Aus der
Neurologischen Universitätsklinik Tübingen
Abteilung Neurologie mit Schwerpunkt Epileptologie

Functional characterization of different epilepsy associated *SCN2A* and *CACNA1E* mutations

Inaugural-Dissertation
zur Erlangung des Doktorgrades der Medizin

der Medizinischen Fakultät
der Eberhard Karls Universität
zu Tübingen

vorgelegt von
Lauerer-Braun, Robert Johannes, geb. Lauerer

2022

Dekan:	Professor Dr. B. Pichler
1. Berichterstatter:	Professor Dr. H. Lerche
2. Berichterstatter:	Professorin Dr. M. Knipper-Breer
3. Berichterstatter:	Professor Dr. C. Kubisch

Tag der Disputation: 25.02.2022

Für meine Eltern

Table of contents

List of figures

List of tables

List of abbreviations

A/D	Analog /Digital
ACTH	Adrenocorticotropic hormone
ANOVA	Analysis of variance
ARX	Aristaless-related homeobox protein
ATP	Adenosine triphosphate
AUC	Area under the curve
B(F)NIS	Benign (familial) neonatal/infantile seizures
CA1...3	Cornu ammonis 1... 3
CACNA1E	Gene encoding the human $Ca_V2.3$ voltage-gated calcium channel
$Ca_V2.3^{-/-}$ mice	Heterozygous knockout mice
CD	Current density
CD8	Cluster of differentiation 8
DEE	Developmental and epilepti encephalopathy
DNA	*Desoxyribonucleid acid*
E. coli	Escherichia coli
EEG	Electroencephalography
EGTA	*Ethylene glycol-bis(2-aminoethylether)-N,N,N',N'-tetraacetic acid*
EIMFS	Epilepsy of infancy with migrating focal seizures
FCS	Fetal calf serum
g	Conductance
g_{Max}	Maximal conductance
GABA	*γ-aminobutyric acid*
GBL	*γ-hydroxybutyrolactone*
GFP	Green flourescent protein
GOF	Gain of function
HEK 293	Human embryonic kidney 293 cells
HEPES	*2-[4-(2-hydroxyethyl)piperazin-1-yl]ethanesulfonic acid*
I	Current
I_{Max}	Maximal current
I…IV	Domain I …. IV
ICD	International Classification of Diseases
ILAE	International league against epilepsy
IRES	Internal ribosome entry site
Iss	Steady-state current
I_{peak}	Peak current
KLD	Kinase-Ligase-Digest
KO	Knockout
k_V	Slope factor
LB	Lysogeny broth
LOF	Loss of function
LTP	Long-term potentiation

MRI	Magnetic resonance imaging
n	Number
PCR	Polymerase chain reaction
r400	Ratio of residual current to the peak current in a 400ms long protocol
S1…S6	Segment 1…6
SCN2A	Gene encoding the human $Na_V1.2$ voltage-gated sodium channel
SEM	Standard error of the mean
t	Time
τ_{act}	Time constant of fast activation
τ_{inact}	Time constant of fast inactivation
τ_{rec}	Time constant of recovery from inactivation
TBE	Tris/Borate/EDTA-Buffer
tsA201	Cell line derived from HEK293 cells
TSC1	Tuberous sclerosis gene 1
TSC2	Tuberous sclerosis gene 2
UV	Ultraviolet
v/v	Volume/Volume
V	Voltage
$V_{½}$	Voltage, at which half maximal activation or inactivation occurs
VGCC	Voltage-gated calcium channel
VGSC	Voltage-gated sodium channel
wt	*Wild type*

1 Introduction

1.1 Epilepsy

The word epilepsy is derived from the Greek verb επιλαμβυειυ which translates to "to seize, possess, afflict" (Magiorkinis *et al.*, 2010). Epileptic patients have been described in the literature since 2000 years B.C. (Magiorkinis *et al.*, 2010). Even though the disease is known to man since at least 4000 years, we only understand a small part of the underlying pathophysiology.

Epilepsy is a neurological disease that is defined by the recurrent occurrence of epileptic seizures. These paroxysmal transient events result from spontaneous synchronous or excessive electrical discharges in groups of brain cells, which cause clinical signs and symptoms (Fisher *et al.*, 2005). Epileptic seizures may result in a wide variety of different symptoms which include involuntary movements of single limbs or the whole body as well as the loss of consciousness, altered sensation or other complex movement or behavior symptoms.

With a point prevalence of approximately 6.4 per 1000 persons in the population, active epilepsy is one the most common neurological disorders in the human population (Fiest *et al.*, 2017). Up to 10% of the population experience a seizure during their lifetime. However, not all of these patients can be diagnosed with epilepsy, as there must be at least a 60 percent chance of recurrent seizures (Fisher *et al.*, 2014; Scheffer *et al.*, 2017).

According to version 11 of the International classification of diseases (ICD), epilepsy can be diagnosed when the disease fulfils one of the three main criteria of the epilepsy definition of the International league against epilepsy (ILAE) (Fisher *et al.*, 2014):

- At least two unprovoked or reflex seizures more than 24 hours apart
- One unprovoked seizure and a probability of further seizures over 60% in the next ten years
- Diagnosis of an epilepsy syndrome
  (ICD 11, 8A60- 8A6Z, WHO, 2018)

Previous to the current definition, epilepsy could only be diagnosed after the occurrence of two seizures in the medical history of a patient. As of now, the possibility for clinicians

to diagnose a patient with epilepsy after the first seizure is added, if the underlying pathology is already clear (Fisher *et al.*, 2014).

In order to find a good treatment for every patient it is crucial to determine the etiology of the epileptic disorder. The current definition of epilepsy distinguishes between epilepsy due to structural changes in brain anatomy found by brain MRI and five additional groups, in which either genetic, infectious, metabolic, and / or immune factors are the cause of disease. It is to mention that mixed etiologies are possible. Epileptic disease in patients in which the etiology remains unclear can be grouped into an unknown group (Scheffer *et al.*, 2017). As better tools for diagnosis such as whole-genome sequencing or high-resolution-MRI become more available nowadays, it is very likely that this group is going to diminish in size in the future.

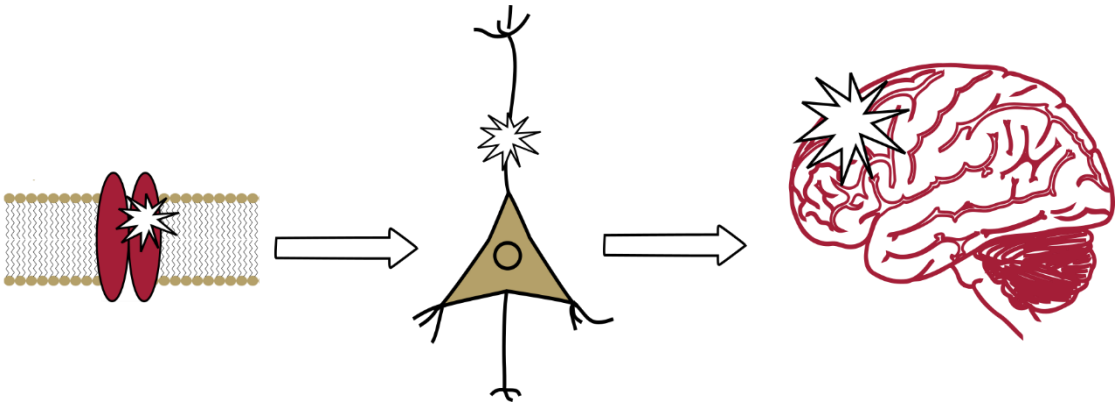

Figure 1: Simplified cartoon of the etiology of genetic epilepsies caused by mutations in ion channels: Altered characteristics of ion channels can result in an altered function of neurons. This might lead to epilepsy. The cartoon of the brain was modified after Mills, 1892.

Various monogenetic alterations have been identified as a cause of a variety of epileptic phenotypes. Here, alterations in a single gene are enough to disturb the physiological function of the brain (Figure 1). Among a wide spectrum of genes involved, often, alterations in genes that encode different types of ion channels can be identified as disease causing (Lerche *et al.*, 2013; Wang *et al.*, 2016; Oyrer *et al.*, 2018). Since a dysfunction of the respective channel is the pathophysiological correlate of the epileptic disease, one can also refer to these epileptic encephalopathies as channelopathies. Channelopathies include a wide variety of diseases (for review see Lehmann-Horn *et al.*, 1999), such as episodic ataxia and other movement disorders (for review see Silveira-Moriyama *et al.*, 2018), migraine (for review see Sutherland *et al.*, 2019), autism

spectrum disorder (for review see Vorstman *et al.*, 2017), chronic pain (for review see Drenth *et al.*, 2007), muscular disorders (for review see Lehmann-Horn *et al.*, 1999) and non-neurological diseases like Long-QT syndrome (for review see Bohnen *et al.*, 2017), Brugada Syndrome (for review see Brugada *et al.*, 2014),Cystic fibrosis (for review see Elborn, 2016) and many other disorders. The knowledge of the disease-causing mutation in a patient and its functional consequences can help to choose an etiology-targeted therapy and predict the prognosis of the disease (see also Figure 1).

In my thesis, I present an electrophysiological evaluation of one mutation in the known epilepsy gene *SCN2A* and three mutations in the new epilepsy gene *CACNA1E,* that were all discovered in patients with different forms of developmental and epileptic encephalopathies.

1.1.1 Developmental and epileptic encephalopathies (DEE)

According to the 2017 classification of epilepsies by the International League Against Epilepsy (ILAE), the term developmental and epileptic encephalopathy (DEE) defines a disorder in which epileptic seizures contribute to severe behavioral and cognitive impairment beyond the symptoms that can be explained by the underlying pathology. The symptoms may add up to further developmental regression as seizures persist and can happen at any age. Per current definition one can distinguish between patients in which the developmental aspect of the disease is the leading symptom from those in which the epileptic activity is the leading aspect by subclassifying further into developmental or epileptic encephalopathies. Both descriptors can be used if both aspects play an equal role in the clinical phenotype. It is important to note that the underlying pathophysiology of the seizures can be of idiopathic, e.g. genetic or lesional nature (Berg *et al.*, 2010; Scheffer *et al.*, 2017).

The disease group of DEE syndromes comprises a very wide range of heterogenic phenotypes and includes many syndromes that have been defined over time.

Among various DEE syndromes, one subset of patients shows distinct symptoms which can be described as infantile spasms or West syndrome (Scheffer *et al.*, 2017; D'Alonzo *et al.*, 2018). This cluster of symptoms is not a strictly defined syndrome and therefore

the definition varies slightly among the literature. The epileptic disorder was first described by W.J. West in 1841 and affects approximately 1-2 of 10.000 children under the age of one (W.J.West, 1841; Pavone *et al.*, 2014). It includes different phenotypes of epileptic seizures, in which the most common phenotype consists of epileptic spasms that cluster in short periods of time. Patients usually show a typical EEG-phenomenon called hypsarrythmia, a chaotic pattern of slow waves and epilepsy-typical potentials in interictal EEG (D'Alonzo *et al.*, 2018). In correlation with this chaotic interictal EEG activity, patients often suffer from delayed brain development. The different possible etiologies of infantile spasms most often include structural alterations like perinatal acquired hypoxic-ischemic-encephalopathy. In other cases, chromosomal deletions and alterations in different genes, including transcription factors like the Aristaless-related homeobox protein *(ARX),* tumor suppressor genes like the tuberous sclerosis-causing genes *TSC1* and *TSC2* or ion channels like the sodium channel *SCN2A* ($Na_V1.2$) (Osborne *et al.*, 2010; Pavone *et al.*, 2014; Wolff *et al.*, 2017) could be identified as the causative factor of disease.

1.2 Ion channels

Ion channels are transmembrane proteins that form ion selective pores across the cell membrane through which ions can passively pass, following their transmembrane gradient, when the channel is open. Their kinetics can be modified by changes in voltage, changes in the concentration of ions, by extra- or intracellular binding molecules or mechanical traction (Kandel *et. al,* 2013). Contrary to other ion carrier proteins, movements of ions through these channels happen passively by diffusion, following forces resulting out of electrical and concentration gradients between both sides of the cell membrane. Ion channels are integral proteins that enable electrical excitability and conduction of action potentials by opening and closing to specific triggers.

Voltage-gated ion channels are a superfamily of channels that share similarities in structure and function as they can be traced back to a common ancestor (Yu *et al.*, 2004; Kandel *et al*., 2013). Although most ion channels share certain similarities in domain architecture and amino acid sequence, different structural ion channel families have evolved over time: K^+ channels show the broadest variety amongst the voltage gated ion

channel families, as different non-voltage-gated K^+ channels can have two, four or six transmembrane domains, still sharing similarities in pore architecture (Yu *et al.*, 2004). Similar to other voltage-gated cation channels, voltage-gated K^+ channels are comprised of 6 transmembrane domains. While Ca^{2+} and Na^+ channels comprise four major domains that each contain six transmembrane segments in one protein that is encoded by a single gene, voltage-gated K^+ channels form homo- or heterotetramers to build up a pore(Anderson *et al.*, 2001; Yu *et al.*, 2004).

The secondary structures of voltage-gated Na^+ and Ca^{2+} channels are closely related to each other. The α-subunit is the pore forming core of the channel, comprised of a total of 24 transmembrane segments in 4 domains.

1.3 The gating and structure of voltage-gated sodium and calcium channels

Voltage-gated ion channels are unique because of their membrane voltage mediated gating mechanism, that enables cells to react to changes in ion concentrations and electrical excitation. They are crucial for the excitability of cells. The current gating theories of ion channels are based on the model of Hodgkin and Huxley (Hodgkin and Huxley, 1952). These two pioneers of neuroscience described a mathematical model for action potentials that they recorded in the giant axons of squids. To simplify, their theory describes the action potential as a sequence of openings and closings of multiple gates in Na^+ and K^+ channels that have a certain probability of opening and closing. Parts of this model were later discovered to be a very accurate description of the three possible main conformations of voltage-gated sodium channels, which account for the major part of the action potentials that Hodgkin and Huxley described (Figure 2). In the open (O) state of the channel, ions can pass the cell membrane trough the channel pore along their electrochemical gradient. In the closed (C) state, the channel does not conduct ionic currents, but can be activated to open. During the inactivated (I) state, the channel also remains in a nonconductive conformation, but cannot be activated directly by changes in voltage, before it has recovered from inactivation by longer lasting membrane repolarisation. As the Hodgkin and Huxley model was initially developed to describe action potentials, its features mainly apply for the gating mechanism of voltage-gated sodium and potassium channels. Nevertheless, the gate theory as a derivation of the

original Hodgkin-Huxley model in ion channels can also be applied when describing the gating behavior of other voltage-gated ion channels such as voltage-gated calcium channels, although the mechanisms of gating, and especially inactivation might differ in parts from those of voltage-gated sodium channels. To better describe the complex gating behavior of ion channels researchers may nowadays also distinguish between a whole set of different closed states, as it better resembles the different states of the ion channel (for review see Bähring *et al.*, 2011).

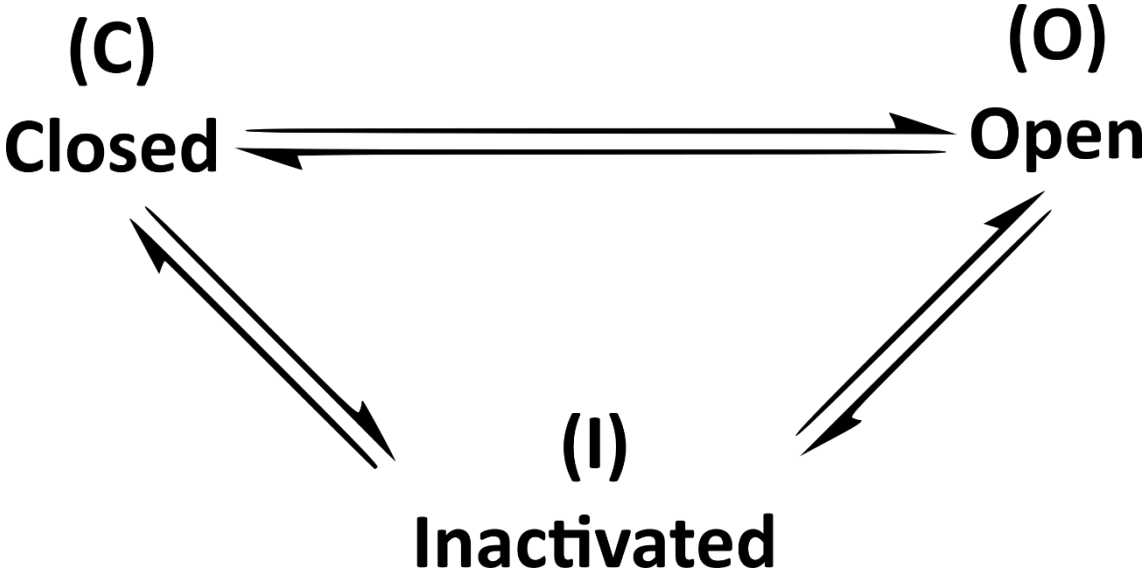

Figure 2 : Simplified scheme of the three main states that occur in voltage-gated cation channels.

Different parts of the channel were identified to be of a great importance for the transition between the three main states.

As ion channels evolved overtime, different domains seem to have preserved their function during gating. For example, we can assume that the functional identity of single transmembrane domains in the six-transmembrane-segment-base-domain-element of voltage-gated sodium, calcium and potassium channels is roughly the same (Figure 3 & Figure 5). This is notable, since four of these elements are conjoined in voltage-gated sodium and calcium channels, while they have stayed separated in voltage-gated potassium channels. Voltage-gated potassium channels can therefore form homo- or heterotetramers, while voltage-gated calcium and sodium channels form a hetereotetramer in themselves.

In each of the four domains, the fourth transmembrane segment S4 acts as a voltage sensor. These α-helical sensor domains contain four to seven positively charged amino acids in distinctive patterns. In most cases, the sequence comprises several arginine residues in alteration with two non-charged hydrophobic amino acids (Catterall, 2012; Clairfeuille *et al.*, 2017) The positive charges of this amino acid residues move during changes in membrane potential and lead to a change in the conformation of the whole channel, that enables the channel to conduct a current (Catterall, 2010). Segments five and six of each domain and their connecting linker form the ion conductive pore through the membrane and are responsible for the ion selectivity and the main gating mechanism of the channel. In voltage-gated sodium channels, an inner part of the channel is responsible for the process of inactivation. The linker between domain III and IV serves as blocking particle that swings into the channel pore like a ball on a chain and enables a second possibility of a closed channel pore (Vassilev *et al.*, 1989; West *et al.*, 1992). Other parts of the pore forming subunit that are mostly located intracellularly, i.e. linkers of the transmembrane segments or the N- and C-terminal, can bind to other proteins and modify kinetics of the channel (Kandel *et al.,* 2013).

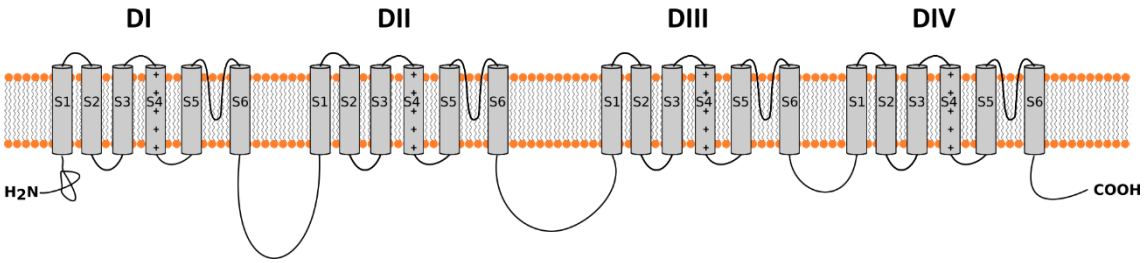

Figure 3: The secondary structure of $Na_V1.2$ α-subunit comprises four domains with each 6 transmembrane segments. In each domain, the fourth transmembrane segment acts as a voltage sensor, while segments five and six form the channel pore.

1.3.1 *SCN2A* / $Na_V1.2$

The *SCN2A* gene encodes the $Na_V1.2$ voltage-gated sodium channel (VGSC).This channel is a member of the family of voltage-gated ion channels that consists of nine channel types from $Na_V1.1$ to $Na_V1.9$ (Figure 4) (Catteral *et al.,* 2005). All voltage-gated sodium channels share sequence similarities with the other members of this class of channels. Furthermore, there is a close relationship with voltage-gated calcium channels, which are considered to be the evolutionary ancestors of sodium channels (Anderson *et*

al., 2001). Voltage-gated sodium channels initiate and propagate action potentials and are therefore important for the electrical properties of excitable cells (Kandel *et al.*, 2013).

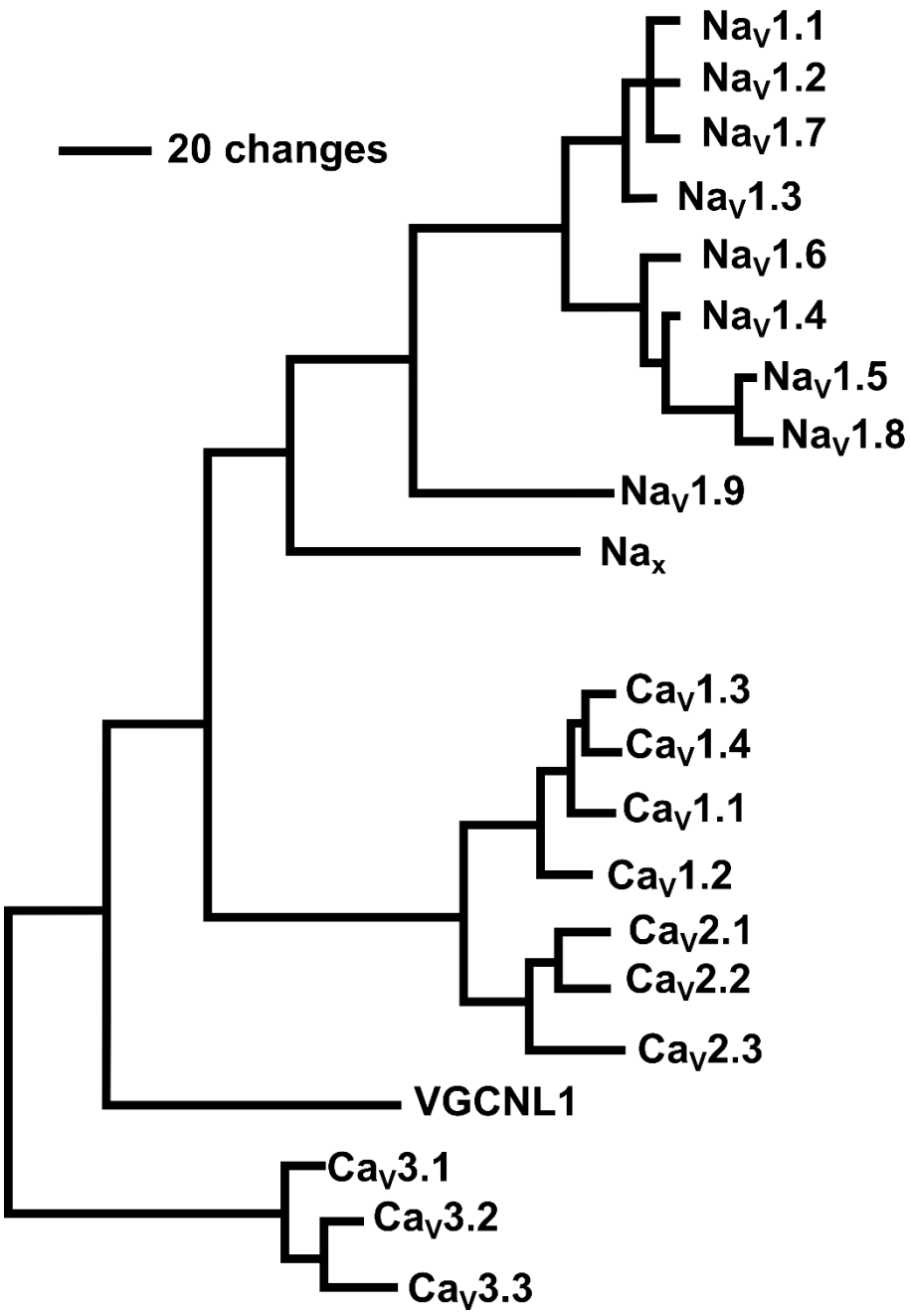

Figure 4: Phylogenic tree of voltage-gated sodium and calcium channels according to the protein sequence of the minimal pore regions from the fourth homologous domain. Adapted from Yu et al, 2004

The $Na_V1.2$ channel complex consists of the pore forming α-subunit (Figure 3) and one or two of four different auxiliary β-subunits β_{1-4} (Catterall *et al.,* 2005). The secondary structure of the α-subunit is similar to that of $Ca_V2.3$ and other voltage-gated sodium and calcium channels with four identical domains, that each are comprised out of six transmembrane domains (Figure 3 & Figure 5). Whereas the α-subunit can form a functioning ion channel on its own, the β-subunits change kinetics and determine the expression rate of the channel similar to the auxiliary subunits in calcium channels (Catterall, 2012)(see also 1.3.2.2).

$Na_V1.2$ is widely expressed throughout the whole central nervous system and is one of the main sodium channels expressed in the brain especially during early stages of development (Liao *et al.,* 2010). In early development, $Na_V1.2$ is mainly expressed at the evolving nodes of Ranvier and then partially replaced by $Na_V1.6$. In adults, $Na_V1.2$ is mainly expressed in unmyelinated axons. (Kaplan *et al.*, 2001; Liao *et al.,* 2010).

Both gain– and loss of function mutations in the *SCN2A* gene are known to cause a wide variety of phenotypes, including different genetic forms of epilepsies, episodic ataxia, autism or developmental delay (for review see Wolff *et al.*, 2017, 2019). Additional disease associations are added constantly. Among the different epileptic phenotypes, two rough main groups can be distinguished by the onset of disease (Wolff *et al.*, 2017). The first group includes patients with epilepsy beginning in the first days to weeks of life, and a relatively good response to sodium channel blocking drugs. Typical syndromes include benign (familial) neonatal/infantile seizures (B(F)NIS) (Heron *et al.*, 2002; Wolff *et al.*, 2017, 2019), Ohtahara syndrome (Nakamura *et al.*, 2013; Wolff *et al.*, 2017, 2019), epilepsy of infancy with migrating focal seizures (EIMFS) (Howell *et al.*, 2015; Wolff *et al.*, 2017, 2019) and unclassified encephalopathies (Wolff *et al.*, 2017). Patients with a later onset of epilepsy in life typically have a more severe phenotype and are more likely exhibit pharmacoresistant seizures. This includes syndromes like West syndrome (Kodera *et al.*, 2013; Nakamura *et al.*, 2013; Wolff *et al.*, 2017, 2019) and Lennox-Gastaut syndrome (Wolff *et al.*, 2017, 2019), myoclonic-atonic epilepsy (Wolff *et al.*, 2017) and focal epilepsies with an electrical status epilepticus during slow-wave-sleep-like phenotype (Wolff *et al.*, 2017).

1.3.2 *CACNA1E* / $Ca_V2.3$

1.3.2.1 The family of voltage-gated calcium channels

The *CACNA1E* gene encodes the voltage-gated calcium channel $Ca_V2.3$. It is a member of the family of voltage-gated calcium channels which consists of three subfamilies that are defined by amino acid sequence similarities (Figure 4). The common molecular structure in these gene families translates to similar electrical kinetics, and to the sensitivity of the channels to different blockers (for review see Catterall *et al.* 2005).

Channels of the $Ca_V1.x$-family correspond to the L-type current. These currents are defined by their long-lasting nature, their activation at high voltages and that they can be blocked by dihydropyridines. $Ca_V1.x$- channels account for the main calcium currents in muscle and endocrine cells and contribute to muscle contraction as well as the secretion of hormones. In neurons, these channels are important for long term potentiation.(for review see Hofmann *et al.*, 2014). The $Ca_V2.x$-familiy is more heterogeneous in terms of sensitivity to channel blockers and gating kinetics of its members than the other two families (Catterall *et al*., 2005; Dolphin, 2006). $Ca_V2.1$ was identified as the channel that conducts the P/Q-Type current and primarily described in measurements of Purkinje neurons of the cerebellum. It is mainly located at pre-synapses and is involved in the release of neurotransmitters (Llinás *et al.*, 1992; Mintz *et al.*, 1995; Catterall et al., 2005). $Ca_V2.2$ conducts the N-Type current (Catterall *et al.*, 2005). $Ca_V2.3$ is thought to be the main corelate of the R-Type current, which was initially defined by its resistance to blockers of other calcium channels as dihydropyridines. $Ca_V2.3$ is blocked by SNX-482, a peptide in the venom of *Hysterocrates gigas,* a tarantula found in Cameroon (Newcomb *et al.*, 1998; Bourinet *et al.*, 2001). $Ca_V3.x$-channels are associated with the T-type current. They are involved in pacemaking and repetitive firing (Catterall *et al.*, 2005).

1.3.2.2 The $Ca_V2.3$ channel complex

The channel complex of the $Ca_V2.3$-channel consist of 4 subunits, which most likely come together in a 1:1:1:1 molar ratio. The α_{1E}-subunit, which is encoded by the *CACNA1E* gene, is the main pore-forming part of this complex (Figure 5). This transmembrane protein is joined by 3 auxiliary subunits: A β-, an $\alpha_2\delta$- and probably a γ-subunit (Catterall *et al.,* 2005; Neely *et al.*, 2014).

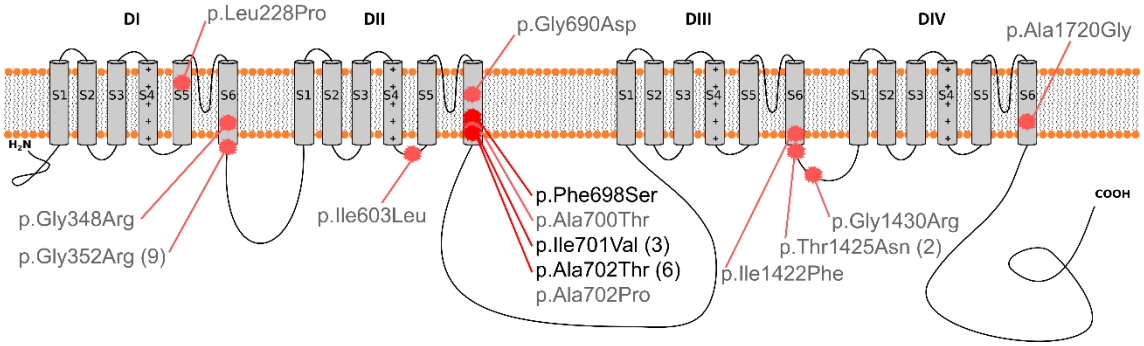

Figure 5: The $Ca_V2.3$ channel has four homologue domains containing each six transmembrane segments. Missense mutations in *CACNA1E* in patients with the *CACNA1E* encephalopathy are highlighted. Numbers in brackets indicate number of patients, if multiple individuals were affected. Functionally studied variants in S6 of DII are highlighted in darker font Adapted from Helbig *et al.,* 2018.

Co-expression studies could show that the β-subunit elevates the expression of the α-subunit and therefore also increases the current density of the channel, when expressed in non-neuronal cells such as HEK293 cells or *Xenopus laevis* oocytes (Williams *et al.*, 1994; Dolphin, 2003). Each of the four different β-subunits β_1 to β_4 exists in different isoforms and splice variants, allowing for different compositions of the channel complex (Birnbaumer *et al.*, 1998). The four different possible $\alpha_2\delta$-subunits consist of two domains, that are separated after translation and then rejoined by disulfide bonds. As shown in co-expression studies, this subunit increases the current density in cells expressing the protein and shifts the activation and inactivation kinetics to more negative voltages (Klugbauer *et al.*, 1999). The $\alpha_2\delta$-subunit is a main targets of gabapentin and pregabalin, two common antiepileptic drugs that are mainly used as a treatment in neuropathic pain (Gee *et al.*, 1996; Taylor *et al.*, 2007). There is limited evidence that this subunit is not an essential part of the channel complex (Müller *et al.*, 2010). The γ-subunit seems to be part of the channel complex in some tissues. Its significance for the channel

complex is not yet fully understood. There are even hints that this subunit is as well not associated with the VGCC complex at all (Müller *et al.*, 2010) .

1.3.2.3 Cellular and subcellular localization of $Ca_V2.3$ and current state of research

$Ca_V2.3$ channels are expressed in many tissues of the human body including testis, kidney and lung with a hotspot of expression in the central nervous system (Fagerberg *et al.*, 2014; *NCBI Gene ID: 777*, 2018). In the central nervous system, $Ca_V2.3$ expression is complex and not yet fully understood. There is evidence of presynaptic (Breustedt *et al.*, 2003; Dietrich *et al.*, 2003) and postsynaptic (Parajuli *et al.*, 2012) expression of $Ca_V2.3$. The macroscopic expression pattern of $Ca_V2.3$ throughout the whole brain is ubiquitous with clustering in some regions (Soong *et al.*, 1993; Williams *et al.*, 1994; Weiergräber *et al.*, 2006; Parajuli *et al.*, 2012). $Ca_V2.3$ is expressed in excitatory cells as well as in GABAergic interneurons of the *reticular thalamus* (Weiergräber *et al.*, 2008). With at least three different splice variants of the channel that show different expression patterns among brain areas, drawing functional clues from tissue expression becomes very complex (Weiergräber *et al.*, 2006). In addition to the complex macroscopic and microscopic expression pattern of $Ca_V2.3$, subcellular mechanisms broaden the possible systemic effects of an altered channel function to a huge extent (Tai *et al.*, 2006; Müller *et al.*, 2010).

To this point in time, the function of $Ca_V2.3$ in the central nervous system was often studied in the context of the cellular correlates of learning: long-term potentiation (LTP) and synaptic plasticity. Located distant from the synapse, $Ca_V2.3$ channels influence the threshold for initiation of presynaptic long-term potentiation at hippocampal mossy fiber synapses, while they are not crucial for LTP in general (Breustedt *et al.*, 2003; Dietrich *et al.*, 2003).

Also, caution should be exercised when interpreting electrophysiological studies on $Ca_V2.3$ and its full correspondence to the R-Type current. Previous research suggest that the R-Type current is not completely congruent with the current of $Ca_V2.3$ channels (Newcomb *et al.*, 1998; Sochivko *et al.*, 2002). Furthermore, commonly used channel

blockers for R-Type currents such as SNX-482 or Ni^+ ions at a low concentration are not fully specific for $Ca_V2.3$ (Lee *et al.*, 1999; Tottene *et al.*, 2000; Bourinet *et al.*, 2001; Kimm *et al.*, 2014). This complicates the interpretation of experiments on the function of $Ca_V2.3$ in neuronal cells, as the currently available blockers will also interact with other channel types and might change neuronal function.

A study in rodent brains showed that the channel contributes to roughly 30% of the Ca^{2+} current in cortical astrocytes (D'Ascenzo *et al.*, 2004). Other studies also suggest the expression of the channel in rat and human astrocytes (Day *et al.*, 1996; Latour *et al.*, 2003). Calcium oscillations in astrocytes contribute to paroxysmal depolarization shifts during epileptic seizure activity and may influence ictal activity by releasing monamine neurotransmitters as glutamate (Tian *et al.*, 2005). Calcium waves in astrocytes and radial glia cells are also an influencing factor of neuronal development (Weissman *et al.*, 2004). In contrast to this, $Ca_V2.3^{-/-}$ mice show a normal macroscopic anatomy of the brain (Weiergräber *et al.*, 2006). Taken together, the role of $Ca_V2.3$ currents in neuronal development is still unknown and might be only relevant on a microscopic level.

1.4 The patch clamp technique

The patch clamp technique was invented by Neher and Sakmann in 1976 and was awarded with the Nobel prize of medicine and physiology in 1991 (Neher and Sakman, 1976). The technique offers multiple possibilities to record the electrical behavior of molecules and cells. Depending on the selected patch clamp mode, one can record either current-voltage relationships in whole cells or investigate single channel behavior. Various patch clamp configurations have been established. All of them involve a piece of cell membrane or patch, hence the name patch clamping, that gets sealed to a glass micropipette which enables electrical recordings of single membrane compartments. A widely-used configuration is the whole cell configuration, in which a hole in the cell membrane allows modifying the overall membrane voltage or injecting current into the cell (Figure 6). In general, two different modes of electrical stimulation are possible: In voltage clamp mode, the membrane potential of the 'patched' cell is changed and the elicited currents are recorded. In current clamp, changes in membrane potential are recorded upon injection of a current into the cell. While current clamp recordings are widely used to study the behavior of excitable cells such as neurons, voltage clamp

recordings are mostly used to study different ionic currents in excitable and none-excitable cells (Molleman, 2002).

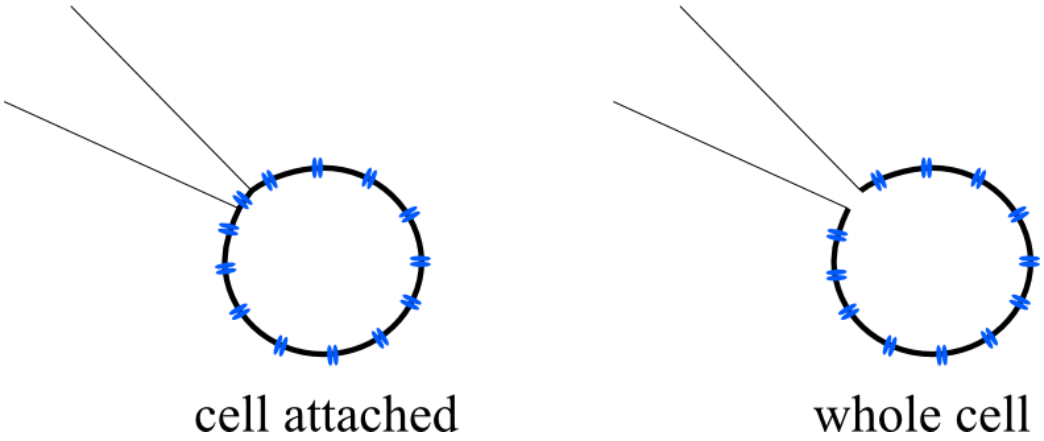

Figure 6: Cell attached and whole cell patch clamp mode. The overexpressed channels are unproportionally magnified in this comic.

1.5 Aim of this thesis

The aim of this work was to electrophysiologically provide a first functional evaluation of the c.632 G>A (p.G211D) mutation in *SCN2A*, a well known epilepsy gene, and the c.2093 T>C (p.F698S), c.2101 A>G (p.I701V), and c.2104 G>A (p.A702T) mutations in *CACNA1E,* a newly established epilepsy gene, all found in patients with severe pharmocoresistant epilepsy.

2 Materials and methods

2.1 Reference sequences and constructs

Table 1 shows the reference sequences that were used to verify the integrity of the cDNA of the desired genes.

The *CACNA1E* gene in the pcDNA3.1 vector (Figure 10) was a generous gift of Prof. Norbert Klugbauer (Institute for Experimental and Clinical Pharmacology and Toxicology, Albert-Ludwigs-Universität Freiburg, Freiburg, Germany) (Vajna *et al.*, 2001). The human β_{2d}-subunit cloned in the pIRES2-EGFP-Vector (Clontech) (Figure 11) and the $\alpha_2\delta_1$-subunit encoded by *CACNA2D1* in the pIRES puro3 vector (Figure 12) were gifts by Prof. Stefan Herzig (Department of Pharmacology, University of Cologne, Cologne, Germany) (Hobom *et al.*, 2000).

The *SCN2A* gene was cloned into the pcDNA3 vector (Figure 7) as described elsewhere (Xu *et al.*, 2007). *SCN1B* and *SCN2B* in the pCLH vector were kindly provided by GlaxoSmithKline (Brentford,UK). The hygromycin coding region in these vectors was exchanged with EGFP in the *SCN1B*-vector and CD8 in the *SCN2B*-vector (Schwarz *et al.*, 2016).

Plasmid DNA was sequenced as stated below and alignments of different sequences were achieved in the CLC Sequence Viewer Software (Quiagen Venlo, The Netherlands).

Table 1: Reference sequences for all genes used in this thesis VGSC voltage-gated sodium channels VGCC voltage-gated calcium channels

Gene name	*Product*	*NCBI Reference*	*Uniprot Reference*
SCN2A	$Na_V1.2$	NM_001040142.1.	Q99250-1
SCN1B	β_1-subunit (VGSC)	NM_001037	Q07699-1
SCN2B	β_2-subunit (VGSC)	NM_004588	O60939-1
CACNA1E	$Ca_V2.3$ / α_{1E}	NM_001205293.1.	Q15878-1
CACNB2d	β_{2d}-subunit (VGCC)	NM_201596.2.	Q08289-1
CACNA2D1	$\alpha_2\delta_1$-subunit (VGCC)	XM_005250570	P54289-1

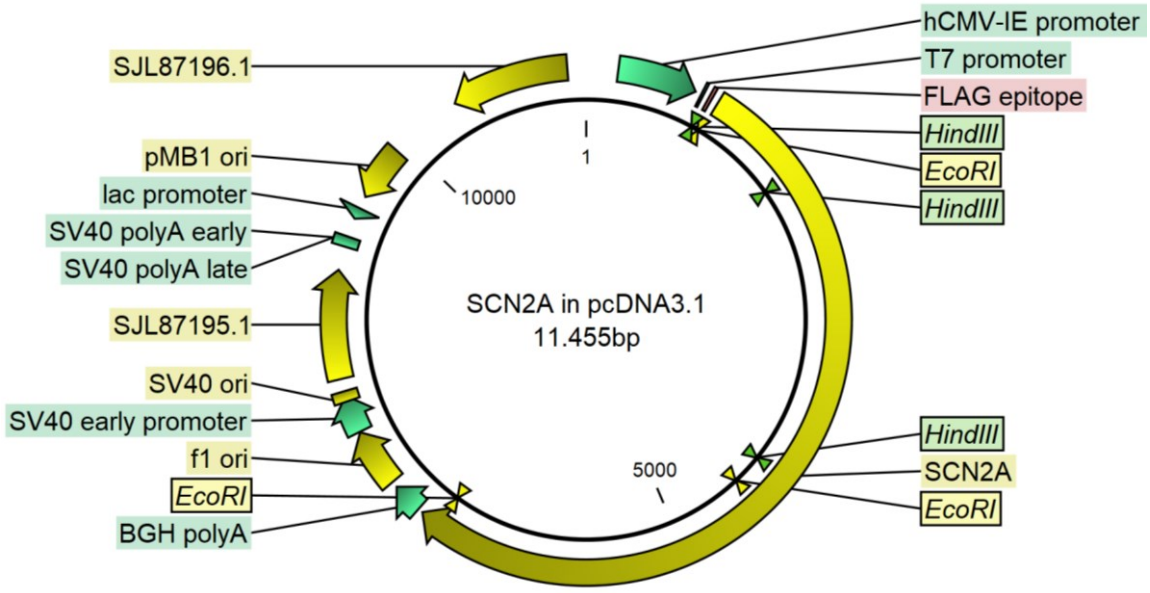

Figure 7 : The *SCN2A* gene was used in the pcDNA3.1 vector. Restriction sites to verify the construct are indicated with small double triangles.

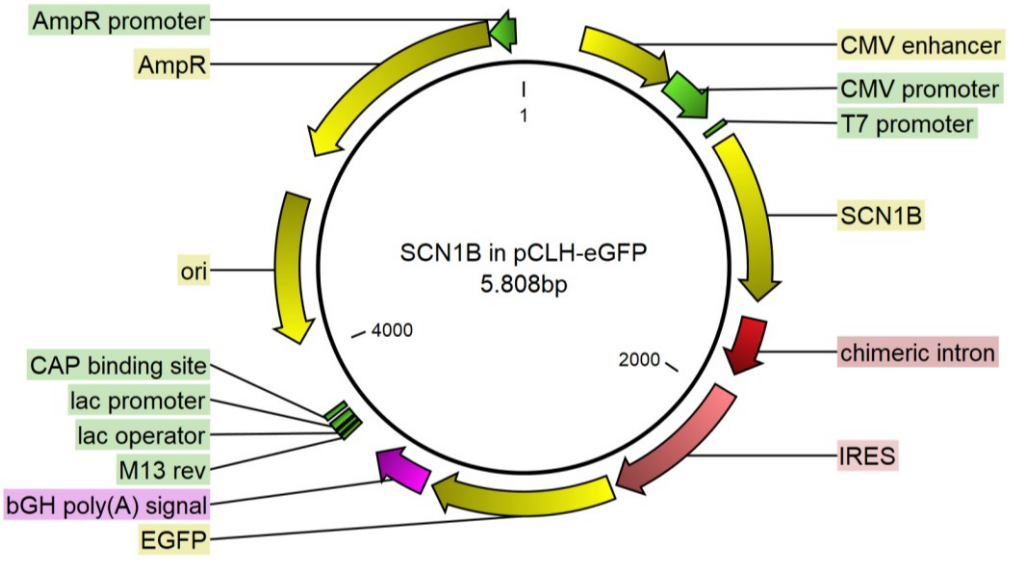

Figure 8: The *SCN1B* gene was used in the pCLH vector with an *eGFP* gene as reporter.

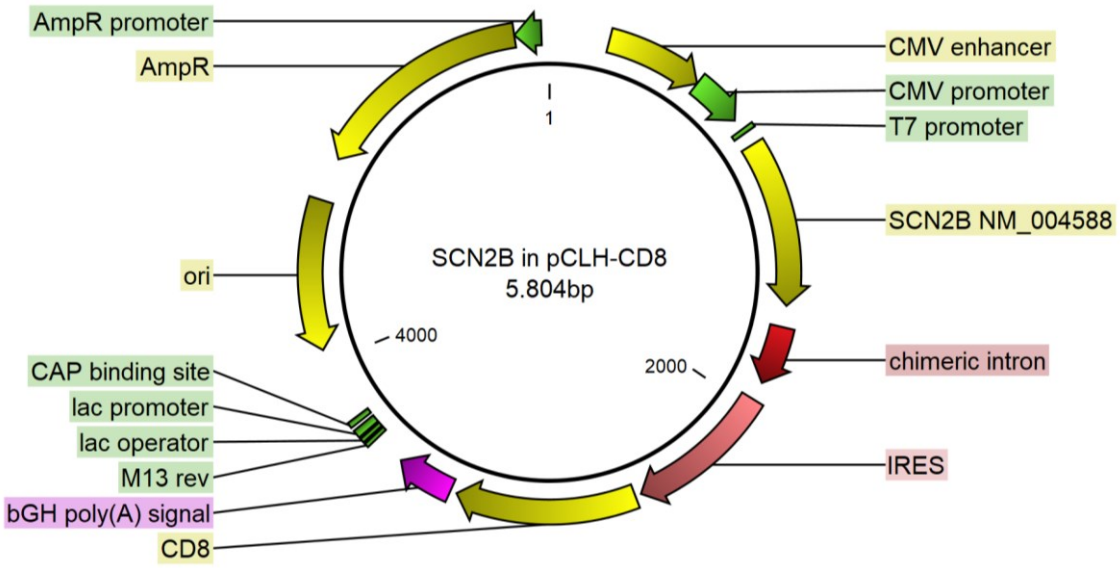

Figure 9: The *SCN2B* gene was used in the pCLH vector with an CD8 gene as reporter.

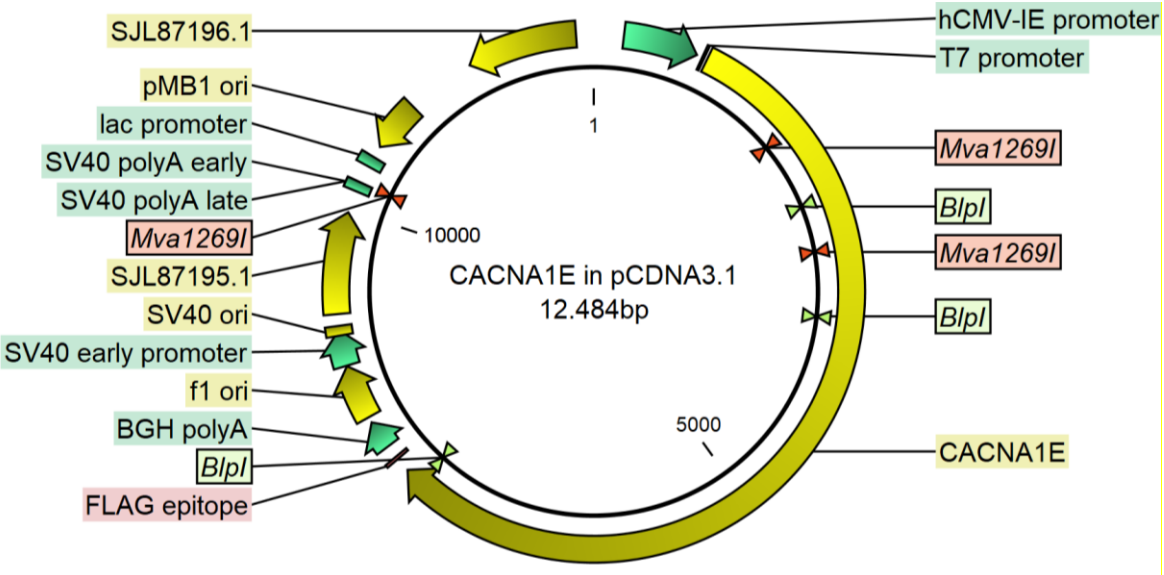

Figure 10: The *CACNA1E* gene was used in the pcDNA3.1 vector. Restriction sites to verify the construct are indicated with small double triangles.

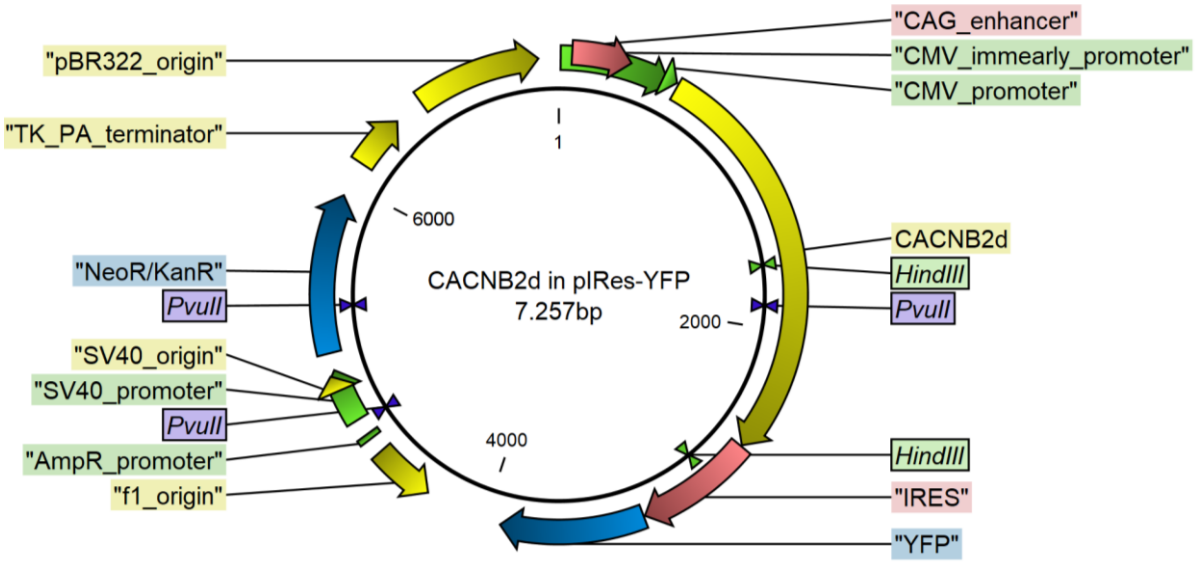

Figure 11 :The *CACNB2d* gene was used in the pIRES-YFP vector. Restriction sites to verify the construct are indicated with small double triangles.

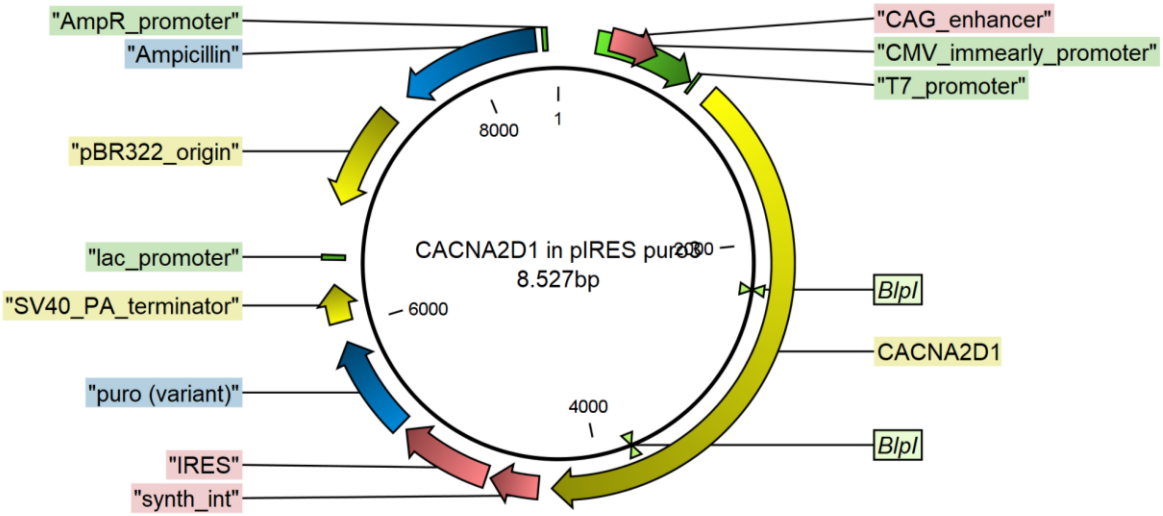

Figure 12 : The *CACNA2D1* gene was used in the pIRES-puro3 vector. Restriction sites to verify the construct are indicated with small double triangles.

2.2 Mutagenesis

Mutations in the cloned constructs were generated by two different polymerase chain reaction (PCR) based single-site directed mutagenesis approaches. In both cases, a PCR with partially mismatching primers (see Table 2) led to a base exchange at the desired position of the construct. Before transformation into bacteria, the original template was digested with DpnI. This restriction enzyme only cleaves methylated DNA and cleans the reaction of the dam^+ methylated DNA template. This ensured that only colonies formed after transformation, which contained a plasmid that originated from the PCR reaction.

The c.632 G>A p.Gly211Asp (G211D) missense mutation in *SCN2A* was generated using a site-directed polymerase chain reaction (PCR) mutagenesis protocol with the Gotaq® Long Polymerase (Promega Corporation,Madison, WI, USA). The primers for this were fully complementary and both included the desired mutation.

For *CACNA1E*, the NEB Q5 Site directed mutagenesis kit was used. In this protocol, non-overlapping primers were generated with the supplied online tool for the kit. After PCR, the linear plasmid was ligated and digested in a single step called KLD (Kinase-Ligase-Digest) reaction.

Primers for mutagenesis

Table 2: Mutagenic primers used to engineer the desired mutations into the cDNA. Corresponding annealing temperatures are given. Altered nucleotides are indicated in bold.

Gene	*Alteration*	*Forward Primer*	*Reverse Primer*	$T_{Annealing}$
SCN2A	c.632 G>A p.Gly211Asp (G211D)	5'-AGACCTAG**A**CAATGTTTC-3'	5'- GAAACATTG**T**CTAGGTCT -3'	41 °C
CACNA1E	c.2093 T>C p.Phe698Ser (F698S)	5'-CTGAATGTGT**C**CTTGGCTATCG-3'	5'-TAGCGTGTAGTTGCCAAAC-3'	61 °C
CACNA1E	c.2101 A>G p.Ile701Val (I701V)	5'-GTTCTTGGCT**G**TCGCTGTGGA-3'	5'-ACATTCAGTAGCGTGTAGTTG-3'	64 °C
CACNA1E	c.2104 G>A p.Ala702Thr (A702T)	5'-CTTGGCTATC**A**CTGTGGATAATC-3'	5'-AACACATTCAGTAGCGTG-3'	59 °C

Polymerase chain reaction protocol

To engineer the c.632 G>A / p.Gly211Asp variant into *SCN2A*, reagents were mixed as follows and the PCR was ran on a BluRay Turbocycler thermocycler (Table 3) (Taipei City, Taiwan):

Table 3: Polymerase chain reaction protocol to engineer the c.632 G>A / p.Gly211Asp mutation into the *SCN2A* gene

Reagent	*Amount*
Forward Primer (10 µmol/l)	2.5 µl
Reverse Primer (10 µmol/l)	2.5 µl
Template (1.6 ng/µl)	1 µl
GoTaq® Long PCR Master Mix, 2X	25 µl
Water	19 µl
	50 µl

Protocol		
Initial denaturation	*95 °C*	*2 min*
30 cycles:		
Denaturation	94 °C	25 s
Annealing	41 °C	25 s
Extension	65 °C	15 min
Final extension	72 °C	10 min
Soak	*4 °C*	*forever*

After PCR, the bacterial template DNA was digested using DpnI (New England Biolabs, Ipswich, MA, USA) at 37°C for one hour.

For mutations in *CACNA1E*, the reaction was prepared according to the Q5 site directed mutagenesis kit's protocol. The PCR protocol was designed as follows and ran on a BluRay thermocycler (Table 4) (BlueRay Biotech, Taipeh, Taiwan):

Table 4: Polymerase chain reaction protocol to engineer mutations into the *CACNA1E* gene.

Reagent	*Amount*
Forward Primer (10µmol/l)	1.25 µl
Reverse Primer (10µmol/l)	1.25 µl
Template (14ng/µl)	1 µl
Q5 Hot Start Polymerase, 2X	12.5 µl
Water	9 µl
	25 µl

Protocol		
Initial denaturation	98°C	30 s
25 cycles:		
Denaturation	98°C	10 s
Annealing	See above	20 s
Extension	72°C	6 min
Final extension	72°C	2 min
Soak	4-10°C	forever

After PCR, a Kinase-Ligase-Digest (KLB) step was applied for 5 min at room temperature (Table 5).

Table 5: Composition of the Kinase-Ligase-Digest reaction for *CACNA1E* constructs.

Reagent	*Amount*
PCR Product	1 µl
KLD Reaction Buffer, 2X	5 µl
KLD Enzyme Mix, 10X	1 µl
Water	3 µl
	10 µl

For both reactions 5 µl of the mixtures were transformed into 5-α competent cells (NEB).

2.3 Sanger sequencing of plasmids

Plasmids were sequenced with the Sanger technique on an ABI 3730xl DNA Analyzer (96 capillary instrument) at an external core facility (GATC Biotech AG, Köln, Germany). The primers for sequencing *SCN2A* and *CACNA1E* were designed by Dr. Niklas Schwarz to have overlapping sequencing products and to be able to sequence the complete gene. Primers for *CACNB2* and *CACNA2D1* were designed by me under the guidance of Dr. Schwarz. Sequences were verfied using CLC Sequence Viewer (Quiagen) and GATC Sequence Viewer (GATC Biotech).

2.4 Diagnostic restriction digest of plasmids

Plasmids used were analyzed in a restriction digest to verify the correct size und integrity of the plasmid of the alpha-subunit and the auxiliary Ca^{2+} channel subunits.

The reaction was set up as follows (Table 6):

Table 6: Composition of diagnostic restriction digest reactions for plasmids

Reagent	*Amount*
Plasmid DNA	0.5-1 µg
Buffer 10X	2.5 µl
Matching restriction enzyme	1.0 µl
H_2O	to 25 µl
	25 µl

The mixture of reagents was incubated for 1-2 h at 37°C and then run on an agarose-gel as stated below.

2.5 Transformation of chemically competent *E. coli*

Chemically competent *E. coli* cells (α-select(Bioline) ,Top Ten(Invitrogen) or 5-alpha (New England Biolabs)) were transformed using a standard heat shock protocol: The bacterial suspension was thawed on ice. After adding 2-5 µl of plasmid DNA, the

suspension was incubated on ice for 30 min. The heat shock consisted of 45 s at 42°C for α-select and Top Ten cells, and 30 s for 5-alpha cells. This was followed by a 2 min incubation time on ice. 900 µl of SOC medium was added and bacteria were allowed develop antibiotic resistance (ampicillin) for 1h at 37°C and 350 rpm in a thermal shaker. After that, 50-200 µl of the cell suspension was platted on *Lysogeny Broth*-agar (LB-agar) plates containing the required selection antibiotic for the transformed plasmid. One day later, colonies were picked and transferred to 8-14 ml LB medium (PanReac Applichem, Darmstadt, Germany) supplemented with the corresponding antibiotic. Cultures were incubated overnight at 37°C and 170 rpm in a shaking incubator. A glycerol stock was made the following day for further cultures using 0.5 ml 80% glycerol and 0.5 ml culture solution. The glycerol stock was frozen at -80°C. Plasmid DNA was isolated out of the remaining culture as stated below.

2.6 Isolation of plasmid DNA

To obtain small amounts of DNA, transformed bacteria were cultured in 7.5 ml of LB medium supplemented with the proper selection antibiotic overnight and DNA was isolated using the EtractMe® Plasmid DNA miniprep kit (BLIRT S.A, DNA GDAŃSK,Gdansk, Poland).

Plasmids were sequenced as stated above. If the mutation was introduced correctly into the α-subunit, no additional mutations could be found and the integrity of the plasmid was verified via restriction digest and gel electrophoresis, a small amount of the glycerol stock was brought back to culture in 350 ml LB-medium supplemented with the corresponding antibiotic. The culture was incubated overnight for 24 h, followed by plasmid DNA isolation with the EtractMe® Plasmid DNA Maxiprep kit (BLIRT S.A., DNA GDAŃSK, Gdansk, Poland).

Plasmid DNA concentrations were measured using a NanoDrop™ ND-1000 (Thermo Fisher Scientific™, Wilington, DE, US) spectrometer with sterile water as blank control. The A_{280}/A_{260} absorbance ratio was used as an indicator of purity. A ratio above 1.8 was considered as pure.

2.7 Agarose gel electrophoresis

To analyze the size of plasmids after PCR or DNA isolation, agarose gel electrophoresis was used. To achieve a 1% agarose gel, Agarose basic (PanReac Applichem, Darmstadt Germany) was dissolved in TBE-buffer (A4348, PanReac Applichem, Darmstadt, Germany) and heated up for approximately 2 min in the microwave. After slight cooling 5 µl of RedSafe nucleid acid staining solution (iNtRON Biotechnology, Jungwon-gu, Seongnam, Gyeonggi-do, Korea) was added per 100 ml of agarose solution to later stain the gel. The gel was poured into the chamber and covered in TBE-buffer 20 min after pouring. 10-25 µl of the PCR products were mixed with 2-5 µl Orange G and loaded into the pockets of the gel. A voltage of 120 V was applied for ~ 1,5 h. After that, the gel was analyzed under UV-light.

2.8 Cell culture

The tsA201 cell line used in this study is derived from the HEK293 cell line trough further transduction of HEK293 cells. The HEK293 cell line is a stable cell line that was achieved by Frank Graham in 1973 by transforming cells that were taken from the kidney of an human embryo with adenovirus type 5 (Graham *et al.*, 1977). HEK293 cells are very persistent cells, that are well established for electrophysiological recordings. Since HEK293 and tsA201 cells only express few ion channels, they are ideal to use as a heterologous expression system for ion channels.

TsA201 cells were cultivated in T12 or T75 flasks (Falcon, Corning, NY, USA) using Dulbecco's Modified Eagle Medium (DMEM) (Gibco) supplemented with 10% (v/v) FCS (PAN-Biotech, Aidenbach, Germany) and 0.02 mM Glutamine (Biochrome) in a 5% CO_2 atmosphere at 37°C. Medium was exchanged once a week and cells were passaged to a new flask every week. Cells were therefore mechanically detached and resuspended in new medium without the use of enzymes. Prior to electrophysiological recordings, 0.7 million cells were subcultured in 35 mm dishes (Greiner Bio-One, Frickenhausen, Germany) and prepared for transfection 24 h after passage. All sterile procedures were carried out under a sterile hood.

2.9 Transient cell transfection

Transient cell transfection was achieved using a lipopolyplex transfection method. TsA201 cells were subcultured in 35 mm dishes with a seeding density of 0.7 million cells 24 h prior to transfection. For transfection, 7.5 µl transfection reagent (TransIT®-LT1, Mirus Bio LLC, Madison, WI, USA) were mixed with 250 µl Optimem Medium (Gibco, Thermofisher scientific, Waltham, MA USA). After a 5-minute incubation period, 2 µg plasmid DNA of the *CACNA1E* α_{1E}-subunit together with DNA encoding the β_{2d}-subunit and in some pre-experiments the $\alpha_2\delta$-subunit was added in a 1:1:1 molar ratio. For *SCN2A* 2 µg of α-subunit plasmid DNA were added together with 0.2 µg of each hβ_1 and hβ_2-subunits. After another 20-minute incubation period, the whole mix was added to the cells. First electrophysiological recordings were carried out 24 h after transfection.

2.10 Electrophysiology

2.10.1 Patch clamp setup

An inverted microscope (Axio-Vert.A1; Zeiss or DM IL LED, Leica) was used to view the cells that were supposed to be recorded. The electrical circuitry consisted of a glass micropipette filled with the 'intracellular solution' in contact with a AgCl covered silver electrode (AG-8W, Science products, Hofheim, Germany) and a AgCl covered silver bath electrode in the 35 mm dish (Greiner Bio one, Frickenhausen, Germany), both connected to the patch clamp amplifier (Axopatch 200B, Axon Instruments, Union City, CA, USA) through a preamplifying headstage and an airtight pipette holder close to the recording setup. The setup was placed on an air suspended table and surrounded by a faraday cage. An electric micromanipulator helped to position the pipettes in the 35 mm dish. Currents were recorded through the amplifier into a Digidata 1320A or 1440A A/D – Converter where they were converted into a digital signal and sent to a computer running the Clampex 8 or 10 electrophysiology software (Axon Instruments, Union City, CA, USA)(Figure 13).

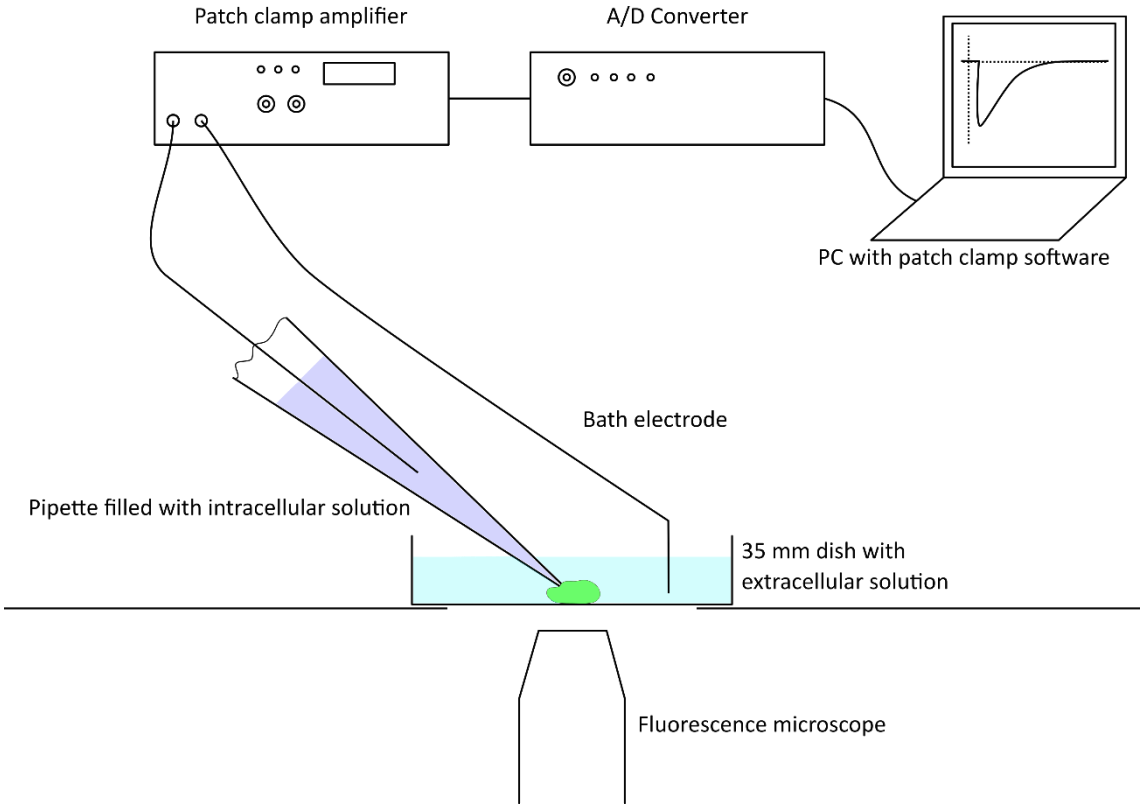

Figure 13: Scheme of the patch clamp setup used.

Silver electrodes were regularly covered with AgCl by putting them in household bleach (DanKlorix, CP GABA GmbH, Hamburg, Germany) overnight.

2.10.2 Experimental procedure

TsA201 cells were transfected as stated above 24-36 h before electrophysiological recordings were obtained. To separate cells, they were split into 35 mm dishes 30-60 min before first measurements started. Prior to using a dish in the patch clamp setup, the cell culture medium was removed and the bath solution was added onto the cells. In experiments with $Na_V1.2$, the transfected cells were washed with a buffer solution containing CD8 binding beads (see below) before adding the bath solution. Each cell culture dish was used for recordings for approximately one hour.

Borosilicate glass pipettes (GB150F-8P, Hofheim, Germany) were pulled on a Model P-97 Flaming/Brown micropipette puller (Sutter Instrument, Novato, CA, USA).

Pipettes filled with intracellular solution had a resistance of 1-2 MΩ when entering the bath solution.

Before entering the bath solution with the pipette, a small positive pressure was applied to the pipette to keep it clean from dirt.

As the co-expression of the auxiliary subunits with $Na_V1.2$ or $Ca_V2.3$ changes their gating parameters, cells that expressed these subunits were identified by the co-expression of tags. For this, the sodium channel β_2-subunit was co-expressed with the cell surface protein CD8 via an IRES-Site (see also 2.1) through the same promoter. The CD8 surface cell antigen could be targeted with the binding of CD8 MACS Beads (ThermoFisher Scientific), that are usually used in Magnetic Cell Sorting (MACS). These small magnetic beads are covered with CD8 targeting antibodies and attach to cells expressing this antigen. In $Na_V1.2$ experiments, the cells were briefly washed with a solution in which CD8 MACS beads were suspended. CD8 and β_2-subunit positive cells were surrounded by at least 2-4 beads and could be identified by this. The sodium channel β_1-subunit and the calcium channel β_{2d}-subunit were tagged with a variant of *Green Fluorescent Protein* (GFP) (see also 2.1). Cells expressing these proteins could be visualized by their green fluorescence under a corresponding microscope.

To record Na^+ or Ba^{2+} currents, the whole cell patch clamp mode was used (Figure 6). To reach this mode, cells were approached with the pipette, until a slight deformation of the cell could be recognized. A mild positive pressure, that was used to ensure a clean pipette tip, was then released to initiate the sealing of the cell to the pipette tip. The pressure was then slightly lowered using a standard medical 30 ml syringe until a *Giga seal* was formed, recognizable by an increased resistance between bath and pipette electrode of more than 1 GΩ. After compensating for pipette resistance with the internal circuit of the patch clamp amplifier, cells could be opened using another short impulse of negative pressure. The resulting capacitance and resistance artefacts were compensated with the internal circuitry of the patch clamp amplifier. In this whole cell mode, pipette solution could enter the cell and lead to controlled ion concentrations in the cell.

2.10.3 Recording solutions

2.10.3.1 Recording solutions for Na^+ currents

Table 7:Recording solutions for Na^+ currents.

	intracellular	*extracellular*
	(mmol/l)	(mmol/l)
CsF	130	-
NaCl	5	140
$MgCl_2 * 6\ H_2O$	2	1
KCl	-	4
$CaCl_2$	-	2
EGTA	5	-
HEPES	10	5
Glucose	-	4

The pH of both solutions was adjusted to 7.4 with CsOH using a pH-meter (Schott).

Osmolarity was adjusted with Mannitol to 300 mosmol for intracellular and 290 mosmol for extracellular solution using an osmometer (Typ OM806, Löser Messtechnik, Berlin Germany).

2.10.3.2 Recording solutions for Ba^{2+} currents

The composition of the solutions used for electrophysiological records of Ba^{2+} currents was adapted from Williams *et al.*, 1994.

To study calcium channel kinetics, Ba^{2+}-ions were used instead of Ca^{2+}-ions to avoid calcium dependent effects, like calcium dependent inactivation and other second messenger effects. Cs^+-ions replaced K^+-ions to block the few potassium channels in tsA201 cells. EGTA was added to bind any excess divalent ions, especially Ca^{2+}. *2-[4-(2-hydroxyethyl)piperazin-1-yl]ethanesulfonic acid (HEPES)* acted as stabilizer of the pH of the solutions. Magnesium chloride was used to stabilize the membrane potential. Choline chloride served as a neutral donor of chloride ions and non-sodium cations.

Table 8: Recording solutions for Ba^{2+} currents.

	intracellular	*extracellular*
	(mmol/l)	(mmol/l)
CsF	105	-
CsCl	30	-
$MgCl_2 * 6\ H_2O$	1	1
$BaCl_2 * 2\ H_2O$	-	15
EGTA	10	-
HEPES	10	10
Choline-Cl	-	150

The pH of both solutions was adjusted to 7.4 with CsOH using a pH-meter (Schott).

Osmolarity was adjusted with Mannitol to 300 mosmol for intracellular and 290 mosmol for extracellular solution using an osmometer (Typ OM806, Löser Messtechnik, Berlin Germany).

2.10.4 Voltage clamp protocols

2.10.4.1 Voltage protocols for Na^+ currents of $Na_V1.2$ (SCN2A) channels

Leak subtraction protocol

A -P/4 leak subtraction protocol was administered before recording most protocols, consisting of four voltage pulses opposite to the test pulse with a voltage amplitude 25% of the test pulse. The resulting currents were automatically summed up and subtracted from the signal by the Clampex 10 software (Axon Instruments, Union City, CA, USA).

Voltage dependence of activation

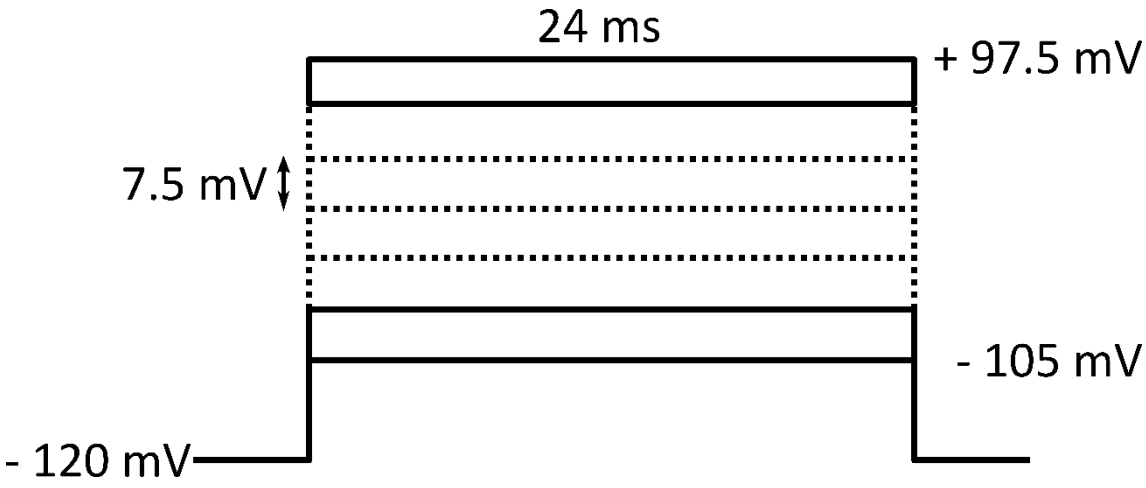

Figure 14: Voltage Protocol for recording activation kinetics in tsA201 cells transfected with $Na_V1.2$, β_1- and β_2-subunits.

Cells were depolarized from a holding potential of -120 mV to different voltage steps ranging from -105 mV to 97.5 mV in 7.5 mV increments for 24 ms (Figure 14). Recordings were obtained at a sampling rate of 20 kHz and filtered using the internal low pass filter of the patch clamp amplifier at a frequency of 5 kH. A -P/4 leak subtraction protocol was applied prior to each sweep as described above.

Tau of fast inactivation / Persistent current I_{SS} /I_{Peak}

Cells were depolarized to different voltages between -80 mV to 10 mV in 10 mV steps for 95 ms from a holding potential of -120 mV (Figure 15). Recordings were obtained at a sampling rate of 20 kHz and filtered using the internal low pass filter of the patch clamp amplifier at a frequency of 5 kHz. A -P/4 leak subtraction protocol was applied prior to each sweep as described above. The time constants of inactivation τ_{fast} and τ_{slow} were determined by fitting the current traces with a two-part exponential fit in Clampfit 10 (Axon Instruments, Union City, CA, USA).

$$I(t) = A_1 * e^{\frac{-t}{\tau_{slow}}} + A_2 * e^{\frac{-t}{\tau_{fast}}} + c$$

Only the fast time component was analyzed, as it accounted for the major inactivating component. To determine the persistent current, the mean current I_{SS} between 70 ms to 90 ms was divided by the peak current I_{Peak} of each sweep.

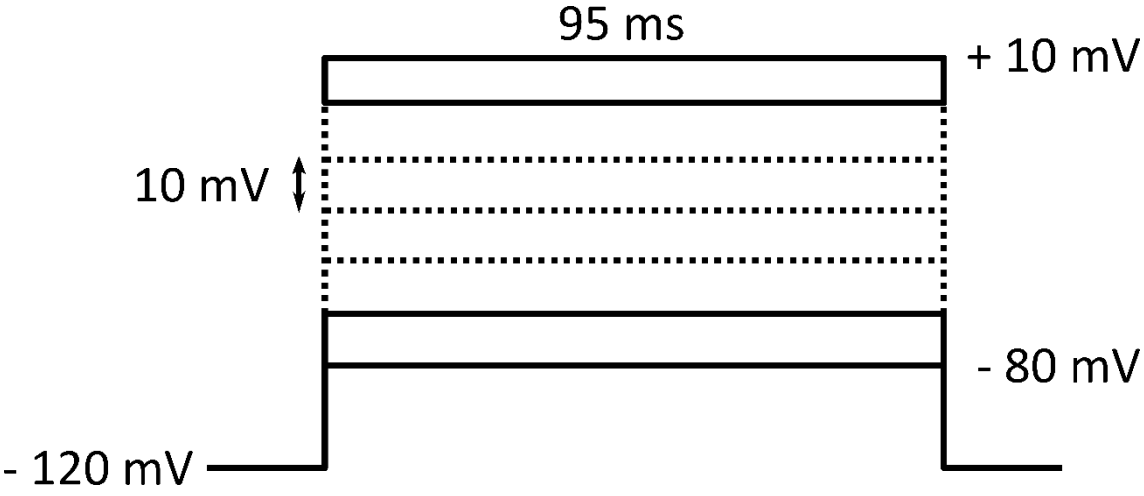

Figure 15: Voltage protocol to elicit Na^+ currents for determine fast inactivation parameters and persistent current I_{SS} / I_{Peak}.

Steady State fast inactivation

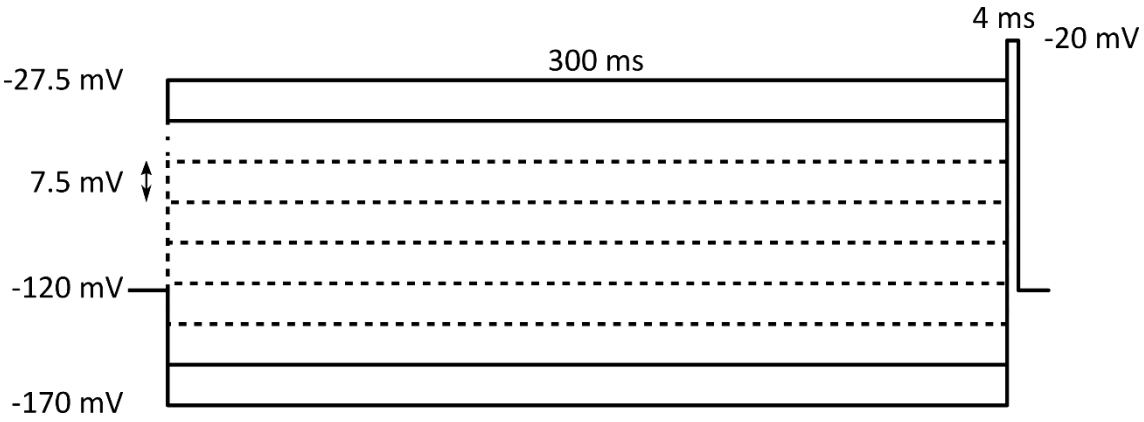

Figure 16: Voltage protocol to determine steady state inactivation parameters.

To determine steady state inactivation parameters, a conditioning pulse to voltages ranging from -170 mV to -27.5 mV in +7.5 mV steps was applied for 300 ms, followed by a test pulse to -20 mV for 4 ms (Figure 16). The elicited currents during this test pulse were normalized against the maximal current peak of each cell and plotted against the conditioning potential during the first pulse. Recordings were obtained at a sampling rate of 50 kHz and filtered using the internal low pass filter of the patch clamp amplifier at a frequency of 5 kHz. Leak subtraction was obtained with a -P/4 leak subtraction protocol prior to each sweep as described above.

Recovery from fast inactivation

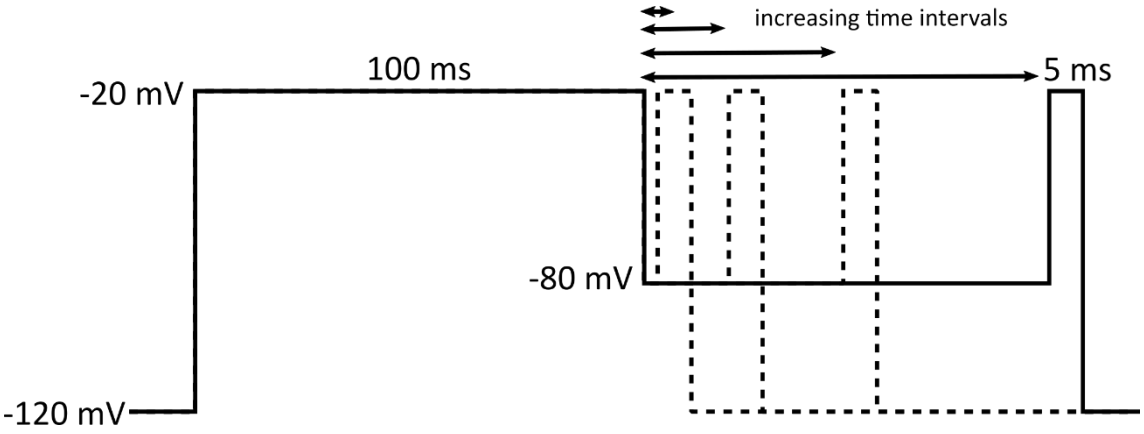

Figure 17: Voltage protocol to determine the recovery of inactivation at -80 mV. Similar protocols were applied at holding voltages of -100 mV and -120 mV.

Recovery from fast inactivation was determined at three different voltages with separate two pulse protocols. A preconditioning voltage pulse to -20 mV activated the channels for 100 ms. The cells were then repolarized to -80 mV, -100 mV or -120 mV for rising durations. After this, cells were depolarized again to -20 mV for 5 ms (-80 mV protocol) or 7.5 ms (Figure 17). Recordings were obtained at a sampling rate of 40 kHz and filtered using the internal low pass filter of the patch clamp amplifier at a frequency of 5 kHz.

2.10.4.2 Voltage protocol for Ba^{2+} currents of $Ca_V2.3$ (CACNA1E) channels

All recordings were obtained with a sampling rate of 10 kHz. The signal was filtered using the internal low pass filter of the patch clamp amplifier at a frequency of 5 kHz. A -P/4 leak subtraction protocol was administered before recording the test current, similar to $Na_V1.2$ recordings (see section 2.10.4.1)

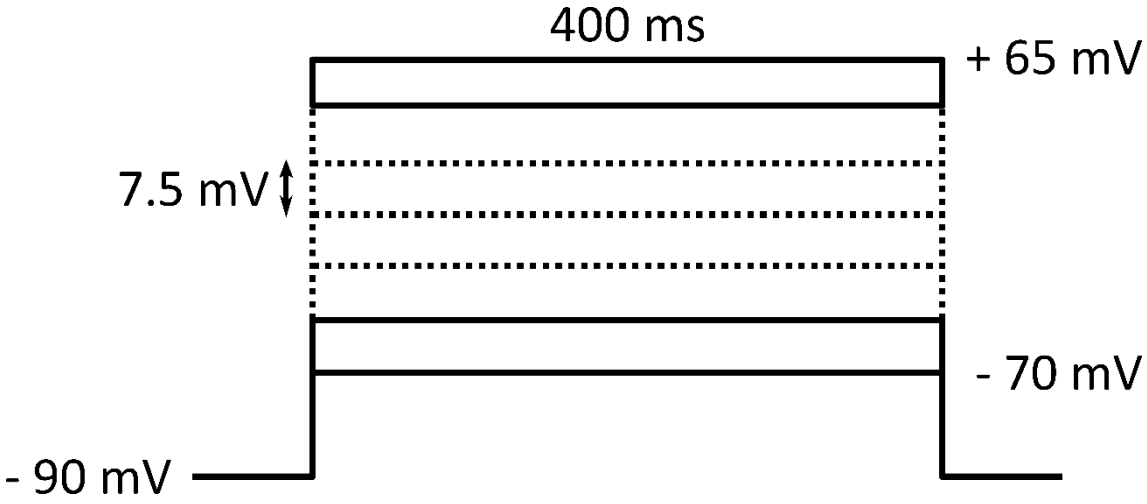

Figure 18: Voltage protocol to elicit Ba^{2+} currents in tsA201 cells expressing $Ca_V2.3$ channels.

A step protocol was used to elicit Ba^{2+} currents in transfected tsA201 cells, that consisted of multiple depolarizations of the membrane in 7.5 mV increments from a holding potential of -90 mV for 400 ms (Figure 18).

2.11 Data analysis and fitting of electrophysiological data

The acquired current traces were analyzed using the ClampFit 10.3 Software (Axon Instruments, Union City, CA, USA)).

Peak currents were normalized in Microsoft Excel. Fitting of the data was achieved using gnuplot 5.0 with self-written scripts. Graphs were created with a combination of Origin 6.1 and inkscape 0.48.4. Statistical tests were achieved using SigmaPlot 12.4 (Systat Software, Inc). Data was checked for normal distribution. For normally distributed data, the t-test or one-way ANOVA with Bonferroni post-hoc test was used. Otherwise, the Mann-Whitney-U-test or ANOVA on ranks with Dunn's posthoc test was used.

2.11.1.1 Fitting of the voltage dependence of activation

The conductance *g* was calculated in Microsoft Excel using the following equation:

$$g(V) = \frac{I_{peak}}{(V - V_{rev})}$$

with I_{peak} being the peak current, V_{rev} the corresponding reversal potential and V the applied voltage.

The conductance curve *g(V)* at different voltages was fit using a standard Boltzmann equation in gnuplot:

$$g(V) = \frac{g_{max}}{1 + e^{\frac{V - V_{½}}{k_V}}} + c$$

With g_{max} being the amplitude, V the applied voltage, $V_{½}$ the reversal potential, k_v the slope and c a constant expression. The amplitude g_{max} of this fit was used to normalize the data followed by a second fit with the same equation.

2.11.1.2 Fitting of steady state inactivation parameters

The voltage dependence of inactivation curve *I(V)* was fit using a Boltzmann equation in gnuplot:

$$I(V) = \frac{I_{max}}{1 + e^{\frac{V - V_{½}}{k_V}}} + c$$

With I_{max} being the amplitude, V the applied voltage, $V_{½}$ the reversal potential, k_v the slope and c a constant expression

2.11.1.3 Fitting of recovery from inactivation parameters

To fit the recovery from inactivation curve *I(t),* a second order exponential equation with an offset and an initial delay was used as best fitting model in gnuplot:

$$I(t) = A_1 * \left(1 - e^{-\frac{t - t_0}{\tau_1}}\right) + A_2 * \left(1 - e^{-\frac{t}{\tau_2}}\right) + c$$

With A_1 and A_2 being the amplitudes of both parts of the fit, t_0 being the delay, c being the offset and τ_1 and τ_2 being the time constants of the two parts of the equation. As values for A_1 ranged between 0.8 and 0.9 , the fast component of the equation was seen as good

approximation of the recovery behavior. Therefore, the faster time-descriptor τ_1 was used for statistical analysis of the recovery from fast inactivation.

2.11.1.4 Analysis of time dependent activation and inactivation

Time constants of activation and inactivation were determined by fitting the corresponding part of the elicited current traces with an exponential function in Clampfit 10 (Axon Instruments, Union City, CA, USA). For the activation time constants of $Ca_V2.3$ a first order exponential function was used:

$$I(t) = A * e^{\frac{-t}{\tau}} + c$$

with I being the current, t being the time, A being the amplitude, τ being the time constant of activation or inactivation and c a constant factor.

To determine the time course of inactivation for $Ca_V2.3$ currents, the residual current I_{res} during the last 10 ms of a 400 ms pulse was divided by the peak current I_{Peak}. The ratio r400 is a surrogate parameter of the time course of inactivation.

$$r400 = \frac{I_{res}}{I_{Peak}}$$

For the time course of inactivation in $Na_V1.2$ currents a second order exponential function was fit in Clampfit 10 (Axon Instruments, Union City, CA, USA).

$$I(t) = A_{fast} * e^{\frac{-t}{\tau_{fast}}} + A_{slow} * e^{\frac{-t}{\tau_{slow}}} + c$$

with I being the current, t being the time, $A_{fast/slow}$ being the fast or respective slow amplitude, $\tau_{fast/slow}$ being the fast or respective slow time constant of inactivation and c a constant expression.

3 Results

3.1 Diagnostic restriction digest

To verify the integrity of the plasmids used for transfection, a restriction digest was setup for each construct as stated above. For each construct, restriction enzymes were chosen to cut preferably more than one time. The reaction was run on an 1% agarose gel for 1,5h and then analyzed under UV light (Figure 19 to Figure 23).

Table 9: Plasmids used and the corresponding restriction enzymes

Gene & vector	*Enzyme*	*Expected size of bands*
SCN2A pcDNA3.1	EcoRI	5.560 kb 3.38 kb 2.507 kb
	HindIII	8.268 kb 2.362 kb 825 bp

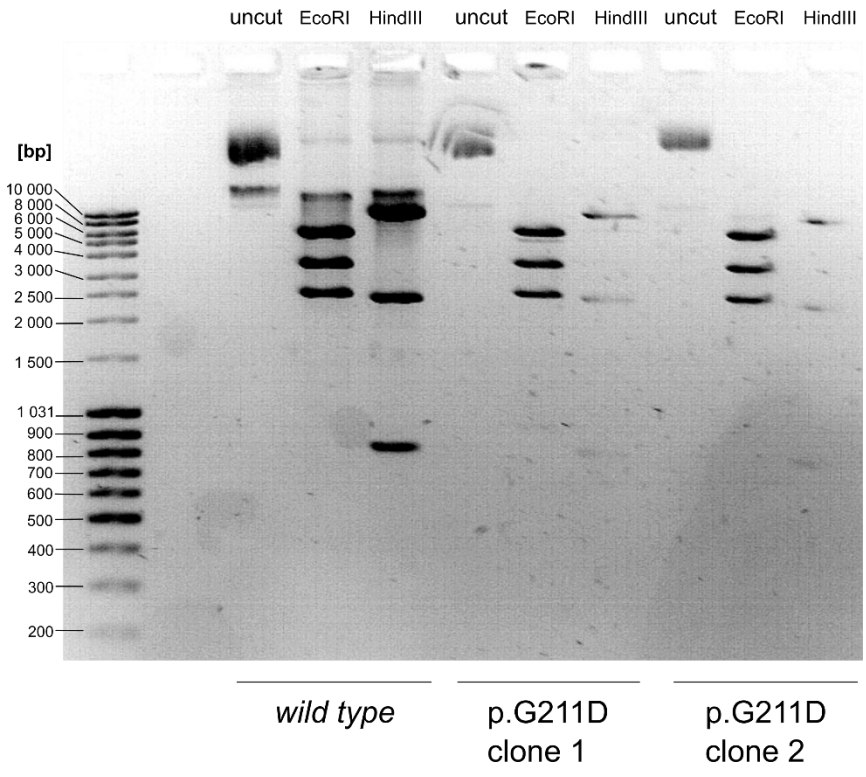

Figure 19: Agarose gel electrophoresis of the restriction digest of *SCN2A* wild type and two p.G211D mutants. Minor quality of electrophoresis: The gel was not aligned properly in the electrophoresis chamber. Uncut clone 1 DNA was not properly filled in the gel pocket. HindII restriction digest of mutants did not contain sufficient amounts of DNA.

Gene & vector	*Enzyme*	*Expected size of bands*
CACNA1E pcDNA3.1	BlpI	7.130 kb 4.361 kb 993 bp
	Mva1269I	7.466 kb 3.988 kb 1.030 kb

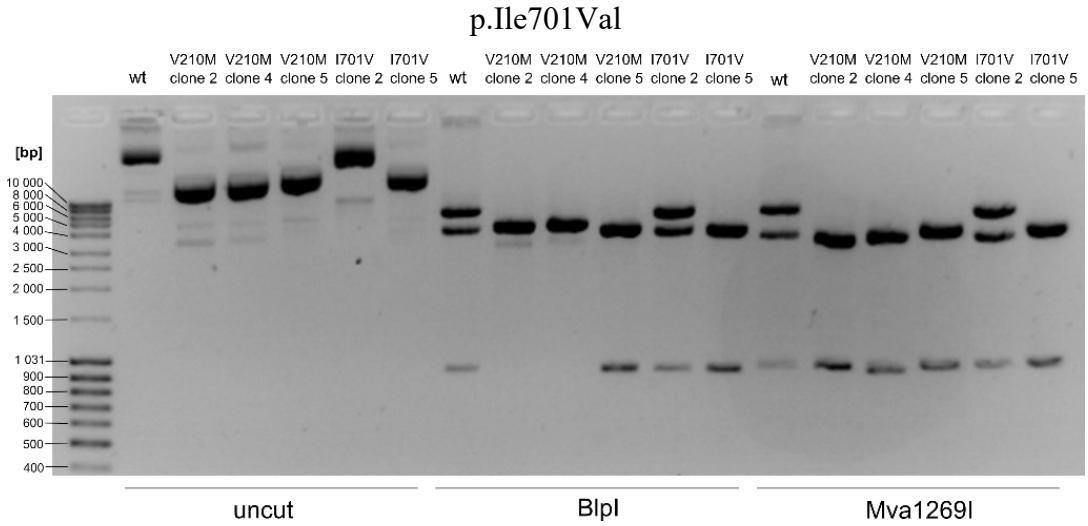

Figure 20:Agarose gel electrophoresis of *CACNA1E* p.Ile701Val mutant DNA. Clone 2 was used for electrophysiological recordings. p.Val210Met mutants and clone 5 of p.Ile701Val show examples in which the diagnostic restriction digest indicated false ligation during the mutagenesis procedure.

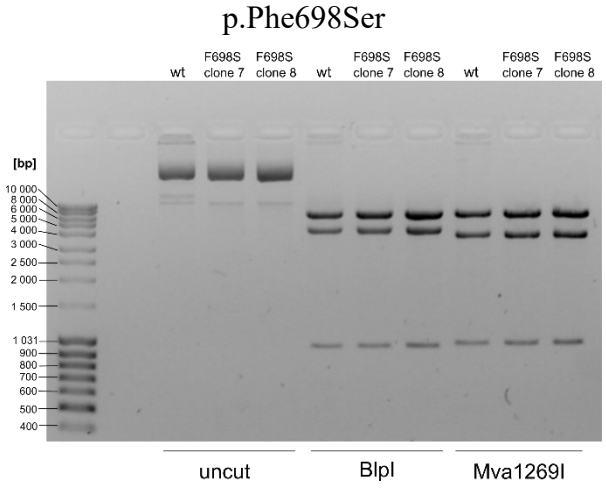

Figure 21: Agarose gel electrophoresis of *CACNA1E* p.Phe698Ser mutant DNA. Clone 7 was used for electrophysiological recordings.

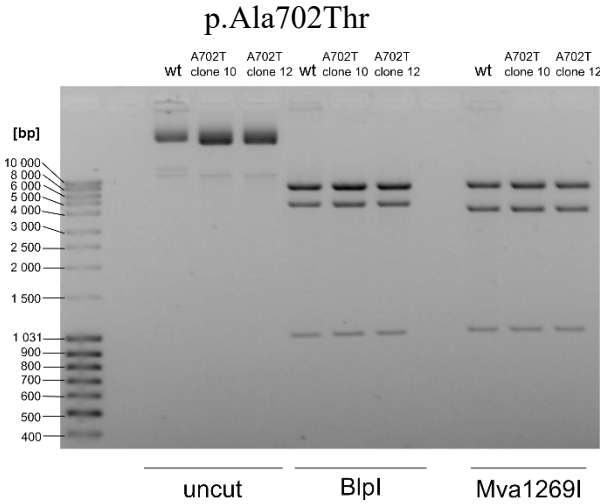

Figure 22: Agarose gel electrophoresis of CACNA1E p.Ala702Thr mutant DNA. Clone 10 was used for electrophysiological recordings.

Gene & vector	*Enzyme*	*Expected size of bands*
CACNB2d pIRES-YFP	PvuII	3.744 kb
		2.905 kb
		608 bp
	HindIII	6.062 kb
		1.195 kb
CACNA2D1 pIRES puro	BlpI	7.098 kb
		1.429 kb

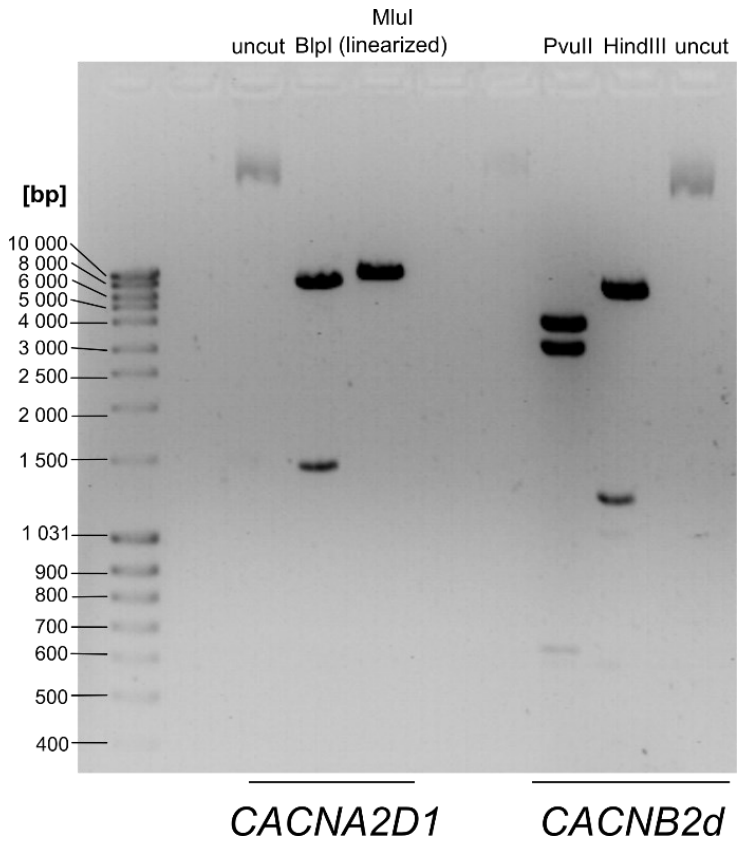

Figure 23 : Agarose gel electrophoresis of a restriction digest of the *CACNA2D1* and *CACNB2d* calcium channel subunit DNA. MluI only linearized the *CACNA2D1* plasmid, although one more cutting site was expected. Due to an outdated enzyme used and the unknown exact sequence of the construct, this was ignored, since the BlpI digest was as expected.

3.2 Results $Na_V1.2$ / *SCN2A* p.Gly211Asp

3.2.1 Representative current traces

The electrophysiological effect in $Na_V1.2$ of the c.632G>A p.Gly211Asp (G211D) mutation in the *SCN2A* gene was compared to the *wild type channel*. The missense mutation in the linker between segment S3 and S4 of domain 1 (see Figure 24) leads to an exchange of amino acids from glycine to aspartate. This mutation was a *de novo* mutation in a French patient with focal seizures, profound intellectual disability and muscular hypotonia.

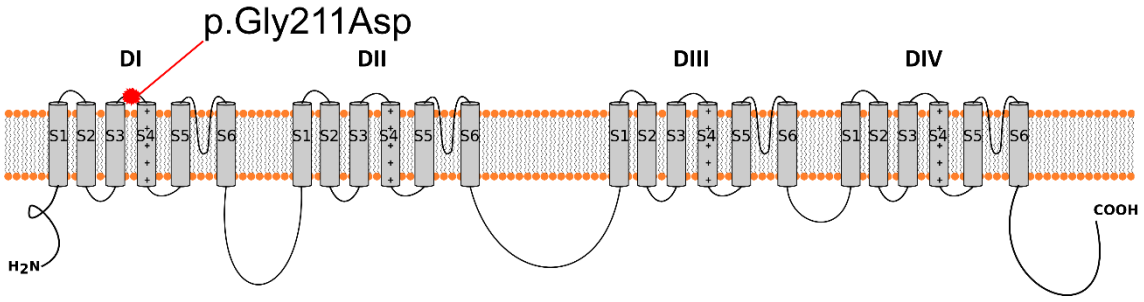

Figure 24: Location of the p.G211D mutation in the secondary structure of $Na_V1.2$.

Figure 25 shows example current traces recorded in cells expressing either *wild type* or p.G211D mutant $Na_V1.2$ channels.

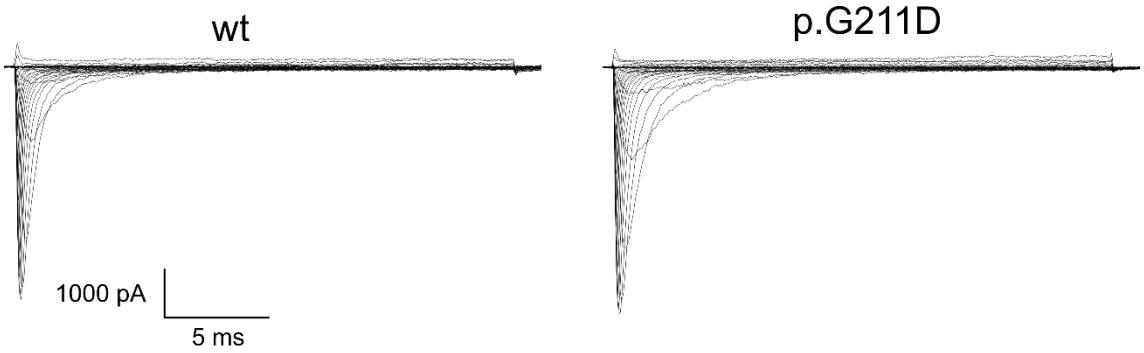

Figure 25: Typical Na^+ current traces of $Na_V1.2$ *wild type* or p.Gly211Asp mutant channels overexpressed in tsA201 cells elicited by a step protocol.

3.2.2 Current density

The current density for $Na_V1.2$ *wild type* and p.G211D mutant channels was calculated as stated above by dividing the current peak of each sweep in a voltage step protocol by the compensated capacitance of the cell at the patch clamp amplifier. The current density of the p.G211D mutation was slightly increased in comparison to the *wild type*, but even though a tendency was distinct, statistical analysis showed no significant difference (Figure 26, Table 10).

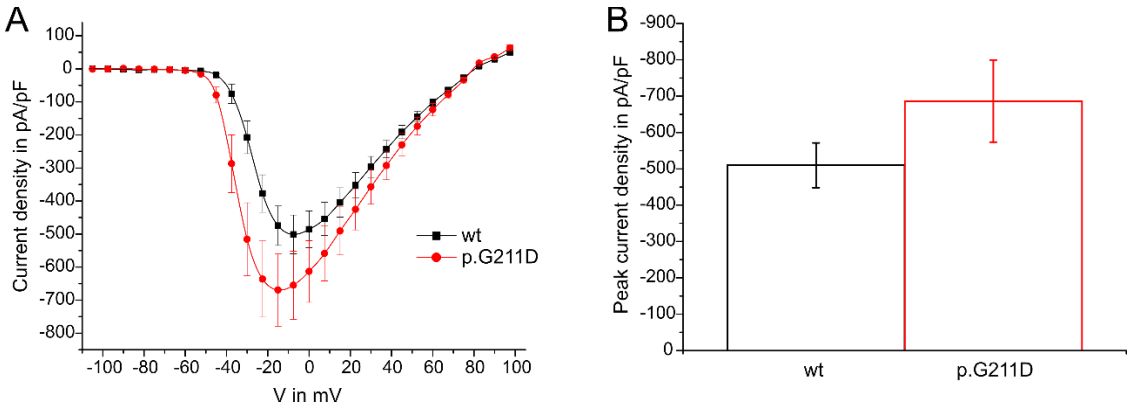

Figure 26: **A** Current density of $Na_V1.2$ *wild type* and p.Gly211Asp (G211D) currents in a voltage step protocol from -105 mV to +97.5 mV **B** Mean of the peak current density of every cell recorded. Error bars indicate the standard error of the mean.

Table 10: Current density of $Na_V1.2$ wild type and p.G211D.

		Peak of mean current density	*Mean of peak current density*
	n	[pA/pF] ± SEM	[pA/pF] ± SEM
wt	20	-501.1 ± 58.6	-509.8 ± 61.63
p.G211D	15	-669.5 ± 109.1	-686.3 ± 113.0

3.2.3 Steady-state activation and fast inactivation

Steady-state activation was determined by calculating the conductance for the current peak of each step in a voltage step protocol and fitting a Boltzmann fit to the data as stated above.

Steady-state fast inactivation was determined in a two-step protocol with a conditioning potential followed by a short test voltage step. The elicited current peak for each potential was normalized against the maximal current peak of each cell and plotted against the conditioning potential during the first pulse. A Boltzmann fit was fit to the data as stated above.

For steady-state inactivation, no significant change could be observed between *wild type* $Na_V1.2$ and p.Gly211Asp mutant channels.

The voltage dependence of activation was shifted to more hyperpolarized potentials for mutant channels in comparison to *wild type* channels, observable in the significant change of the $V_{½}$-value by -7.2 mV, while the slope factor k remained unchanged (Figure 27 & Table 11).

Table 11 : Parameters of steady state activation and inactivation parameters of $Na_V1.2$ *wild type* and p.G211D *** p<0.001

	Steady state activation			*Steady state inactivation*		
	n	$V_{½}$ [mV] ± SEM	k ± SEM	n	$V_{½}$ [mV] ± SEM	k ± SEM
wt	20	-24.3*** ± 0.9	-5.5 ± 0.2	15	-67.5 ± 0.7	4.9 ± 0.2
p.G211D	15	-31.5*** ± 1.3	-5.3 ± 0.3	14	-67.8 ± 0.8	4.5 ± 0.1

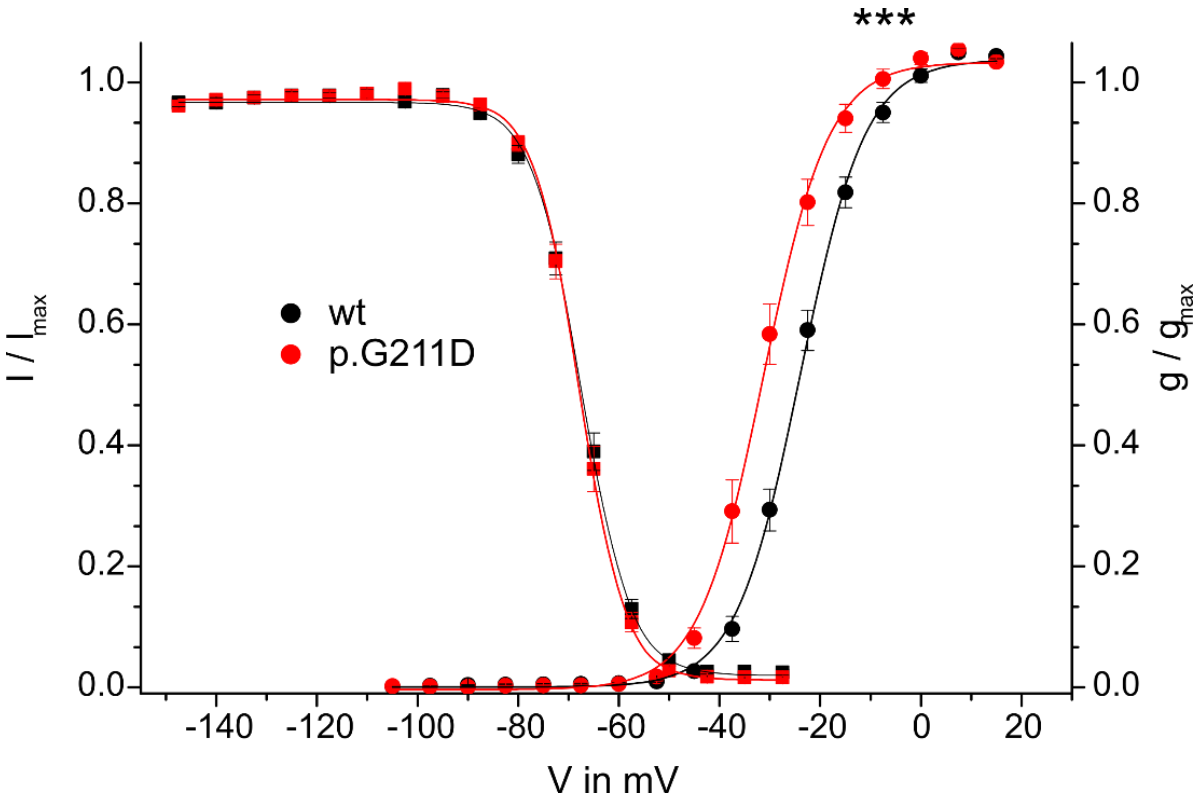

Figure 27 Voltage-dependence of steady state activation and fast inactivation for $Na_V1.2$ *wild type* and pG211D mutant channels *** p< 0.001.

3.2.4 Recovery from fast inactivation

Recovery from fast inactivation was determined at three different voltages with separate two pulse protocols as stated in the methods section. In short, the voltage protocol consisted of two depolarizing pulses with a time-variable holding voltage step in between. The first voltage step served to inactivate the channels, that could then recover from inactivation at the holding voltage. The current that was elicited by the second voltage-pulse was plotted against the holding time between the two voltage-pulses. Data points were fit using a second order exponential equation with an offset and an initial delay. Since the fast component of recovery accounted for 80-90% of the whole recovery process, the faster time-descriptor τ_1 was used for statistical analysis. Recovery from fast inactivation remained unchanged by the mutation (Figure 28 & Table 12).

Table 12: Time constants of recovery of fast inactivation for $Na_V1.2$ *wild type* and p.G211D mutant channels

	-120 mV		*-100 mV*		*-80 mV*	
	τ_{rec} [ms] ± SEM	n	τ_{rec} [ms] ± SEM	n	τ_{rec} [ms] ± SEM	n
wt	1.57 ± 0.13	10	3.48 ± 0.28	11	12.65 ± 1.00	14
p.G211D	1.59 ± 0.01	11	3.56 ± 0.25	13	11.57 ± 0.93	13

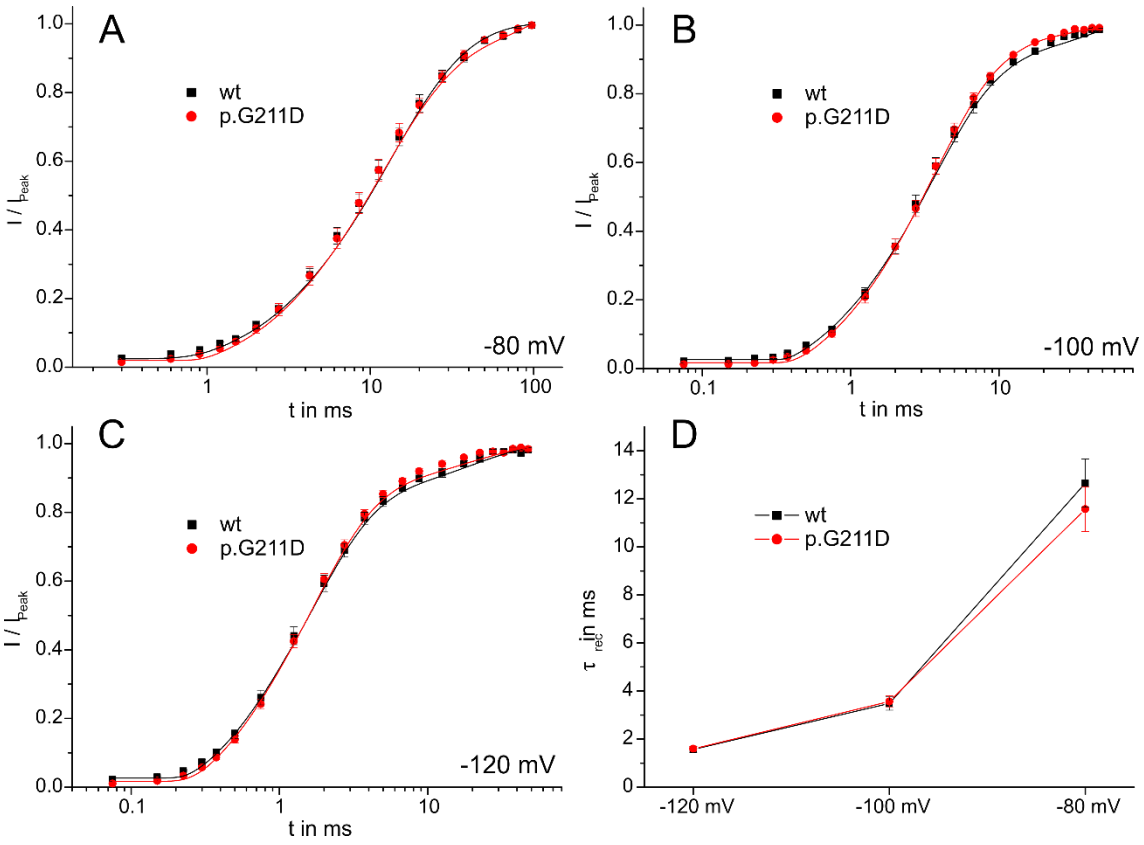

Figure 28: **A** I-t curve of the recovery from fast inactivation at -80 mV for $Na_V1.2$ *wild type* and mutant channels. **B** I-t curve of the recovery from fast inactivation at -100 mV **C** I-t curve of the recovery from fast inactivation at -120 mV. **D** τ of the recovery from fast inactivation at different voltages for $Na_V1.2$ *wild type* and mutant channels resulting out of the fit of data points in A - C.

3.2.1 Time course of fast inactivation

The time constant τ_{fast} of fast inactivation was determined by fitting the decay of the elicited current trace per voltage in a voltage step protocol with a second-order exponential equation in ClampFit10 as described in the methods section (Figure 29A). As the fast component accounted for over 90% of the fit, the faster time parameter τ was used for comparison between *wild type* and p.G211D mutant channels. It is to mention, that the accuracy and the scatter range of the resulting parameters improve at more depolarized voltages as the elicited current peaks become bigger and the relative amount of noise to the current peak decreases. For this reason and to account for repeated measurements, significance was only tested at 0 mV.

Table 13: The time constant of fast inactivation τ_{inact} at 0 mV for *wild type* and p.G211D mutant $Na_V1.2$ channels.

	n	τ_{inact} [ms] ± SEM
wt	15	0.35 ± 0.02
p.G211D	14	0.34 ± 0.02

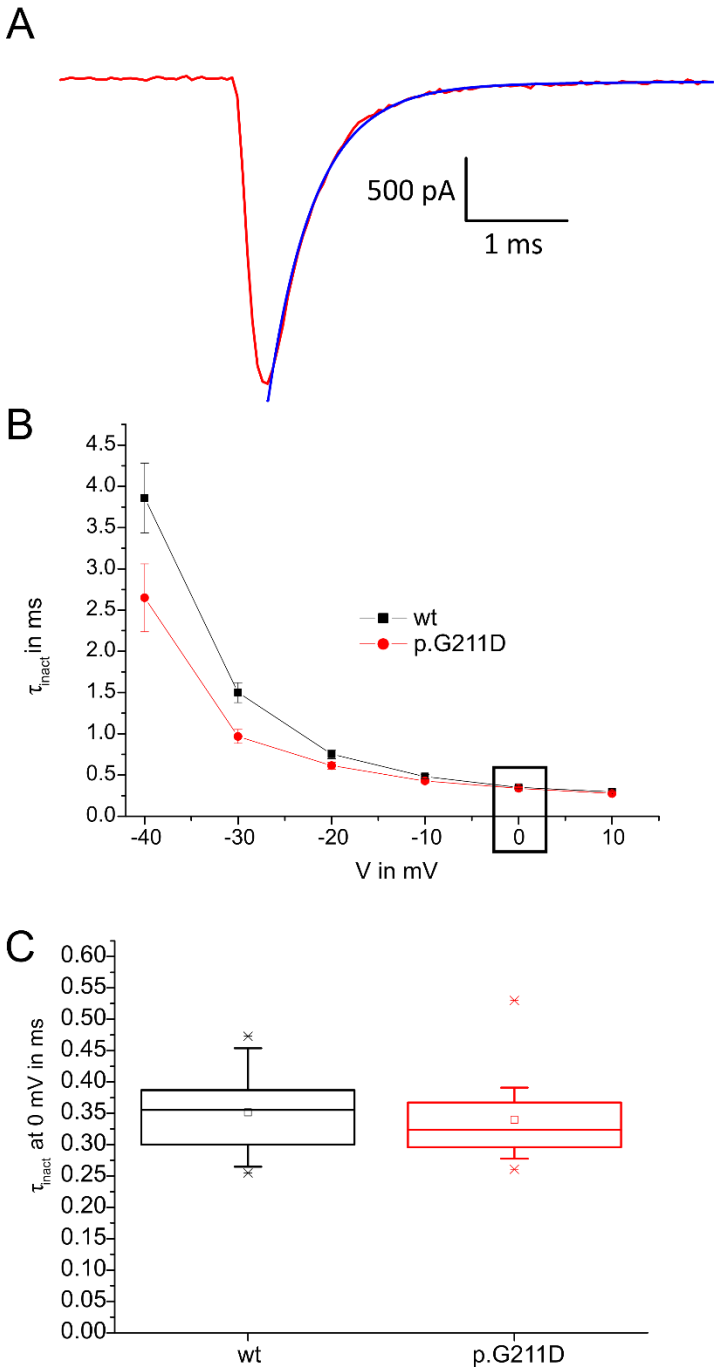

Figure 29: τ_{inact} of fast inactivation of $Na_V1.2$ *wild type* and p.G211D mutant channels **A** Example fit for a single $Na_V1.2$ *wild type* current to determine the time course of fast inactivation in a voltage step protocol at -10 mV. The inactivating part of the current (plotted in red) was fit in ClampFit10 using a two-exponential equation (plotted in blue). The figure shows only a small excerpt of the whole recording which is 100ms long. **B** τ_{inact} of fast inactivation at different voltage steps determined by fitting the decaying part of the current trace in a voltage step protocol. To account for repeated measurements, significance was only tested at 0 mV. **C** τ_{inact} of fast inactivation at 0 mV for *wild type* and p.G211D $Na_V1.2$ channels. There was no significant difference observable.

3.2.2 Persistent current I_{SS} / I_{Peak}

The persistent current was calculated by dividing the mean current at the end of a 90 ms pulse by the peak current of the same pulse at voltages between -40 mV and +10 mV. To compare currents of mutant and *wild type* channels, the total area under the curve (AUC) for the voltage-dependent I_{ss}/I_{Peak} was approximated by calculating the surface area of trapezoids under the curve. This revealed a significant reduction of the persistent current for p.G211D mutant channels compared to the wild type that resulted out of a moderately increased peak current and non-significant reduction of the absolute persistent current (Figure 30 & Table 13). Even though the cumulated data indicates a significant difference, the result is not fully conclusive, as the steady-state current might be a constant artefact of the recording conditions and there are multiple outliers in the *wild type* dataset. Furthermore, a decreased persistent current has never been established as a functional phenotype caused by a missense mutation, whereas an increased persistent current was previously described as electrophysiological effect a mutation in *SCN2A* (Lauxmann *et al.*, 2013).

Table 14: Area under the curve for the persistent current of $Na_V1.2$ *wild type* and p.G211D mutant channels between -40 mV and + 10 mV ** $p < 0.01$.

Area under the curve

	n	[mV*(pA/pA)]		
		25%	median	75%
wt	15	0.4	0.68	1.19
p.G211D	14	0.16	0.33**	0.40

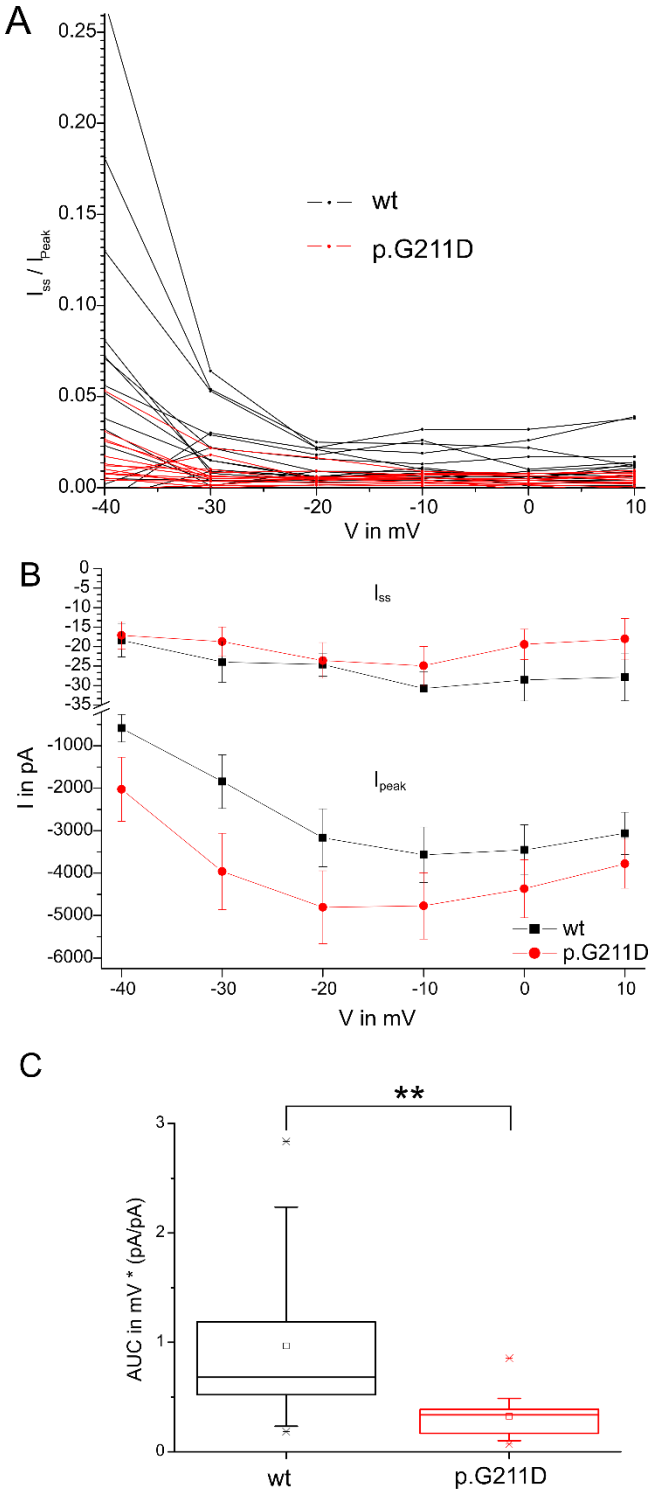

Figure 30: **A** Persistent Na^+ current I_{ss}/I_{Peak} of all cells recorded for voltages between -40 mV to +10 mV for $Na_V1.2$ *wild type* and p.G211D mutant channels **B** Mean I_{SS} and I_{Peak} for $Na_V1.2$ *wild type* and p.G211D mutant channels. **C** Area under the curve for I_{ss}/I_{Peak} between -40 mV to +10 mV. Boxes in boxplots depict the 25% to 75% interquartile range. Horizontal lines depict the median. Whiskers indicate the 5% to 95% quantile. Small cross markings indicate maxima and minima. Small box markings indicate the mean. ** $p < 0.01$.

3.3 Results $Ca_V2.3$ / *CACNA1E*

3.3.1 Rundown of calcium currents

During the recording of currents through $Ca_V2.3$ channels in the whole cell patch clamp mode, a continuous rundown of the Ba^{2+} current was observed over time, even though other parameters of the recording, such as seal and access resistance, remained stable. This phenomenon was previously described by former investigators of calcium currents (Korn, 1989; Sarantopoulos *et al.*, 2004). Figure 31 shows the decrease of current density in three voltage step protocols during the time course of recordings, in which we examined *wild type* $Ca_V2.3$ channels co-expressed with the β_{2d} and the $\alpha_2\delta_1$ subunit. Current density decreased over time, while no shift in activation occurred. The same relationship could also be observed in other protocols. An additional effect that should be considered is a cumulative inactivation of channels during multiple activating current pulses. Rundown could not be diminished by ATP in the pipette solution nor perforated patch clamping using β-Escin (Sarantopoulos *et al.*, 2004). Experiments with β-Escin in our lab were mainly conducted by my colleague Jacqueline Bahr. This made it impossible to record steady-state-inactivation or recovery kinetics as these would have required stable recording conditions.

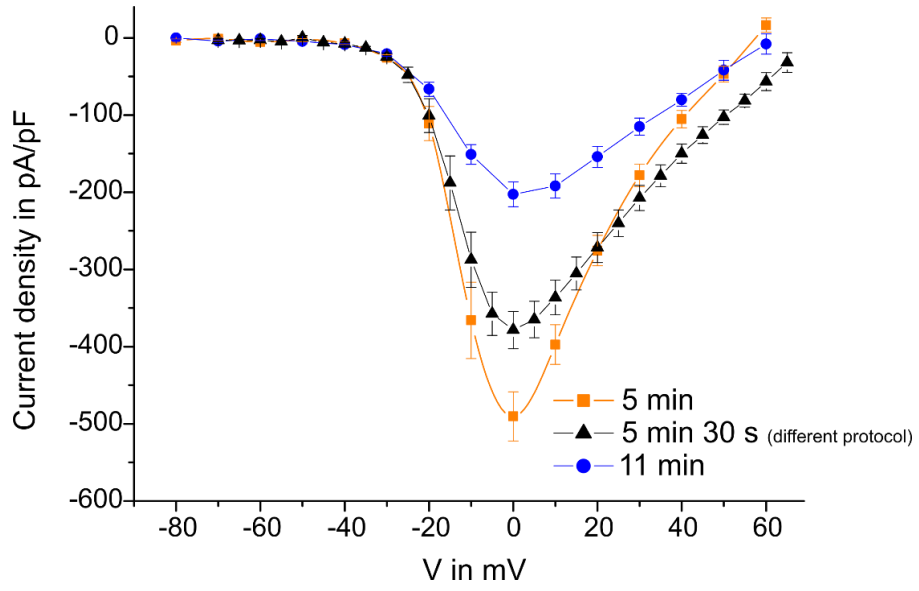

Figure 31 : Rundown of Ba^{2+} currents during the time course of recordings in a pre-experiment in tsA201 cells expressing the *wild type* $Ca_V2.3$ channel together with the β_{2d} and the $\alpha_2\delta_1$-subunit. The current density decreases, while $V_{1/2}$ of activation appears to remain stable, n= 10.

3.3.2 Investigating pathological *CACNA1E* mutations

Mutations in *CACNA1E* were identified in a worldwide cooperation of clinicians and geneticists in patients with severe epilepsy and developmental delay. Katherine Helbig and Heather Mefford collected the genetic data of *CACNA1E* encephalopathy patients (Figure 5)(Helbig *et al.*, 2018).

Electrophysiological recordings were conducted by my colleagues Jacqueline Bahr, Betül Üysal and me. Jacqueline Bahr recorded an extensive amount of cells that went into statistical analysis. The data is pooled here to reach a reasonable n. I conducted the analysis and statistics as well as the preparation and pre-experiments to the project (see also Declaration of contribution to the thesis). Representative current traces of the different mutants and *wild type* channels are shown in Figure 32.

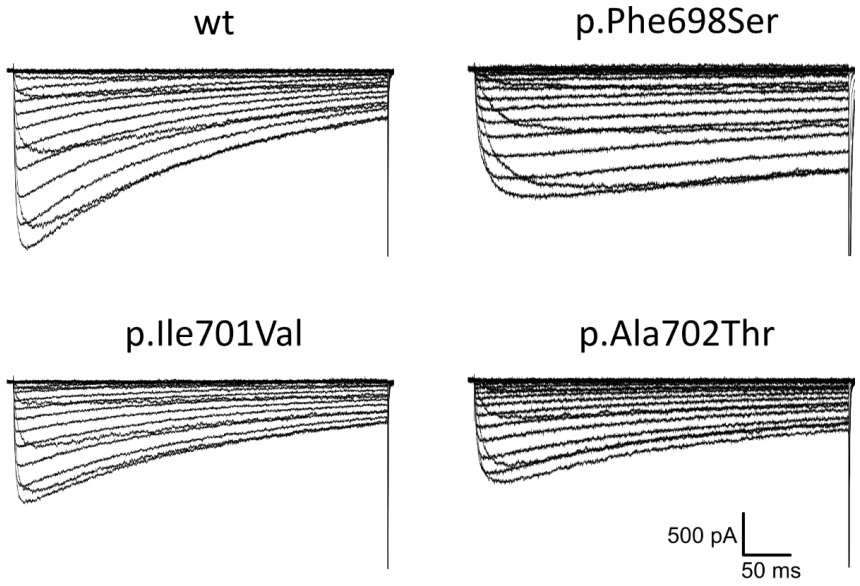

Figure 32: Representative current traces of $Ca_V2.3$ *wild type* and mutant Ba^{2+} currents. Adapted from Helbig *et al.,* 2018.

3.3.3 Current density

Current density in cells was estimated by dividing the peak current of the test protocol by the capacity of the cell, which was determined via compensation at the patch clamp amplifier. Statistical testing showed no significant difference between the different mutant and the wild type channels in current density (Figure 33 & Table 15.

Table 15: Mean current density of $Ca_V2.3$ *wild type* and mutant channels

	n	[pA/pF] ± SEM
wt	24	-183.1 ± 17.7
p.F698S	11	-121.4 ± 17.1
p.I701V	10	-186.9 ± 27.8
p.A702T	9	184.5 ± 34.2

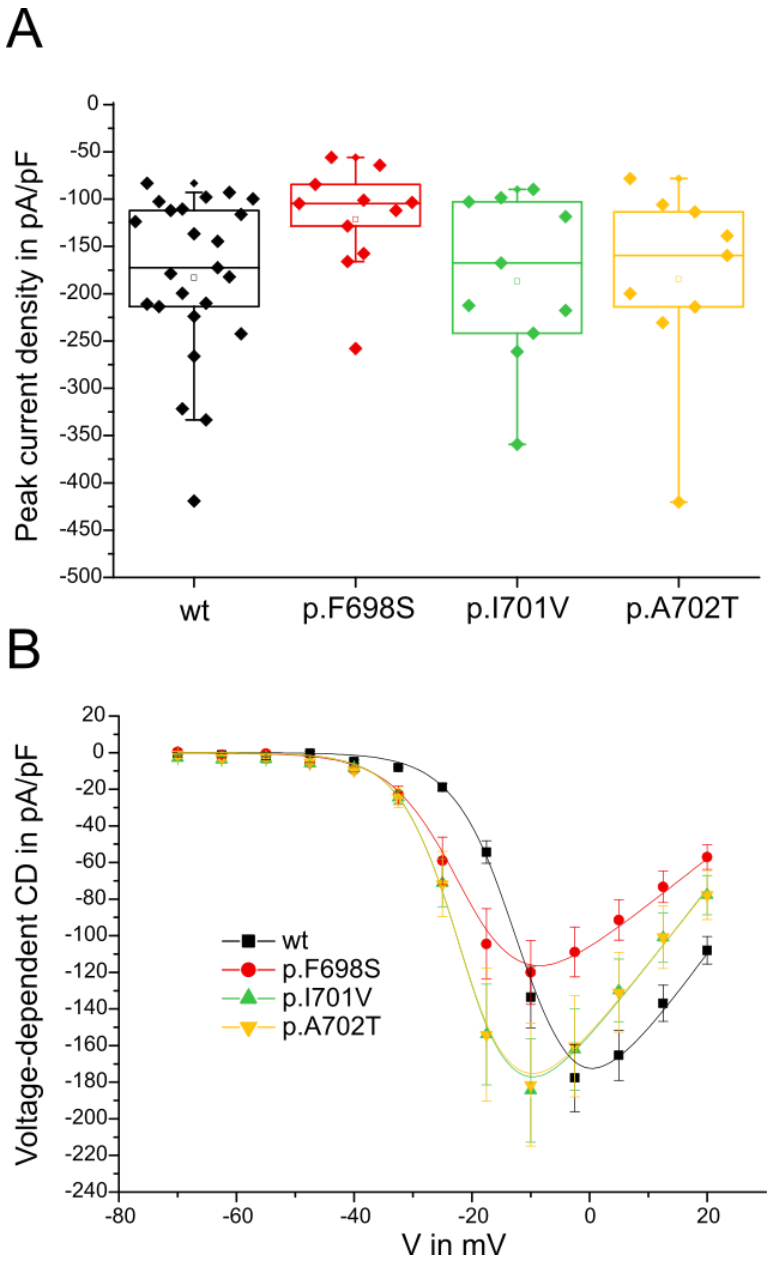

Figure 33 : **A** Peak current density of $Ca_V2.3$ *wild type* and mutant channels. Boxes in boxplots depict the 25% to 75% interquartile range. Horizontal lines depict the median. Whiskers indicate the 5% to 95% quantile. Small cross markings indicate maxima and minima. Small box markings indicate the mean. **B** Mean current density of $Ca_V2.3$ *wild type* and mutant channels at different voltages adapted from Helbig *et al.,* 2018

3.3.4 Voltage dependence of activation

The voltage dependence of activation was determined by calculating the conductance at different voltages in a step protocol as described in section 2.11.1.1 and fitting a Boltzmann-function to the data points. For all three *CACNA1E* mutants, the voltage dependence of activation was shifted by ~10 mV to more hyperpolarized potentials in comparison to the *wild type,* while the slope of the activation curves showed no significant difference (Figure 34 & Table 16).

Table 16: Activation parameters of $Ca_V2.3$ *wild type* and mutant channels. $V_{1/2}$ is the half maximal voltage of activation; k_V indicates the slope of the curve *** p<0.001.

		$V_{½}$	k_V
	n	[mV] ± SEM	[mV] ± SEM
wt	24	-9.7 ± 0.8	5.0 ± 1.1
p.F698S	11	-20.1 ± 1.2***	5.1 ± 0.7
p.I701V	10	-20.5 ±1.2***	4.3 ± 0.7
p.A702T	9	-20.4 ± 1.4***	4.2 ± 0.3

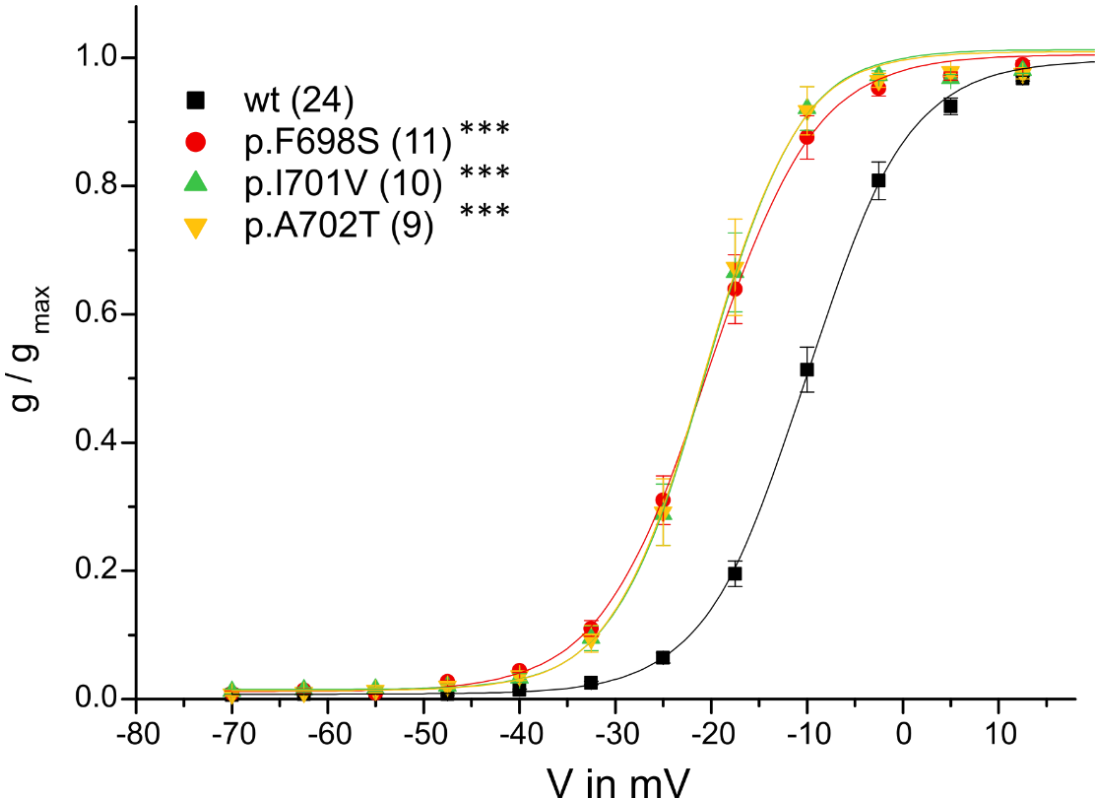

Figure 34: Voltage dependence of activation of *wild type* and mutant $Ca_V2.3$ channels. The numbers in brackets give the number of cells recorded. Adapted from Helbig *et al.,* 2018 *** $p<0.001$.

3.3.5 Time course of activation

To determine the time course of activation, a first order exponential function was fit to the rising current in a voltage protocol from the beginning of the current to its peak. When we determined the area under the curve (AUC) over multiple voltages, no significant difference could be observed (Figure 35 & Table 17).

Table 17: Time-dependent activation parameters of $Ca_V2.3$ *wild type* and mutant channels derived from a monoexponential fit of the current trace at different voltages.

		τ_{act} *at 5 mV*			*area under the curve from-17.5 mV to +42.5 mV*		
	n	ms			ms * mV		
		25%	Median	75%	25%	Median	75%
wt	24	1.71	1.94	2.19	105.69	117.28	134.14
p.F698S	11	1.68	2.33	3.12	109.57	170.44	240.04
p.I701V	10	1.27	1.5	2.25	82.4	107.79	178.80
p.A702T	9	1.45	1.68	2.28	112.61	119.04	192.85

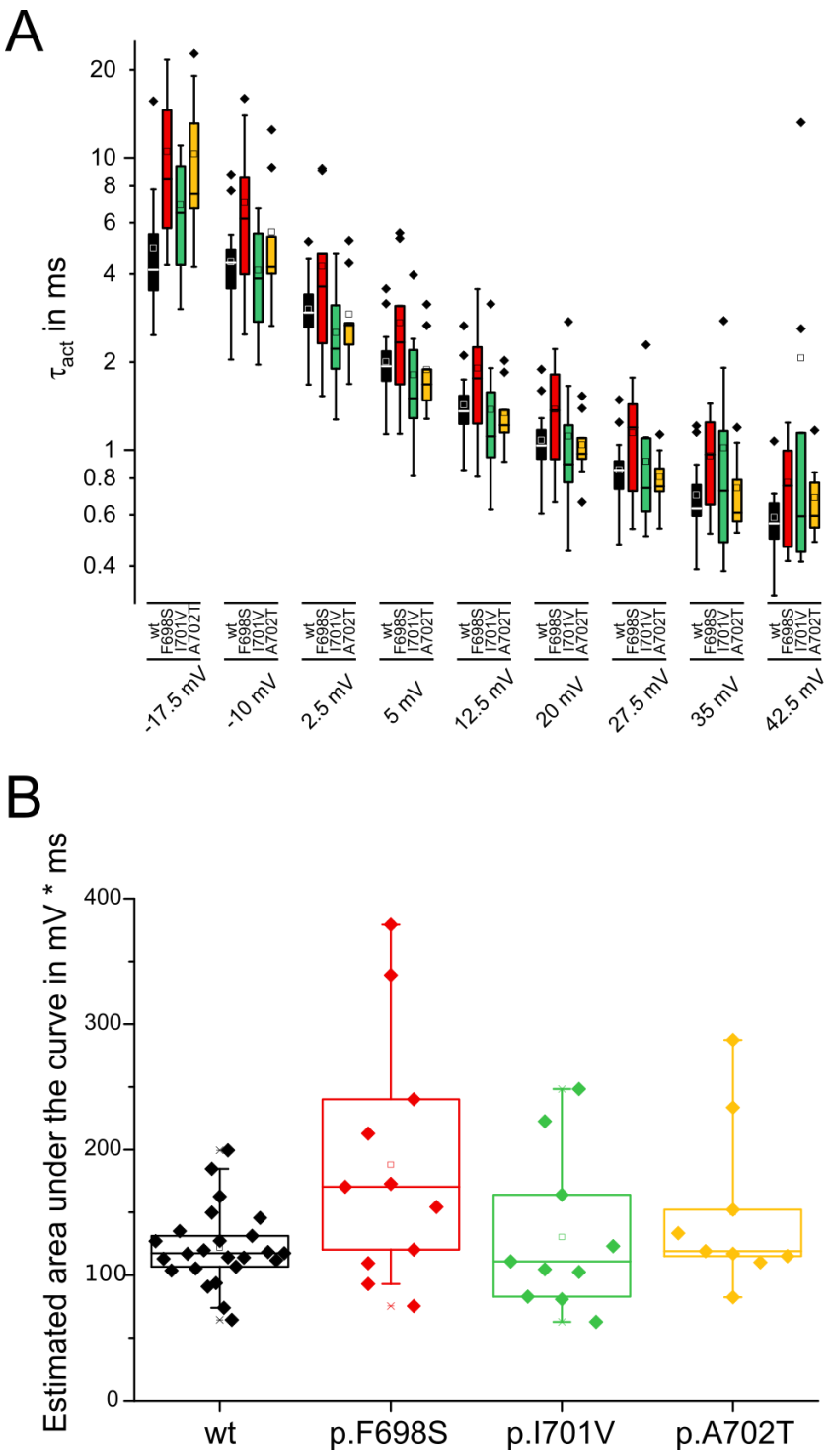

Figure 35 **A** t_{act} at different voltages for $Ca_V2.3$ channels **B** Area under the curve between -17.5 mV and +42.5 mV. Values for single cells are indicated by data points. Boxes in boxplots depict the 25% to 75% interquartile range. Horizontal lines depict the median. Whiskers indicate the 5% to 95% quantile. Small cross markings indicate maxima and minima. Small box markings indicate the mean. Adapted from Helbig *et al.*, 2018.

3.3.6 Time course of inactivation

To determine the time course of inactivation, the surrogate parameter r400 was used. r400 was determined by dividing the peak current of each current trace by the mean residual during the last 10 ms elicited by a 400 ms second long voltage pulse:

To adjust for repeated measurements, the area under the curve (AUC) was calculated. When the AUC was compared between *wild type* and mutant channels, the time course of inactivation was significantly slowed for p.F698S and p.A702T mutants. However, when we compared the r400 value at a single voltage e.g. 5 mV, all three mutations showed a significant slowing of the inactivation (Figure 36 &Table 18).

Table 18: Time dependent inactivation parameters of $Ca_V2.3$ *wild type* and mutant channels at 5mV as example and the area under the curve * $p < 0.05$, ** $p < 0.01$

		r400 at 5 mV	*area under the curve from -17.5 mV to +42.5 mV*		
	n	[pA/pA]	[pA/pA] * mV		
		Mean ± SEM	25%	Median	75%
wt	24	0.27 ± 0.09	11.92	16.47	20.82
p.F698S	11	0.53 ± 0.05**	20.03	27.83**	41.63
p.I701V	10	0.40 ± 0.04*	18.82	22.77	28.05
p.A702T	9	0.45 ± 0.05**	15.65	27.89*	35.52

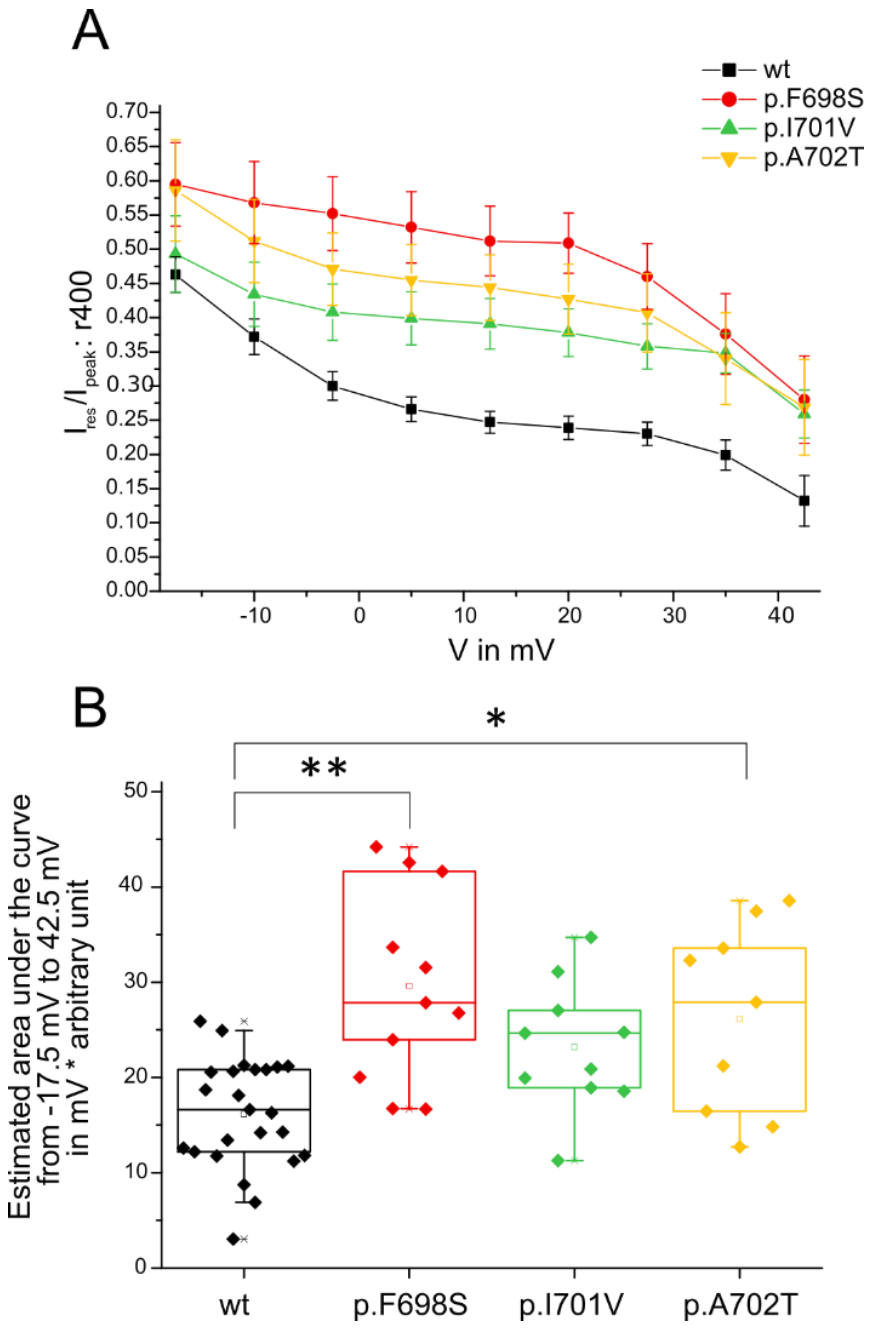

Figure 36: **A** Residual current after 400ms as surrogate parameter of time dependent inactivation in $Ca_V2.3$ channels at different voltages **B** Area under the curve for A. Boxes in boxplots depict the 25% to 75% interquartile range. Horizontal lines depict the median. Whiskers indicate the 5% to 95% quantile. Small cross markings indicate maxima and minima. Small box markings indicate the mean. * $p< 0.05$, ** $p<0.01$ Adapted from Helbig *et al.*, 2018.

4 Discussion

4.1 *SCN2A*

4.1.1 *In vitro* effect of p.G211D in $Na_V1.2$ (*SCN2A)*

The p.G211D mutation in $Na_V1.2$ (*SCN2A)* showed two distinctive effects in electrophysiological recordings: Most distinctive was a shift in the voltage dependence of activation by approximately -7mV. In neuronal cells this will lower the threshold for the initiation of action potentials, which compared to other *SCN2A* mutations would correspond to a gain of function (GOF) (Lauxmann *et al.*, 2018). As a second effect, the persistent current was smaller in the mutated channel, although the data is not fully conclusive. This corresponds to a loss of function (LOF) effect in the channel as it results in a smaller area under the curve of the current trace. Less Na^+ ions will cross the cell membrane when the channel is open. However, given the tendency of an increased current density in the mutated channel and the possible strong effect of noise in this parameter, the relevance of this second effect is not very clear whereas a shift in the activation curve as a first effect is a well-established GOF parameter.

4.1.2 Phenotype of patients with the *SCN2A* p.G211D mutation

A patient with the p.G211D mutation in the neonatal isoform (NM_001040143) of *SCN2A* was previously described by Kodera *et al.* in 2013. The patient was reported to have symptoms of West syndrome and hypotonia. Unfortunately, further information on this patient is not available.

In contrast to this, another unpublished case in France carrying this mutation presented with focal seizures, profound intellectual disability and muscular hypotonia. In this patient, seizures could be reduced in frequency, but not fully controlled by Phenytoin, a sodium channel blocker. This underlines the major gain of function of $Na_V1.2$ channels in this patient.

Previous research has shown that patients who suffer from *SCN2A* encephalopathy and show West syndrome as main clinical feature, in general carry loss of function mutations in *SCN2A* (Wolff *et al.*, 2017). For example the p.Arg853Gln mutation, that is often found

in *SCN2A* associated West syndrome, shows a loss of function of the channel (Wolff *et al.*, 2017; Berecki *et al.*, 2018).

Therefore, our results, indicating mainly a gain of function effect, would much better fit to the severe epilepsy described by our collaborators in Paris, although the onset of seizures in this patient is not known.

4.1.2.1 The S3-S4 linker in $Na_V1.2$

Amino acid position 211 is located in the linker between segments S3 and S4 of domain I of the $Na_V1.2$ α-subunit (Figure 24). As the glycine residue at this position is highly conserved among voltage-gated sodium channels (Figure 37) and the different orthologues of *SCN2A* in different species (Figure 38), one can assume that this position is of high importance for channel function.

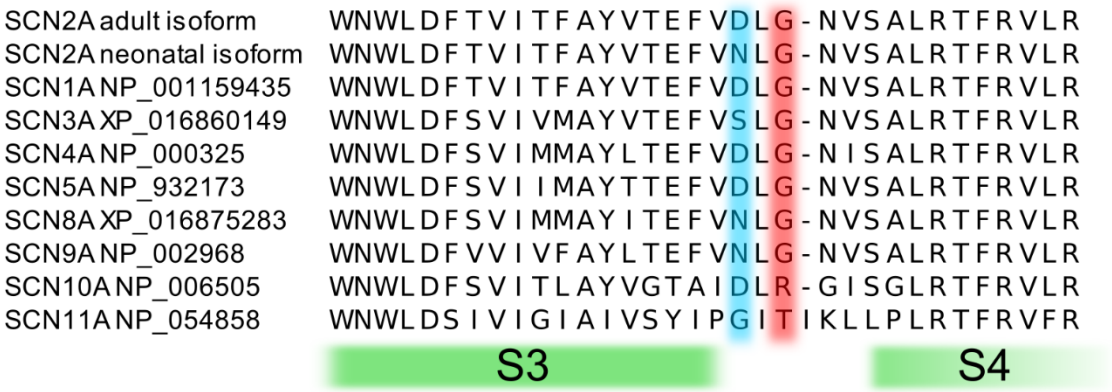

Figure 37: Comparison of the protein sequence of voltage-gated sodium channels. Segment S3 and the beginning of segment S4 of Domain I are marked with green boxes. Highlighted in blue is the position of variation between adult and neonatal isoforms. Highlighted in red is position 211 in *SCN2A*, highly conserved in the channel family. The NCBI accession number is given for the compared channels.

Remarkably, the p.Gly211Asp mutation observed here is very close to a variation of amino acids at position 209 that occurs physiologically among different isoforms of voltage-gated sodium channels (Figure 37 and Figure 38). In *SCN2A,* this variation of amino acids is a result of alternative splicing between exon 6A and exon 6N and might play a modulating role in the onset of disease, as different isoforms are expressed at different time points of development (Kasai *et al.*, 2001; Liao *et al.,* 2010). The close relationship between this physiological exchange in amino acids during development

becomes more interesting as both exchanges result in a change in amino acid charge. In both cases an uncharged amino acid, asparagine or glycine, is exchanged by aspartic acid, a negatively charged amino acid. This change in charge is at an important site, near the positively charged RxxRxxR arginine motif of the voltage sensor domain in the S4 segment, which is present in most voltage-gated ion channels (Catterall, 2012; Clairfeuille *et al.*, 2017) (see also Figure 37 and Figure 38).

Figure 38: Comparison of *SCN2A* homologues in different species. Segment S3 and the beginning of segment S4 of Domain I are marked in green. Highlighted in blue is the position that is changed in the neonatal isoform of *SCN2A*. Position 211 in human *SCN2A* is depicted by a red box.

It is known, that the physiologically occurring change in amino acids at position 209 changes gating parameters and may modulate the effect of other mutations in *SCN2A*. Xu *et al*. observed a faster inactivation, a shift in steady-state fast inactivation and a slower recovery from fast inactivation of the neonatal *wild type* isoform compared to the adult isoform when the α-subunit of the channel was expressed alone. However, some gating changes were only significant if the pathological missense mutation p.Leu1563Val was present in the neonatal isoform of the channel. Liao *et al*. found comparable results, but only when they did not coexpress the auxiliary β-subunits (Liao *et al*., 2010). With co-expression of the β-subunits an effect could only be observed if other amino acid exchanges where present in the channel(Xu *et al.*, 2007; Liao et al., 2010 a; Liao et. al, 2010 b). Changes of the inactivation kinetics due to the physiological exchange of amino acids by alternative splicing are also present in other sodium channels as $Na_V1.1$ (*SCN1A*), although this can only be seen with certain recording conditions (Fletcher *et al.*, 2011). Similar to the p.Gly211Asp mutation, the very close p.Val208Glu mutation in *SCN2A*, that was identified in a family of patients with benign neonatal-infantile epilepsy (BFNIE), also shifts the activation curve into the hyperpolarizing direction (Lauxmann *et al.*, 2018).

As the here described p.Gly211Asp mutation was discovered in the adult isoform of the *SCN2A* gene, my recordings took place in this isoform of the channel. However, Kodera *et al.* previously described a patient with West syndrome and severe hypotonia. The mutation of this patient was located in the neonatal splice variant of the channel (Kodera *et al.*, 2013) Further research is needed to determine if the p.Gly211Asp mutation in the neonatal splice variant alters channel function in a similar way as was observed in the adult splice variant.

The discrepancy of the changes in channel functions observed between the adult and neonatal isoforms and the altered activation threshold between p.Gly211Asp and the adult *wild type*, can possibly be explained by the closer location of position 211 to the positive charges in the voltage sensor. Previous research proved that negative amino acid residues in domains outside of S4, can form ion interaction pairs with the positively charged arginine residues during the movement of the S4-subunit (Payandeh *et al.*, 2011; Catterall, 2012).

Strikingly, an exchange of the homologous glycine in Na$_V$1.5, encoded by *SCN5A,* showed similar effects on the gating of this channel. *SCN5A* is a gene in which GOF mutations are well associated with heart diseases like Long-QT-syndrome. LOF mutations in *SCN5A* cause Brugada syndrome, while both GOF and LOF mutations may as well cause cardiomyopathy (for review see Brugada *et al.*, 2014; Wilde *et al.*, 2018). The p.Gly213Asp mutation in this gene leads to multifocal atrial and ventricular ectopy in ECG and a dilated cardiomyopathy via a GOF effect by shifting the voltage dependence of activation by -3.7 mV. Additionally this mutation shifts the voltage dependence of inactivation to depolarized potentials suggesting that the function of this position is not completely similar among sodium channels (Calloe *et al.*, 2018).

4.1.3 Possible pathophysiology of epilepsy syndromes caused by mutations in *SCN2A*

The electrophysiological gain or loss of function of the channel has implications for the clinical phenotype of the patient. Gain of function mutations are associated with an earlier onset of the disease and a better response to sodium channel blocking drugs than loss of

function mutations. Patients with loss of function mutations show a later onset of the epilepsy or autism spectrum disorder and do not respond to sodium channel blocking drugs (Wolff *et al.*, 2017).

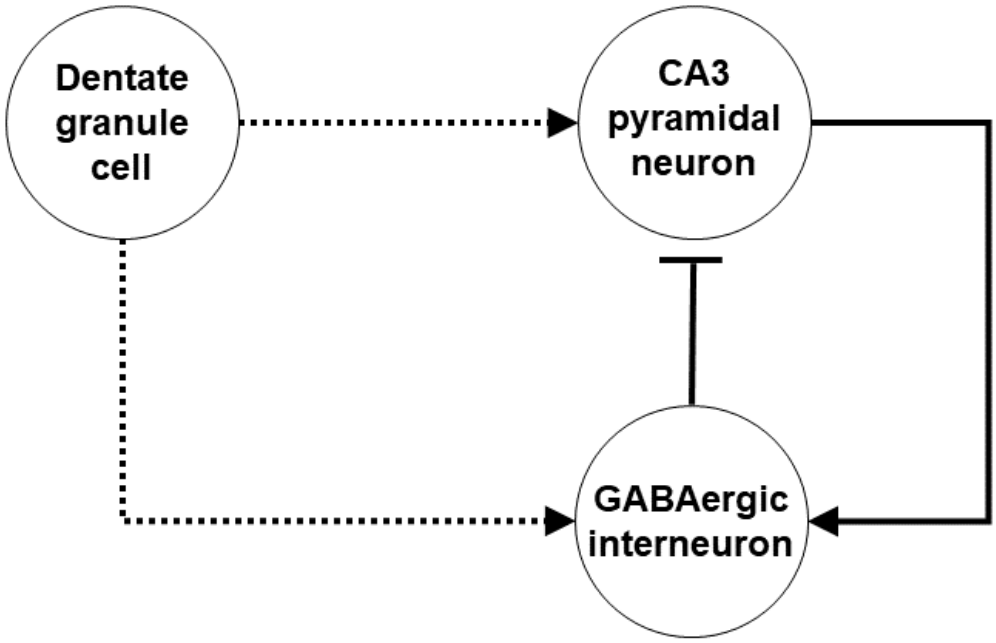

Figure 39: The neuronal circuit in the hippocampus in between dentate granule cells and CA3 neurons. The mossy fibers (dotted lines) connect the granule cells of the dentate gyrus with CA3 neurons and provide feed forward inhibition via GABAergic interneurons (Acsády *et al.*, 1998; Rebola *et al.*, 2017).

$Na_V1.2$ is expressed in axon initial segments and the nodes of Ranvier of mouse hippocampus and cortex and then partially replaced by $Na_V1.6$, later in life, the expression of $Na_V1.2$ increases in unmyelinated fibers, like the mossy fibers of the hippocampus (Kaplan *et al.*, 2001; Liao *et al.,* 2010). $Na_V1.2$ is therefore an important player of action potential initiation and crucially influences the firing of neurons especially in the developing brain. The expression of $Na_V1.2$ in unmyelinated mossy fibers of dentate granule cells in the adult brain could provide a possible explanation for the phenotype of the patients associated with LOF mutations. As mossy fibers target GABAergic parvalbumin-positive interneurons besides CA3 pyramidal neurons they contribute to the feed-forward inhibition of CA3 neurons (Figure 39) (Acsády *et al.*, 1998; Rebola *et al.*, 2017). The hypothesized pathophysiology of epileptic activity in patients with loss of

function mutations results in a reduced input to GABAergic interneurons and a disinhibition of following CA3 neurons (Wolff *et al.*, 2017).

4.2 CACNA1E

4.2.1 *In vitro* effects of mutations in $Ca_V2.3$ / *CACNA1E*

The three missense mutations in *CACNA1E,* c.2093 T>C (p.F698S), c.2101 A>G (p.I701V), and c.2104 G>A (p.A702T), that were studied in this work are all located in the S6 transmembrane segment of domain II of the $Ca_V2.3$ channel (Figure 5).

The majority of missense mutations in patients with *CACNA1E* encephalopathy are located in the S6 segments of the channel and thereby affecting a highly conserved domain of the channel (Figure 40) (Helbig *et al.*, 2018). All three mutations showed a distinct shift in the voltage dependence of activation to hyperpolarized potentials of ~10 mV and a prolonged inactivation. To summarize, both alterations in gating kinetics lead to gain of function effect, that increases the flux of barium or calcium ions across the cell surface. Interestingly, almost all of the disease-causing mutations in *CACNA1E* that have been studied functionally show similar effects on activation and inactivation kinetics (Raybaud *et al.*, 2006, 2007; Helbig *et al.*, 2018).

The p.Gly348Asp and p.Gly352Arg mutations in the S6 segment of domain I (Figure 5) of the $Ca_V2.3$ channel have been expressed in *Xenopus laevis* oocytes before by incidence. Raybaud *et al.* studied the importance of the IS6 segment in the gating of calcium channels and found that in their experimental setup the p.Gly348Asp mutant led to a faster inactivation of the channel, whereas the p.Gly352Arg mutation shifted the voltage dependence of activation to more negative potentials and the voltage dependence of inactivation towards more depolarized potentials, both resulting in a gain of function of the mutant channel. Moreover, the p.Gly352Arg mutation prolonged inactivation of the channel, which is another gain of function aspect. (Raybaud *et al.*, 2006).

The p.Ile603Leu is one the few mutations in *CACNA1E* patients that is not located in one of the S6 segments of the channel, but in the intracellular linker between S4 and S5 of domain II (Figure 5). Nevertheless, it shows a similar effect on channel function, shifting the voltage dependence of activation to more negative potentials and prolonging

inactivation (Helbig *et al.*, 2018). This is in line with previous assumptions that the S4-S5 linker interacts with the S6 segment during gating movements in the $Ca_V2.3$ channel (Raybaud *et al.*, 2007; Wall-Lacelle *et al.*, 2011). However, this mutation also increased the current density of the channel, which is another gain of function aspect (Helbig *et al.*, 2018).

Similar to the mutations in domain I of the channel, the p.Ile701Val has been studied previously in *Xenopus laevis* oocytes co-expressed with the β_3 and a $\alpha_2\delta$-subunit. Consistent with our results, the mutation slowed down time-dependent inactivation and shifted the voltage dependence of activation by ~ 10 mV towards more negative voltages (Raybaud *et al.*, 2007). Changes in homologue amino acids to this isoleucine in other calcium channels have similar effects on the gating behavior in these channels (Figure 40). The homologous p.Ile770Met mutation in $Ca_V1.3$ (*CACNA1D*) shifted the activation and inactivation to hyperpolarized potentials (Scholl *et al.*, 2013). In $Ca_V1.4$ (*CACNA1F)* the p.Ile745Thr mutation leads to a shift of the voltage dependence of activation to more negative potentials and a prolonged inactivation (Hemara-Wahanui *et al.*, 2005).

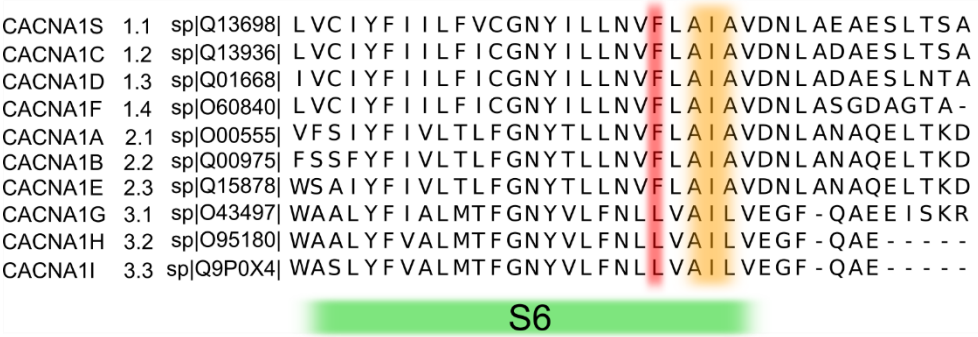

Figure 40: Alignment of domain II S6 segments in human voltage-gated calcium channels. Sequences were obtained from Uniprot. Identifiers indicate gene name, numerical name of the channel as per current nomenclature and the uniprot.org identifier of the sequence. Residues that were characterized are highlighted in red, orange and pink.

Similarly, the p.Ala702Gly and p.Ala1720Gly (in Raybaud *et al.*, 2007 p.Ala1719Gly) mutations have been tested previously in *Xenopus laevis* oocytes. In the *CACNA1E* encephalopathy patients published by us in Helbig *et. al*, 2018, the p.Ala702 site in $Ca_V2.3$ is substituted by threonine in six patients and by proline in one patient (Figure 5). Comparable to our results with threonine, a substitution of this residue by glycine prolongs inactivation drastically, but does not change activation kinetics significantly (Raybaud *et al.*, 2007). The reason for this is most likely the fact that an exchange of

alanine to threonine as a polar amino acid and Proline as 'helix-breaking' amino acid is in each case a stronger change in residue properties than the p.Ala702Gly exchange. We only conducted few experiments with the p.Ala702Pro mutant and could not observe any barium currents. We expect the proline residue to interfere with the helix of the transmembrane segment and cause a major disruption of the channel's function.

The p.Ala1720Gly mutation is a similar substitution in domain IV of the channel that corresponds to the alanine at position 700 in domain II of the channel (Figure 5). Substitution of alanine to glycine at these positions both shift the voltage dependence of activation towards more negative voltages and prolong inactivation. Both mutations additionally also shift the voltage dependence of inactivation towards more negative potentials which translates to a mixed gain and loss of function in mutated channels (Raybaud *et al.*, 2007).

Taken together, all these findings strengthen the view of the importance of distal S6 residues in the $Ca_V2.3$ channel for voltage-dependent activation and time-dependent inactivation. Except for the p.Gly348Ala mutation, all functionally examined mutations, that we describe as disease-causing in these patients, prolong inactivation and shift the voltage dependence of activation towards more negative potentials. From the current point of research, one can suspect that this gain of function is a typical effect of missense mutations in *CACNA1E* encephalopathy patients.
Because of their proximity to the pore region, S6-segments get associated with the activation gate in voltage-gated ion channels. Mutations in the distal S6 of $Ca_V2.1$ and $Ca_V2.3$ have been shown to stabilize the open state of the channel as they probably disrupt a hydrophobic seal that stabilizes the closed state formed by amino acids at positions 349, 701, 1420 and 1720 (Raybaud *et al.*, 2007).

4.2.2 Phenotypes of patients with mutations in *CACNA1E*

Patients with missense mutations in *CACNA1E* were identified worldwide in an international collaborative network of clinicians and geneticists. In total, 30 individuals with 14 different missense mutations could be identified by Whole Exome or Genome Trio-Sequencing (Helbig *et al.*, 2018) (Figure 5).

Among the whole study collective, a distinct phenotype was emerging. All patients showed developmental delay and most individuals showed pharmacoresistant epilepsy. Strikingly, many patients also showed hyperkinetic movement disorders, post-partal hypotonia and congenital contractures.

The phenotype of patients that were affected by mutations in *CACNA1E* studied in this thesis are described below. All of this clinical data was reported in brief in Helbig *et al,* 2018:

One female patient in our study collective was affected by the p.Phe698Ser mutation. She suffered from epileptic spasms and tonic seizures starting in the first week of her life. Video EEG monitoring studies at 15 days of life, 33 weeks and 3 years showed epileptiform discharges, disturbances in age appropriate vertebral electrical activity and multifocal spike wave discharges. Other EEG changes included hypsarrhythmia, a key symptom of West syndrome. The seizures remained refractory to ACTH, phenobarbital, Levetiracetame, Lacosamide, Vigabatrine and Valproic acid. A brain MRI was obtained at 8 days of age and showed no pathological features. Her head circumference was at the 49th percentile. The patient had severe global developmental delay, with no progress in milestones. She suffered from profound hypotonia and was not able to achieve purposeful movements. She furthermore suffered from distal arthrogryposis and left talipes equinovarus. She was also diagnosed with unilateral hydronephrosis. At the age of 4.5 years the patient died from cardiorespiratory failure.

In three female patients of the study collective the p.Ile701Val variant could be detected (Figure 5). All three patients were diagnosed with DEE. Epileptic seizures started at 19, 5.5 and 9 months. There was a huge variety of seizure types in these patients, including myoclonic, tonic focal seizures with impaired awareness and epileptic spasms. EEG patterns had a similar variety with interictal multifocal discharges to normal interictal EEG. One patient had a typical ictal pattern of infantile spasms. Two patients showed minimal brain abnormalities in MRI with slight asymmetry in the hippocampal formation and a small T2 hyperintensity, respective bifrontal cortical, discrete central and basal bitemporal atrophy at the age of 6 years. All patients showed global developmental delay with one patient showing regression after the beginning of epileptic seizures. One patient could communicate with few words and signs, another did not achieve eye contact, the

third one could not communicate verbally as well. None of the patients were able to walk independently. All patients showed hypotonia which developed into increased tone in some parts of the body, whilst other party stayed hypotone in two individuals during development. Furthermore, these two patients showed choreiformic movements. They both responded well to Topiramate which controls seizures in both individuals in the combination with levetiracetam. One of them was seizure free for 2 years under this combination. The third patient has never received Topiramate but responded to Prednisolone. None of the patients had congenital contractures but two had macrocephaly in infancy.

p.Ala702Thr was a recurrent mutation that occurred in six out of 30 affected patients (Figure 5). All of them showed the key symptoms of the *CACNA1E* encephalopathy with epileptic spasms as main epileptic phenotype, developmental delay and axial hypotonia. Five individuals had congenital contractures, one individual showed dyskinetic movements. Except for one patient, all patients presented with macrocephaly. All individuals were severely disabled with a further regression of global developmental delay after the beginning of the epileptic seizures in at least three out of six patients. Two individuals died at the age of 1 respective 3.25 years from acute airway obstruction respective status epilepticus. Hypsarrythmia was present in half of the patients, others showed EEG abnormalities such as multifocal discharges. One patient was seizure free for 18 months under a therapy with Topiramate until status epilepticus occurred. In all other patient's seizures remained refractory to medication. Three individuals showed abnormal MRI morphology with altered signal intensities that involved the basal ganglia and other parts of the brain.

4.2.3 Possible pathophysiology of the *CACNA1E* encephalopathy

As mentioned in 1.3.2.3 the physiological function and expression of $Ca_V2.3$ channels is very complex and not yet fully understood.

Although *CACNA1E* was not known as an epilepsy gene so far, previous studies in rodents focused on the possible function of $Ca_V2.3$ in absence seizures and memory (Breustedt *et al.*, 2003; Dietrich *et al.*, 2003; Weiergräber *et al.*, 2008). Few studies addressed the different seizure susceptibility of *CANA1E* knock out mice. The ablation of

$Ca_V2.3$ alters the chance of absence seizures and reduces the strength of induced convulsive seizures (Weiergräber *et al.*, 2006, 2008; Weiergraber *et al.*, 2007; Zaman *et al.*, 2011). *CACNA1E* KO mice show no spontaneous epileptic phenotype (Weiergräber *et al.*, 2006; Weiergraber *et al.*, 2007). Moreover, $Ca_V2.3^{-/-}$ mice show an increased seizure resistance to Kainate and Pentylenetetrazol induced seizures, but not 4-Aminopyridine induced seizures. They are less likely to show status epilepticus upon Kainate seizure induction and less likely to die from seizures induced by Kainate or pentylenetetrazol (Weiergräber *et al.*, 2006; Weiergraber *et al.*, 2007). KO mice also show a reduced excitotoxicity in the hippocampus after Kainate induced seizures (Weiergraber *et al.*, 2007). The seizure susceptibility of $Ca_V2.3^{-/-}$ mice to γ-hydroxybutyrolactone (GBL) is unclear. In two different studies, $Ca_V2.3^{-/-}$ mice showed either an increased or decreased seizure susceptibility to GBL induced absence seizures and a different EEG seizure architecture than *wild type* mice. (Weiergräber *et al.*, 2008; Zaman *et al.*, 2011). All of this fits to our findings, that gain of function mutations cause an epileptic phenotype with a convulsive seizure type. One might suspect that a gain of function in the channel will result in elevated excitotoxicity, which can further irrupt neurons and their circuits, resulting in a profound encephalopathy.

$Ca_V2.3$ channels contribute to long term potentiation (Breustedt *et al.*, 2003; Dietrich *et al.*, 2003) and the rhythmic firing of neurons (Zaman *et al.*, 2011). Although the mechanism are not fully understood, this involvement in the rhythmic activity of neurons could be a pathophysiological aspect of the *CACNA1E* encephalopathy.

In the *CACNA1E* study collective, the seizures of most patients were pharmacoresistant to multiple drugs (Helbig *et al.*, 2018). However, five out of 20 patients, for whom data were available, responded to the antiepileptic drug Topiramate, which was previously identified to inhibit cholinergic plateau potentials in CA1 neurons via a hyperpolarizing shift in the inactivation curve and a general current reduction of $Ca_V2.3$ channels (Kuzmiski *et al.*, 2005). This blocking action of Topiramate on $Ca_V2.3$ can explain its effectiveness in patients, who all carry gain of function mutations. Other studies also suggest that Lamotrigine, another common antiepileptic drug has influence on the gating of $Ca_V2.3$ channels and seizure susceptibility in $Ca_V2.3^{-/-}$ mice (Hainsworth *et al.*, 2003; Dibué-Adjei *et al.*, 2017). In our small study collective, we could not identify Lamotrigine

as an outstanding effective drug, but it should be considered as a possible drug in future patients.

Based on the few studies on the role of $Ca_V2.3$ during neurodevelopment, it can be assumed that calcium entry through $Ca_V2.3$ channels seems to be an important factor during neural development via Semaphorin 3A signaling (Nishiyama *et al.*, 2011). Furthermore, the astrocytal expression of $Ca_V2.3$ could be another factor of the *CACNA1E* encephalopathy (Day *et al.*, 1996; Latour *et al.*, 2003; D'Ascenzo *et al.*, 2004), as astrocytes play a role in epileptic activity (Tian *et al.*, 2005) and neurodevelopment (Weissman *et al.*, 2004). These aspects could contribute to a global malfunction of the brain along with the neuronal dysfunction and the profound phenotype of *CACNA1E* encephalopathy patients with pathological $Ca_V2.3$ function.

There are multiple possible pathomechanisms for *CACNA1E* associated syndromes. Based on the currently available literature, mutated $Ca_V2.3$ channels may not only influence epileptic activity, but also the proper microscopic architecture of the human brain. Taken together with the complex expression pattern of the channel, drawing hypothesizes on the effect of mutations in the channel *in vivo* is almost impossible and further research needs to be accounted on the function of the channel in the mammalian brain.

5 Summary

5.1 English

Epilepsy is one of the most common neurological diseases worldwide. Even though many etiologies exist, only a small percentage of epilepsy cases can be traced back to monogenetic alterations. In this work, mutations in two genes, encoding a sodium or a calcium channel, that occur in patients with genetic epilepsy were studied.

A patient in France with focal epilepsy and severe intellectual disability was diagnosed with the c.632 G>A (p.G211D) mutation in *SCN2A*, a well-known epilepsy gene. *SCN2A* encodes for $Na_V1.2$, one of the main sodium channels in the human brain during early stages of development. The mutation was introduced into the *wild type* gene and overexpressed in tsA201 cells. Voltage clamp recordings of the transfected cells showed a -7 mV shift in the voltage dependence of activation and a debatable smaller persistent current compared to the *wild type* channel. We suspect the major gain of function in the channel, resulting out of the shift in the activation curve, to be the main cause of disease in this patient. Furthermore, the reduced persistent current might indicate an additional loss of function, that we consider unlikely to be disease-relevant.

In another worldwide collaborative study, mutations in the novel epilepsy gene *CACNA1E* were identified in 30 children with early infantile epilepsy and developmental delay. Most patients were severely affected and showed pharmacoresistant epilepsy and congenital hypotonia and contractures. *CACNA1E* encodes the R-Type calcium channel $Ca_V2.3$, which is widely expressed in the central nervous system. Three missense mutations c.2093 T>C (p.F698S), c.2101 A>G (p.I701V), and c.2104 G>A (p.A702T) were introduced into the wild type gene and expressed heterologously in tsA201 cells. Voltage clamp recordings of the transfected non-neuronal cells showed a distinctive electrophysiological phenotype with a shift of the voltage dependence of activation to more negative values and a prolonged inactivation in comparison to the wild type. We suspect that this very consistent gain of function in the channel is the cause of disease in these patients.

5.2 German

Epilepsie ist eine der häufigsten neurologischen Erkrankungen weltweit. Epilepsie kann viele unterschiedliche Ätiologien haben. Monogetische Veränderungen machen einen kleinen Bruchteil hieran aus. In dieser Arbeit wurden Mutationen in zwei Genen untersucht, die bei Patienten mit genetischer Epilepsie gefunden wurden. Diese kodieren für einen Kalzium- oder für einen Natriumkanal

Bei einem französischen Patienten mit fokaler Epilepsie und schwerer geistiger Retardierung wurde die c.632 G>A (p.G211D) Mutation in *SCN2A,* einem bereits bekannten Epilepsiegen, gefunden. *SCN2A* kodiert $Na_V1.2$, einen der Hauptnatriumkanäle des menschlichen Gehirns während der Phasen der neuronalen Entwicklung. Die Mutation wurde in das Wildtyp Gen eingeführt und in tsA201 Zellen überexprimiert. Voltage-clamp Aufnahmen der transfizierten Zellen zeigten eine Verschiebung der Aktivierungskurve um -7mV und einen fraglichen kleineren Reststrom im Vergleich zum Wildtyp-Kanal. Wir gehen davon aus, dass der hauptsächliche Funktionsgewinn in diesem Kanal, welcher aus der Verschiebung der Aktivierungskurve resultiert, der Grund für die Erkrankung des Patienten ist. Der kleinere Reststrom könnte Hinweis auf einen zusätzlichen Funktionsverlust sein, den wir jedoch nicht als krankheitsrelevant ansehen.

In einer weiteren weltweiten Kollaboration wurden Mutationen im neuen Epilepsiegen *CACNA1E* bei 30 Kindern mit frühkindlicher Epilepsie und geistiger Retardierung identifiziert. Die meisten Patienten waren schwer betroffen und zeigten eine pharmakoresistente Epilepsie, sowie eine kongenitale Hypotonie und Kontrakturen. *CACNA1E* kodiert den im zentralen Nervensystem weithin exprimierten R-Typ Kalzium Kanal $Ca_V2.3$. Die drei Missense-Mutationen c.2093 T>C (p.F698S), c.2101 A>G (p.I701V) und c.2104 G>A (p.A702T) wurden in das Wildtyp- Gen eingeführt und heterolog in tsA201 Zellen exprimiert. Elektrophysiologische Messungen dieser transfizierten nicht-neuronalen Zellen mit der Patch-clamp Technik zeigten einen charakteristischen elektrophysiologischen Phänotyp, der aus einer Verschiebung der Aktivierungskurve in die negative Richtung, sowie einer verlängerten Inaktivierung im Vergleich zum Wildtyp bestand. Wir gehen davon aus, dass dieser sehr konsistente Funktionsgewinn in diesem Kanal der Grund für die Erkrankung der Patienten ist.

6 Publications

Helbig KL*, **Lauerer RJ**,* Bahr JC, Souza IA, Myers CT, Uysal B, Schwarz N, Gandini MA, Huang S, Keren B, Mignot C, Afenjar A, Billette de Villemeur T, Héron D, Nava C, Valence S, Buratti J, Fagerberg CR, Soerensen KP, Kibaek M, Kamsteeg EJ, Koolen DA, Gunning B, Schelhaas HJ, Kruer MC, Fox J, Bakhtiari S, Jarrar R, Padilla-Lopez S, Lindstrom K, Jin SC, Zeng X, Bilguvar K, Papavasileiou A, Xing Q, Zhu C, Boysen K, Vairo F, Lanpher BC, Klee EW, Tillema JM, Payne ET, Cousin MA, Kruisselbrink TM, Wick MJ, Baker J, Haan E, Smith N, Sadeghpour A, Davis EE, Katsanis N; Task Force for Neonatal Genomics, Corbett MA, MacLennan AH, Gecz J, Biskup S, Goldmann E, Rodan LH, Kichula E, Segal E, Jackson KE, Asamoah A, Dimmock D, McCarrier J, Botto LD, Filloux F, Tvrdik T, Cascino GD, Klingerman S, Neumann C, Wang R, Jacobsen JC, Nolan MA, Snell RG, Lehnert K, Sadleir LG, Anderlid BM, Kvarnung M, Guerrini R, Friez MJ, Lyons MJ, Leonhard J, Kringlen G, Casas K, El Achkar CM, Smith LA, Rotenberg A, Poduri A, Sanchis-Juan A, Carss KJ, Rankin J, Zeman A, Raymond FL, Blyth M, Kerr B, Ruiz K, Urquhart J, Hughes I, Banka S; Deciphering Developmental Disorders Study, Hedrich UBS, Scheffer IE, Helbig I, Zamponi GW, Lerche H*, Mefford HC*.

De Novo Pathogenic Variants in CACNA1E Cause Developmental and Epileptic Encephalopathy with Contractures, Macrocephaly, and Dyskinesias

Am J Hum Genet. 2018 Nov 1;103(5):666-678. doi: 10.1016/j.ajhg.2018.09.006. Epub 2018 Oct 18. Erratum in*: Am J Hum Genet.* 2019 Mar 7;104(3):562. PMID: 30343943; PMCID: PMC6216110.

*These authors contributed equally.

7 References

Acsády, L. *et al.* (1998) 'GABAergic cells are the major postsynaptic targets of mossy fibers in the rat hippocampus.', *The Journal of neuroscience : the official journal of the Society for Neuroscience*, 18(9), pp. 3386–403. doi: 10.1523/JNEUROSCI.18-09-03386.1998.

Anderson, P. A. V and Greenberg, R. M. (2001) 'Phylogeny of ion channels: Clues to structure and function', *Comparative Biochemistry and Physiology - B Biochemistry and Molecular Biology*, pp. 17–28. doi: 10.1016/S1096-4959(01)00376-1.

Bähring, R. and Covarrubias, M. (2011) 'Mechanisms of closed-state inactivation in voltage-gated ion channels', *Journal of Physiology*, 589(3), pp. 461–479. doi: 10.1113/jphysiol.2010.191965.

Berecki, G. *et al.* (2018) 'Dynamic action potential clamp predicts functional separation in mild familial and severe de novo forms of SCN2A epilepsy', *Proceedings of the National Academy of Sciences*, 115(24), pp. E5516–E5525. doi: 10.1073/pnas.1800077115.

Berg, A. T. *et al.* (2010) 'Revised terminology and concepts for organization of seizures and epilepsies: Report of the ILAE Commission on Classification and Terminology, 2005-2009', *Epilepsia*, 51(4), pp. 676–685. doi: 10.1111/j.1528-1167.2010.02522.x.

Birnbaumer, L. *et al.* (1998) 'Structures and functions of calcium channel beta subunits', *Journal of bioenergetics and biomembranes*, 30(4), pp. 357–375. doi: 10.1023/A:1021989622656.

Bohnen, M. S. *et al.* (2017) 'Molecular Pathophysiology of Congenital Long QT Syndrome.', *Physiological reviews*, 97(1), pp. 89–134. doi: 10.1152/physrev.00008.2016.

Bourinet, E. *et al.* (2001) 'Interaction of SNX482 with domains III and IV inhibits activation gating of alpha1E (CaV2.3) calcium channels.', *Biophysical journal*, 81(1), pp. 79–88. doi: 10.1016/S0006-3495(01)75681-0.

Breustedt, J. *et al.* (2003) 'Alpha1E-containing Ca2+ channels are involved in synaptic plasticity.', *Proceedings of the National Academy of Sciences of the United States of*

America, 100(21), pp. 12450–5. doi: 10.1073/pnas.2035117100.

Brugada, R. *et al.* (2014) 'Brugada syndrome.', *Methodist DeBakey cardiovascular journal*, 10(1), pp. 25–8. doi: 10.14797/mdcj-10-1-25.

Calloe, K. *et al.* (2018) 'Multifocal atrial and ventricular premature contractions with an increased risk of dilated cardiomyopathy caused by a Nav1.5 gain-of-function mutation (G213D)', *International Journal of Cardiology*. Elsevier, 257, pp. 160–167. doi: 10.1016/j.ijcard.2017.11.095.

Catterall, W. A., Perez-Reyes, E., *et al.* (2005) 'International Union of Pharmacology. XLVIII. Nomenclature and structure-function relationships of voltage-gated calcium channels.', *Pharmacological reviews*, 57(4), pp. 411–25. doi: 10.1124/pr.57.4.5.

Catterall, W. A. (2010) 'Ion channel voltage sensors: Structure, function, and pathophysiology', *Neuron*. Elsevier Inc., 67(6), pp. 915–928. doi: 10.1016/j.neuron.2010.08.021.

Catterall, W. A. (2012) 'Voltage-gated sodium channels at 60: structure, function and pathophysiology', *The Journal of Physiology*, 590(11), pp. 2577–2589. doi: 10.1113/jphysiol.2011.224204.

Catterall, W. A., Goldin, A. L. and Waxman, S. G. (2005) 'International Union of Pharmacology. XLVII. Nomenclature and Structure-Function Relationships of Voltage-Gated Sodium Channels', *Pharmacological Reviews*, 57(4), pp. 397–409. doi: 10.1124/pr.57.4.4.

Clairfeuille, T. *et al.* (2017) 'Voltage-gated sodium channels viewed through a structural biology lens', *Current Opinion in Structural Biology*. Elsevier Current Trends, 45, pp. 74–84. doi: 10.1016/j.sbi.2016.11.022.

D'Alonzo, R. *et al.* (2018) 'West Syndrome: A Review and Guide for Paediatricians', *Clinical Drug Investigation*. Springer International Publishing, 38(2), pp. 113–124. doi: 10.1007/s40261-017-0595-z.

D'Ascenzo, M. *et al.* (2004) 'Electrophysiological and molecular evidence of L-(Cav1), N- (Cav2.2), and R- (Cav2.3) type Ca2+ channels in rat cortical astrocytes', *Glia*. Wiley Subscription Services, Inc., A Wiley Company, 45(4), pp. 354–363. doi:

10.1002/glia.10336.

Day, N. C. *et al.* (1996) 'Distribution of alpha 1A, alpha 1B and alpha 1E voltage-dependent calcium channel subunits in the human hippocampus and parahippocampal gyrus.', *Neuroscience*, 71(4), pp. 1013–1024. doi: 10.1016/0306-4522(95)00514-5.

Dibué-Adjei, M. *et al.* (2017) 'Cav2.3 (R-Type) Calcium Channels are Critical for Mediating Anticonvulsive and Neuroprotective Properties of Lamotrigine In Vivo.', *Cellular physiology and biochemistry : international journal of experimental cellular physiology, biochemistry, and pharmacology*. Karger Publishers, 44(3), pp. 935–947. doi: 10.1159/000485361.

Dietrich, D. *et al.* (2003) 'Functional specialization of presynaptic Cav2.3 Ca2+ channels', *Neuron*, 39(3), pp. 483–496. doi: 10.1016/S0896-6273(03)00430-6.

Dolphin, A. C. (2003) 'Beta subunits of voltage-gated calcium channels.', *Journal of bioenergetics and biomembranes*, 35(6), pp. 599–620. doi: 10.1023/B:JOBB.0000008026.37790.5a.

Dolphin, A. C. (2006) 'A short history of voltage-gated calcium channels', *British Journal of Pharmacology*, 147, pp. S56–S62. doi: 10.1038/sj.bjp.0706442.

Drenth, J. P. H. and Waxman, S. G. (2007) 'Mutations in sodium-channel gene SCN9A cause a spectrum of human genetic pain disorders.', *The Journal of clinical investigation*, 117(12), pp. 3603–9. doi: 10.1172/JCI33297.

Elborn, J. S. (2016) 'Cystic fibrosis', *The Lancet*, 388(10059), pp. 2519–2531. doi: 10.1016/S0140-6736(16)00576-6.

Fagerberg, L. *et al.* (2014) 'Analysis of the Human Tissue-specific Expression by Genome-wide Integration of Transcriptomics and Antibody-based Proteomics', *Molecular & Cellular Proteomics*, 13(2), pp. 397–406. doi: 10.1074/mcp.M113.035600.

Fiest, K. M. *et al.* (2017) 'Prevalence and incidence of epilepsy: A systematic review and meta-analysis of international studies.', *Neurology*, 89(6), p. 642. doi: 10.1212/WNL.0000000000004317.

Fisher, R. S. *et al.* (2005) 'Epileptic seizures and epilepsy: definitions proposed by the

International League Against Epilepsy (ILAE) and the International Bureau for Epilepsy (IBE).', *Epilepsia*, 46(10), pp. 1698–9; author reply 1701-2. doi: 10.1111/j.1528-1167.2005.00273_1.x.

Fisher, R. S. *et al.* (2014) 'ILAE Official Report: A practical clinical definition of epilepsy', *Epilepsia*, 55(4), pp. 475–482. doi: 10.1111/epi.12550.

Fletcher, E. V, Kullmann, D. M. and Schorge, S. (2011) 'Alternative Splicing Modulates Inactivation of Type 1 Voltage-gated Sodium Channels by Toggling an Amino Acid in the First S3-S4 Linker', *Journal of Biological Chemistry*, 286(42), pp. 36700–36708. doi: 10.1074/jbc.M111.250225.

Gee, N. S. *et al.* (1996) 'The novel anticonvulsant drug, gabapentin (Neurontin), binds to the alpha2delta subunit of a calcium channel.', *The Journal of biological chemistry*, 271(10), pp. 5768–76. doi: 10.1074/jbc.271.10.5768.

Graham, F. L. *et al.* (1977) 'Characteristics of a Human Cell Line Transformed by DNA from Human Adenovirus Type 5', *Journal of General Virology*, 36(1), pp. 59–72. doi: 10.1099/0022-1317-36-1-59.

Hainsworth, A. H. *et al.* (2003) 'Actions of sipatrigine, 202W92 and lamotrigine on R-type and T-type Ca2+ channel currents', *European Journal of Pharmacology*, 467(1–3), pp. 77–80. doi: 10.1016/S0014-2999(03)01625-X.

Helbig, K. L. *et al.* (2018) 'De Novo Pathogenic Variants in CACNA1E Cause Developmental and Epileptic Encephalopathy with Contractures, Macrocephaly, and Dyskinesias.', *American journal of human genetics*. Elsevier, 104(3), p. 562. doi: 10.1016/j.ajhg.2019.02.015.

Hemara-Wahanui, A. *et al.* (2005) 'A CACNA1F mutation identified in an X-linked retinal disorder shifts the voltage dependence of Cav1.4 channel activation', *Proceedings of the National Academy of Sciences*, 102(21), pp. 7553–7558. doi: 10.1073/pnas.0501907102.

Heron, S. E. *et al.* (2002) 'Sodium-channel defects in benign familial neonatal-infantile seizures', *Lancet*, 360(9336), pp. 851–852. doi: 10.1016/S0140-6736(02)09968-3.

Hobom, M. *et al.* (2000) 'Neuronal distribution and functional characterization of the

calcium channel alpha2delta-2 subunit', *European Journal of Neuroscience*. Blackwell Science Ltd, 12(4), pp. 1217–1226. doi: 10.1046/j.1460-9568.2000.01009.x.

Hodgkin, A. L. and Huxley, A. F. (1952) 'A quantitative description of membrane current and its application to conduction and excitation in nerve', *The Journal of Physiology*, 117(4), pp. 500–544. doi: 10.1113/jphysiol.1952.sp004764.

Hofmann, F. *et al.* (2014) 'L-Type Ca v 1.2 Calcium Channels: From In Vitro Findings to In Vivo Function', *Physiological Reviews*, 94(1), pp. 303–326. doi: 10.1152/physrev.00016.2013.

Howell, K. B. *et al.* (2015) 'SCN2A encephalopathy: A major cause of epilepsy of infancy with migrating focal seizures.', *Neurology*, 85(11), pp. 958–66. doi: 10.1212/WNL.0000000000001926.

Kandel, E R *et al.* (2013) '5 Ion Channels', in *Principles of Neural Science, Fifth Edition*. McGraw-Hill Education (Principles of Neural Science), pp. 105–125.

Kandel, Eric R *et al.* (2013) *Principles of neural science*. 5. ed. New York [u.a.]: McGraw-Hill Medical (McGraw-Hill medical).

Kaplan, M. R. *et al.* (2001) 'Differential Control of Clustering of the Sodium Channels Nav1.2 and Nav1.6 at Developing CNS Nodes of Ranvier', *Neuron*, 30(1), pp. 105–119. doi: 10.1016/S0896-6273(01)00266-5.

Kasai, N. *et al.* (2001) 'Genomic structures of SCN2A and SCN3A - Candidate genes for deafness at the DFNA16 locus', *Gene*, 264(1), pp. 113–122. doi: 10.1016/S0378-1119(00)00594-1.

Kimm, T. and Bean, B. P. (2014) 'Inhibition of A-Type Potassium Current by the Peptide Toxin SNX-482', *Journal of Neuroscience*, 34(28), pp. 9182–9189. doi: 10.1523/JNEUROSCI.0339-14.2014.

Klugbauer, N. *et al.* (1999) 'Molecular diversity of the calcium channel alpha2delta subunit', *The Journal of Neuroscience : The official Journal of the Society for Neuroscience*. Society for Neuroscience, 19(2), pp. 684–91. doi: 10.1016/0014-5793(95)01475-6.

Kodera, H. *et al.* (2013) 'Targeted capture and sequencing for detection of mutations causing early onset epileptic encephalopathy', *Epilepsia*, 54(7), pp. 1262–1269. doi: 10.1111/epi.12203.

Korn, S. J. (1989) 'Influence of sodium-calcium exchange on calcium current rundown and the duration of calcium-dependent chloride currents in pituitary cells, studied with whole cell and perforated patch recording', *The Journal of General Physiology*. Rockefeller University Press, 94(5), pp. 789–812. doi: 10.1085/jgp.94.5.789.

Kuzmiski, J. B. *et al.* (2005) 'Topiramate inhibits the initiation of plateau potentials in CA1 neurons by depressing R-type calcium channels.', *Epilepsia*. Blackwell Science Inc, 46(4), pp. 481–9. doi: 10.1111/j.0013-9580.2005.35304.x.

Latour, I. *et al.* (2003) 'Expression of voltage-gated Ca2+ channel subtypes in cultured astrocytes', *Glia*, 41(4), pp. 347–353. doi: 10.1002/glia.10162.

Lauxmann, S. *et al.* (2013) 'An SCN2A mutation in a family with infantile seizures from Madagascar reveals an increased subthreshold Na + current', *Epilepsia*, 54(9), pp. e117–e121. doi: 10.1111/epi.12241.

Lauxmann, S. *et al.* (2018) 'Relationship of electrophysiological dysfunction and clinical severity in SCN2A -related epilepsies', *Human Mutation*, 39(12), pp. 1942–1956. doi: 10.1002/humu.23619.

Lee, J. H. *et al.* (1999) 'Nickel block of three cloned T-type calcium channels: low concentrations selectively block alpha1H.', *Biophysical journal*, 77(6), pp. 3034–42. doi: 10.1016/S0006-3495(99)77134-1.

Lehmann-Horn, F. and Jurkat-Rott, K. (1999) 'Voltage-gated ion channels and hereditary disease', *Physiological Reviews*, 79(4), pp. 1317–1372. doi: 10.1152/physrev.1999.79.4.1317.

Lerche, H. *et al.* (2013) 'Ion channels in genetic and acquired forms of epilepsy', *J Physiol The Journal of Physiology Neuroscience S The Journal of Physiology The Physiological Society J Physiol*, 5914(5914), pp. 753–764. doi: 10.1113/jphysiol.2012.240606.

Liao, Y., Deprez, L., *et al.* (2010) 'Molecular correlates of age-dependent seizures in an

inherited neonatal-infantile epilepsy', *Brain*, 133(5), pp. 1403–1414. doi: 10.1093/brain/awq057.

Liao, Y., Anttonen, A. K., *et al.* (2010) 'SCN2A mutation associated with neonatal epilepsy, late-onset episodic ataxia, myoclonus, and pain', *Neurology*, 75(16), pp. 1454–1458. doi: 10.1212/WNL.0b013e3181f8812e.

Llinás, R. *et al.* (1992) 'Distribution and functional significance of the P-type, voltage-dependent Ca2+ channels in the mammalian central nervous system', *Trends in Neurosciences*, 15(9), pp. 351–355. doi: 10.1016/0166-2236(92)90053-B.

Magiorkinis, E., Sidiropoulou, K. and Diamantis, A. (2010) 'Hallmarks in the history of epilepsy: Epilepsy in antiquity', *Epilepsy and Behavior*. Elsevier Inc., 17(1), pp. 103–108. doi: 10.1016/j.yebeh.2009.10.023.

Mills, T. W. (1892) *Popular Science Monthly/Volume 42/November 1892/The Natural or Scientific Method in Education - Wikisource, the free online library*, *Popular Science Monthly Volume 42 November 1892*. Available at: https://en.wikisource.org/wiki/Popular_Science_Monthly/Volume_42/November_1892/The_Natural_or_Scientific_Method_in_Education (Accessed: 12 December 2017).

Mintz, I. M., Sabatini, B. L. and Regehr, W. G. (1995) 'Calcium control of transmitter release at a cerebellar synapse', *Neuron*, 15(3), pp. 675–688. doi: 10.1016/0896-6273(95)90155-8.

Molleman, A. (2002) *Patch Clamping*. Wiley. doi: 10.1002/0470856521.

Müller, C. S. *et al.* (2010) 'Quantitative proteomics of the Cav2 channel nano-environments in the mammalian brain.', *Proceedings of the National Academy of Sciences of the United States of America*, 107(34), pp. 14950–7. doi: 10.1073/pnas.1005940107.

Nakamura, K. *et al.* (2013) 'Clinical spectrum of SCN2A mutations expanding to Ohtahara syndrome', *Neurology*. Lippincott Williams & Wilkins, 81(11), pp. 992–998. doi: 10.1212/WNL.0b013e3182a43e57.

NCBI Gene ID: 777 (2018). Available at: https://www.ncbi.nlm.nih.gov/gene/777?report=expression&bioproject=PRJEB4337

(Accessed: 13 November 2018).

Neely, A. and Hidalgo, P. (2014) 'Structure-function of proteins interacting with the alpha1 pore-forming subunit of high-voltage-activated calcium channels', *Frontiers in Physiology*, 5 JUN(June), pp. 1–19. doi: 10.3389/fphys.2014.00209.

Neher, E. and Sakmann, B. (1976) 'Single-channel currents recorded from membrane of denervated frog muscle fibres', *Nature*. Nature Publishing Group, 260(5554), pp. 799–802. doi: 10.1038/260799a0.

Newcomb, R. *et al.* (1998) 'Selective peptide antagonist of the class E calcium channel from the venom of the tarantula Hysterocrates gigas', *Biochemistry*, 37(44), pp. 15353–15362. doi: 10.1021/bi981255g.

Nishiyama, M. *et al.* (2011) 'Semaphorin 3A induces CaV2.3 channel-dependent conversion of axons to dendrites', *Nature Cell Biology*, 13(6), pp. 676–685. doi: 10.1038/ncb2255.

Osborne, J. P. *et al.* (2010) 'The underlying etiology of infantile spasms (West syndrome): information from the United Kingdom Infantile Spasms Study (UKISS) on contemporary causes and their classification.', *Epilepsia*, 51(10), pp. 2168–74. doi: 10.1111/j.1528-1167.2010.02695.x.

Oyrer, J. *et al.* (2018) 'Ion Channels in Genetic Epilepsy: From Genes and Mechanisms to Disease-Targeted Therapies', *Pharmacological Reviews*, 70(1), pp. 142–173. doi: 10.1124/pr.117.014456.

Parajuli, L. K. *et al.* (2012) 'Quantitative regional and ultrastructural localization of the Ca(v)2.3 subunit of R-type calcium channel in mouse brain.', *Journal of Neuroscience*, 32(39), pp. 13555–13567. doi: 10.1523/JNEUROSCI.1142-12.2012.

Pavone, P. *et al.* (2014) 'Infantile spasms syndrome, West syndrome and related phenotypes: What we know in 2013', *Brain and Development*, pp. 739–751. doi: 10.1016/j.braindev.2013.10.008.

Payandeh, J. *et al.* (2011) 'The crystal structure of a voltage-gated sodium channel', *Nature*. Nature Publishing Group, 475(7356), pp. 353–359. doi: 10.1038/nature10238.

Raybaud, A. *et al.* (2006) 'The role of the GX9GX3G motif in the gating of high voltage-activated Ca2+ channels.', *The Journal of biological chemistry*, 281(51), pp. 39424–36. doi: 10.1074/jbc.M607405200.

Raybaud, A. *et al.* (2007) 'The role of distal S6 hydrophobic residues in the voltage-dependent gating of CaV2.3 channels', *Journal of Biological Chemistry*, 282(38), pp. 27944–27952. doi: 10.1074/jbc.M703895200.

Rebola, N., Carta, M. and Mulle, C. (2017) 'Operation and plasticity of hippocampal CA3 circuits: Implications for memory encoding', *Nature Reviews Neuroscience*. Nature Publishing Group, 18(4), pp. 209–221. doi: 10.1038/nrn.2017.10.

Sarantopoulos, C. *et al.* (2004) 'beta-Escin Diminishes Voltage-Gated Calcium Current Rundown in Perforated Patch-Clamp Recordings From Rat Primary Afferent Neurons', *Journal of Neuroscience Methods*, 139(1), pp. 61–68. doi: 10.1016/j.jneumeth.2004.04.015.

Scheffer, I. E. *et al.* (2017) 'ILAE classification of the epilepsies: Position paper of the ILAE Commission for Classification and Terminology', *Epilepsia*, 58(4), pp. 512–521. doi: 10.1111/epi.13709.

Scholl, U. I. *et al.* (2013) 'Somatic and germline CACNA1D calcium channel mutations in aldosterone-producing adenomas and primary aldosteronism', *Nature Genetics*. Nature Publishing Group, 45(9), pp. 1050–1054. doi: 10.1038/ng.2695.

Schwarz, N. *et al.* (2016) 'Mutations in the sodium channel gene SCN2A cause neonatal epilepsy with late-onset episodic ataxia', *Journal of Neurology*, 263(2), pp. 334–343. doi: 10.1007/s00415-015-7984-0.

Silveira-Moriyama, L. *et al.* (2018) 'Phenotypes, genotypes, and the management of paroxysmal movement disorders', *Developmental Medicine and Child Neurology*, 60(6), pp. 559–565. doi: 10.1111/dmcn.13744.

Sochivko, D. *et al.* (2002) 'The Cav2.3 Ca2+channel subunit contributes to R-type Ca2+currents in murine hippocampal and neocortical neurones', *Journal of Physiology*. Blackwell Publishing Ltd, 542(3), pp. 699–710. doi: 10.1113/jphysiol.2002.020677.

Soong, T. W. *et al.* (1993) 'Structure and functional expression of a member of the low

voltage-activated calcium channel family.', *Science (New York, N.Y.)*, 260(5111), pp. 1133–6. doi: 10.1126/science.8388125.

Sutherland, H. G., Albury, C. L. and Griffiths, L. R. (2019) 'Advances in genetics of migraine', *Journal of Headache and Pain*. The Journal of Headache and Pain, 20(1). doi: 10.1186/s10194-019-1017-9.

Tai, C., Kuzmiski, J. B. and MacVicar, B. A. (2006) 'Muscarinic Enhancement of R-Type Calcium Currents in Hippocampal CA1 Pyramidal Neurons', *Journal of Neuroscience*, 26(23), pp. 6249–6258. doi: 10.1523/jneurosci.1009-06.2006.

Taylor, C. P., Angelotti, T. and Fauman, E. (2007) 'Pharmacology and mechanism of action of pregabalin: The calcium channel α2–δ (alpha2–delta) subunit as a target for antiepileptic drug discovery', *Epilepsy Research*, 73(2), pp. 137–150. doi: 10.1016/j.eplepsyres.2006.09.008.

Tian, G. F. *et al.* (2005) 'An astrocytic basis of epilepsy', *Nature Medicine*, 11(9), pp. 973–981. doi: 10.1038/nm1277.

Tottene, A., Volsen, S. and Pietrobon, D. (2000) 'alpha(1E) subunits form the pore of three cerebellar R-type calcium channels with different pharmacological and permeation properties.', *The Journal of neuroscience : the official journal of the Society for Neuroscience*, 20(1), pp. 171–8. doi: 10.1523/JNEUROSCI.20-01-00171.2000.

Vajna, R. *et al.* (2001) 'Functional coupling between "R-type" Ca 2+ channels and insulin secretion in the insulinoma cell line INS-1', *European Journal of Biochemistry*, 268(4), pp. 1066–1075. doi: 10.1046/j.1432-1327.2001.01969.x.

Vassilev, P., Scheuer, T. and Catterall, W. A. (1989) 'Inhibition of inactivation of single sodium channels by a site-directed antibody', *Proceedings of the National Academy of Sciences of the United States of America*, 86(20), pp. 8147–8151. doi: 10.1073/pnas.86.20.8147.

Vorstman, J. A. S. *et al.* (2017) 'Autism genetics: Opportunities and challenges for clinical translation', *Nature Reviews Genetics*. Nature Publishing Group, 18(6), pp. 362–376. doi: 10.1038/nrg.2017.4.

W.J.West (1841) 'On a peculiar form of infantile convulsion', *Lancet*, 1, pp. 724–725.

doi: 10.1016/0305-4179(84)90176-1.

Wall-Lacelle, S. *et al.* (2011) 'Double mutant cycle analysis identified a critical leucine residue in the IIS4S5 linker for the activation of the Cav2.3 calcium channel', *Journal of Biological Chemistry*. American Society for Biochemistry and Molecular Biology, 286(31), pp. 27197–27205. doi: 10.1074/jbc.M111.237412.

Wang, J. *et al.* (2016) 'Epilepsy-associated genes', *Seizure*, 44(In Press), pp. 11–20. doi: 10.1016/j.seizure.2016.11.030.

Weiergräber, M. *et al.* (2007) 'Hippocampal Seizure Resistance and Reduced Neuronal Excitotoxicity in Mice Lacking the Cav2.3 E/R-Type Voltage-Gated Calcium Channel', *Journal of Neurophysiology*, 97(5), pp. 3660–3669. doi: 10.1152/jn.01193.2006.

Weiergräber, M. *et al.* (2006) 'Altered Seizure Susceptibility in Mice Lacking the Cav2.3 E-type Ca2+ Channel', *Epilepsia*, 47(5), pp. 839–850. doi: 10.1111/j.1528-1167.2006.00541.x.

Weiergräber, M. *et al.* (2008) 'Altered thalamocortical rhythmicity in Cav2.3-deficient mice', *Molecular and Cellular Neuroscience*, 39(4), pp. 605–618. doi: 10.1016/j.mcn.2008.08.007.

Weissman, T. A. *et al.* (2004) 'Calcium waves propagate through radial glial cells and modulate proliferation in the developing neocortex', *Neuron*, 43(5), pp. 647–661. doi: 10.1016/j.neuron.2004.08.015.

West, J. W. *et al.* (1992) 'A cluster of Hydrophobic amino acid residues required for fast Na+-channel inactivation', *Proceedings of the National Academy of Sciences of the United States of America*, 89(22), pp. 10910–10914. doi: 10.1073/pnas.89.22.10910.

WHO (2018) *International Classification of Diseases, 11th Revision (ICD-11)*. Available at: https://icd.who.int/browse11/l-m/en#/http%3A%2F%2Fid.who.int%2Ficd%2Fentity%2F1397288146 (Accessed: 14 November 2018).

Wilde, A. A. M. and Amin, A. S. (2018) 'Clinical Spectrum of SCN5A Mutations: Long QT Syndrome, Brugada Syndrome, and Cardiomyopathy', *JACC: Clinical Electrophysiology*, 4(5), pp. 569–579. doi: 10.1016/j.jacep.2018.03.006.

Williams, M. E. *et al.* (1994) 'Structure and functional characterization of neuronal alpha1E calcium channel subtypes', *J. Biol. Chem.*, 269(35), pp. 22347–22357.

Wolff, M. *et al.* (2017) 'Genetic and phenotypic heterogeneity suggest therapeutic implications in SCN2A-related disorders', *Brain*, 140(5), pp. 1316–1336. doi: 10.1093/brain/awx054.

Wolff, M., Brunklaus, A. and Zuberi, S. M. (2019) 'Phenotypic spectrum and genetics of SCN2A-related disorders, treatment options, and outcomes in epilepsy and beyond', *Epilepsia*, 60(S3), pp. S59–S67. doi: 10.1111/epi.14935.

Xu, R. *et al.* (2007) 'A childhood epilepsy mutation reveals a role for developmentally regulated splicing of a sodium channel', *Molecular and Cellular Neuroscience*, 35(2), pp. 292–301. doi: 10.1016/j.mcn.2007.03.003.

Yu, F. H. and Catterall, W. A. (2004) 'The VGL-Chanome: A Protein Superfamily Specialized for Electrical Signaling and Ionic Homeostasis', *Science Signaling*, 2004(253), pp. re15–re15. doi: 10.1126/stke.2532004re15.

Zaman, T. *et al.* (2011) 'Cav2.3 channels are critical for oscillatory burst discharges in the reticular thalamus and absence epilepsy.', *Neuron*. Elsevier Inc., 70(1), pp. 95–108. doi: 10.1016/j.neuron.2011.02.042.

8 Declaration of contribution to the thesis - Erklärung zum Eigenanteil

Die Arbeit wurde am Hertie-Institut für klinische Hirnforschung in der Arbeitsgruppe Experimentelle Epileptologie unter Betreuung von Herrn Prof. Dr. Holger Lerche durchgeführt.

Die Konzeption des elektrophysiologischen Teils der Studie erfolgte in Zusammenarbeit mit Dr.Ulrike B. S. Hedrich-Klimosch und Dr.Niklas Schwarz. Die Koordination der genetischen und klinischen Daten aus der *CACNA1E* Forschergruppe erfolgte durch Katherine Helbig und Heather Mefford. Die klinischen und gentischen Informationen zur p.G211D Mutation in *SCN2A* wurden durch Prof. Rima Nabbout berichtet.

Sämtliche elektrophysiologischen Versuche zur p.G211D Mutante in *SCN2A* wurden nach Einarbeitung durch Dr.Ulrike B. S. Hedrich-Klimosch und Dr.Niklas Schwarz von mir durchgeführt. Die Primer zur Mutagenese und Sequenzierung von *SCN2A* wurden von Dr. Niklas Schwarz designt. Das Primerdesign für *CACNA1E* erfolgte durch mich. Die elektrophysiologischen Versuche zu *CACNA1E* erfolgten in Zusammenarbeit mit Jacqueline Bahr und Betül Uysal, wobei neben mir Jacqueline Bahr einen großen Anteil an den elektrophysiologischen Messungen trug.

Die statistische Auswertung erfolgte nach Anleitung durch Dr.Ulrike B. S. Hedrich-Klimosch durch mich.

Ich versichere, das Manuskript selbständig verfasst zu haben und keine weiteren als die von mir angegebenen Quellen verwendet zu haben.

Tübingen, den

Robert Lauerer-Braun

9 Acknowledgments

First of all, I want to thank Prof. Dr. Holger Lerche for giving me the opportunity to work at his laboratory and to support my work. Thank you for being a considerate doctoral father and a thoughtful scientific teacher.

I want to thank Dr. Niklas Schwarz and Dr. Ulrike Hedrich-Klimosch for supervising me and supporting me in all the questions and frustrations I had. Thank you for teaching me so many hard and soft skills and for integrating me so warmly into the team.

I want to thank Jacqueline Bahr and Betül Uysal for extensively engaging in this project. Jacqueline Bahr recorded most of the *CACNA1E* p.I701V mutant as well as other mutants. Thank you for going through all the *"KACK-NA-Stress"* we had together.

A special thanks goes to all the collaborators that were engaged into this research. Without their clinical data, my work would be useless. I want to thank the *CACNA1E* collaborative group and especially Katherine Helbig and Heather Mefford for collecting all the clinical data and engaging in such a nice collaboration. I furthermore thank the *SCN2A* Team for providing short info on the clinical phenotype and reporting the underlying genetics.

I am deeply grateful for the funding that I received from the Sigmund-Kiener-Stiftung and its founder, Sigmund Kiener. It enabled me to take the time for research without worrying about my financial situation . It furthermore enabled me to take part in the IZKF program of the medical faculty.

I thank Theresa Braun for being my best friend and partner and recently my wife during all highs and downs. Thank you for all your support and proofreading. I am very lucky to have you by my side and I am looking forward to our future as doctors.

I thank my parents for supporting me over the whole time of my studies. Thank you for enabling me to fulfil my dreams and supporting me in all I do.